Advance Automation 833

April 2015

Introductory course to aircraft dynamics

J.A.A. Engelbrecht

---

1 Course Overview

Aircraft dynamics deals with the equations of motion that describe the flight of an aircraft through space. This course aims to derive and provide an intuitive understanding of those dynamics. It begins with the general six degree of freedom equations of motion for a rigid body and ends by analysing the classic modes of motion of an aircraft about straight and level trimmed flight. The table below provides a summary of what will be handled in the course as well as a summary of the associated homework exercises.

LECTURES	TOPICS COVERED	HOMEWORK
Lecture 1	Standard definitions and notation used in aircraft modelling. Derivation of the six degree of freedom equations of motion. Classic force and moment models for aircraft. Summary of entire aircraft dynamics model.	Development and testing of a 6DOF Model in Simulink. Development and testing of a Force and Moment model in Simulink.
Lecture 2	Defining and calculating trim. Linearising the aircraft dynamics. Analysis of classic aircraft modes of motion.	Calculating trim and verifying trim condition in Simulink simulation. Analyse modes of motion of example aircraft.
Lecture 3	Overview of classic controllers for aircraft. Design of longitudinal controllers.	Design, implement and verify longitudinal controllers in Simulink.
Lecture 4	Design of lateral controllers	Design, implement and verify lateral controllers in Simulink.
Lecture 5	Guidance and Waypoint Navigation	Design, implement and verify guidance and waypoint navigation in Simulink.
Lecture 6	Aircraft State Estimation	None

A student that has completed this course should have a good understanding of the fundamentals of aircraft dynamics, have a physical understanding of the various aircraft modes of motion and the stability derivatives associated with the modes, and have an understanding of how these modes are classically controlled.

2 Axis Systems and Notation

This section introduces the axis systems and notation commonly used in aircraft dynamics modelling.

2.1 Axis Systems

To obtain a mathematical grip on the aircraft for modelling purposes, a number of axis systems first need to be defined. Inertial, Body and Wind axis systems are defined in the subsections that follow.

2.1.1 Inertial Axes

An inertial axis system is required if we are to apply Newton's equations of motion. For typical short range UAV applications, the standard North-East-Down (NED) axis system, shown in Figure 1, adequately approximates an inertial axis system. The NED axis system assumes a flat earth that is non-rotating. The centre of the axis system is chosen to coincide with some convenient reference point on the earth's surface e.g. the starting position on a runway. From there, the x-axis points in the north direction, the y-axis points in the east direction and the z-axis completes the right handed, orthogonal axis system and points in the down direction (towards the centre of the earth).

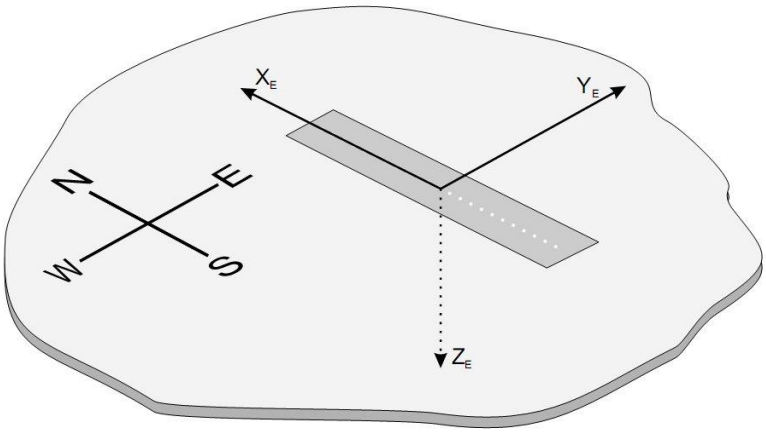

Figure 1 – North-East-Down Axis System

2.1.2 Body Axes

Body axes, as shown in Figure 2, are fixed to the aircraft with their origin chosen to coincide with the aircraft's centre of mass. The x-axis lies in the plane of symmetry and points along some convenient reference line e.g. zero angle of attack line of the wing or watermark line of the fuselage. The y-axis lies perpendicular to the plane of symmetry in the direction of the starboard (right hand) wing. The z-axis completes the right handed, orthogonal axis system and points downwards relative to the aircraft cockpit.

2.1.3 Wind Axes

Wind axes, often referred to as *stability axes*, are similar to body axes in that their origin coincides with the centre of mass and thus move with the aircraft. However, the x-axis points in the direction of the velocity vector, while the z-axis lies in the aircraft's plane of symmetry and points in the down direction relative to the cockpit. The y-axis completes the right hand axis system and points in the direction of the starboard wing.

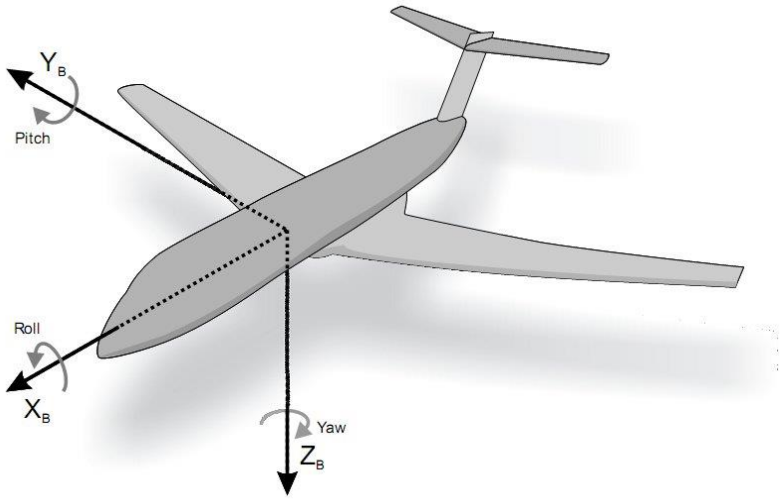

Figure 2 – Aircraft Body Axis System

2.2 Notation

This section introduces the standard notation used in aircraft modelling. Consider Figure 3 below.

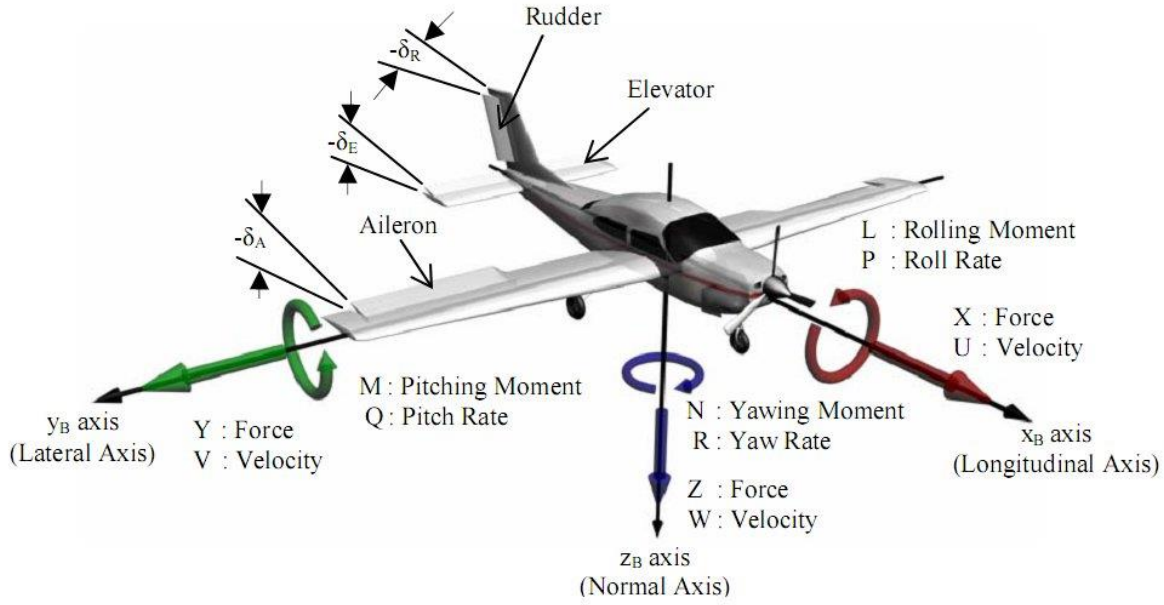

Figure 3 – Standard Aircraft Notation

The figure displays the following symbols and their positive directions,

X, Y, Z :	Coordinates of the force vector in body axes respectively (axial, lateral and normal force)
L, M, N :	Coordinates of the moment vector in body axes respectively (roll, pitch and yaw moments)
U, V, W :	Coordinates of the linear velocity vector in body axes (axial, lateral and normal velocity)
P, Q, R :	Coordinates of the angular velocity vector in body axes (roll, pitch and yaw rates)
$\delta_A, \delta_E, \delta_R$:	Aileron, elevator and rudder control surface deflections respectively. A positive deflection is defined as one that produces a negative moment.

It is often more convenient to express the velocity vector in polar form i.e. using a magnitude and two angles as shown in Figure 4 below.

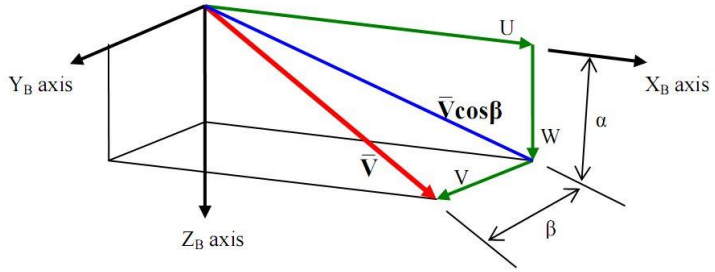

Figure 4 – Polar Velocity Coordinates

The velocity magnitude ($\bar{V}$), angle of attack (α) and angle of sideslip (β) are defined in terms of the Cartesian velocity coordinates above as follows,

$$\bar{V} = \sqrt{U^2 + V^2 + W^2} \tag{2.1}$$

$$\alpha = \tan^{-1}\left(\frac{W}{U}\right) \tag{2.2}$$

$$\beta = \sin^{-1}\left(\frac{V}{\bar{V}}\right) \tag{2.3}$$

The inverse relationships are,

$$U = \bar{V}\cos\alpha\cos\beta \tag{2.4}$$

$$V = \bar{V}\sin\beta \tag{2.5}$$

$$W = \bar{V}\sin\alpha\cos\beta \tag{2.6}$$

3 Six Degree of Freedom Equations of Motion

For control system design purposes, an aircraft is well modelled as a six degree of freedom rigid body. The six degrees of freedom are the aircraft's 3 translational degrees of freedom and its 3 rotational degrees of freedom. A rigid body implies that the position of each mass element on the aircraft remains fixed relative to the body axis system at all times. Although most aircraft, especially large ones, display structural flexibility, theses modes of motion are most often outside the bandwidth of conventional controllers and thus do not need to be taken into account in the modelling process. This section investigates the six degree of freedom equations of motion for a rigid body.

3.1 Kinetics

Kinetics is the branch of mechanics that relates the forces and moments acting on an object to the kinematic state of the object i.e. its position, velocity and acceleration. Newton's laws of motion for six degree of freedom rigid bodies can be used to model this relationship. There are a number of different forms of the kinetic equations of motion depending on which axis systems are used during the coordination of the vectors involved. Presented below are the equations of motion in their classic form where all vectors are coordinated in body axes,

$$X = m\left(\dot{U} - VR + WQ\right) \tag{3.1}$$

$$Y = m\left(\dot{V} + UR - WP\right) \tag{3.2}$$

$$Z = m\left(\dot{W} - UQ + VP\right) \tag{3.3}$$

$$L = \dot{P}I_{xx} + QR\left(I_{zz} - I_{yy}\right) \tag{3.4}$$

$$M = \dot{Q}I_{yy} + PR\left(I_{xx} - I_{zz}\right) \tag{3.5}$$

$$N = \dot{R}I_{zz} + PQ\left(I_{yy} - I_{xx}\right) \tag{3.6}$$

where m is the aircraft mass and I_{xx}, I_{yy} and I_{zz} are the principle moments of inertia about the respective body axes. For a complete derivation of the above equations see Chapter 1 of [3]. The above equations make the following two simplifying assumptions,

- The aircraft is symmetrical about its XZ-plane. This implies that the cross products of inertia I_{xy} and I_{yz} are exactly zero. This is a very accurate assumption for all conventional aircraft.
- The cross product of inertia I_{xz} is negligibly small. This is most often the case for conventional aircraft.

Equations (3.1) to (3.6) relate the forces and moments that act on an aircraft to the time rate of change of its velocity coordinates (using Newton's second law). The various cross product terms on the right hand side of the equations that may appear unfamiliar arise because the force, moment, velocity and angular velocity vectors have been coordinated in body axes and not in inertial axes. Given the forces and moments that act on a body together with its mass and moment of inertia properties, equations (3.1) to (3.6) allow the linear and angular velocity to be propagated over time.

3.2 Kinematics

Kinematics is the field of mechanics that relates various motion variables, such as linear velocity, angular velocity, attitude and position, to each other over time. To this end, the position and angular position (more commonly referred to as attitude) coordinates/parameters commonly used in aircraft dynamics are defined below,

N, E, D:	Coordinates of the position vector in inertial axes
Φ, Θ, Ψ:	The Euler 3-2-1 attitude parameters of the body axis system with respect to inertial space

The position parameters are straightforward to understand. The attitude parameters however require more explanation. The following subsection addresses Euler 3-2-1 attitude parameterisation.

3.2.1 Euler 3-2-1 Attitude Parameterisation

Euler angles are commonly used to parameterise aircraft attitude because they are simple and intuitive to work with. Other means of parameterising attitude, such as Quaternions and DCM parameters do exist, but are less intuitive and more mathematically complex to work with. The major drawback with Euler angles is that they always result in a singularity in the attitude dynamics whereas Quaternions and DCM parameters avoid this singularity. However, for conventional flight, this singularity (at ±90 deg pitch angle for Euler 3-2-1 angles) never comes into play, thus explaining the popularity of Euler angles.

The philosophy behind Euler angles is to use three angles and a predefined order of rotation to describe the attitude of the body axis system (B) with respect to the inertial axis system (I). The Euler 3-2-1 sequence is the most commonly used. This sequence starts with the two axis systems aligned and then moves the body axis system through the following set of ordered rotations:

- Yaw the body axis system positively through the heading angle Ψ
- Pitch the body axis system positively through the pitch angle Θ
- Roll the body axis system positively through the roll angle Φ

The rotations are expressed graphically in Figure 5 below – the yaw rotation is shown on the right, the pitch rotation is shown on the left and the roll rotation is shown in the middle. Note that the roll rotation shown is not strictly correct since roll rotations take place relative to the *pitch plane*, which is not in general the horizon as shown.

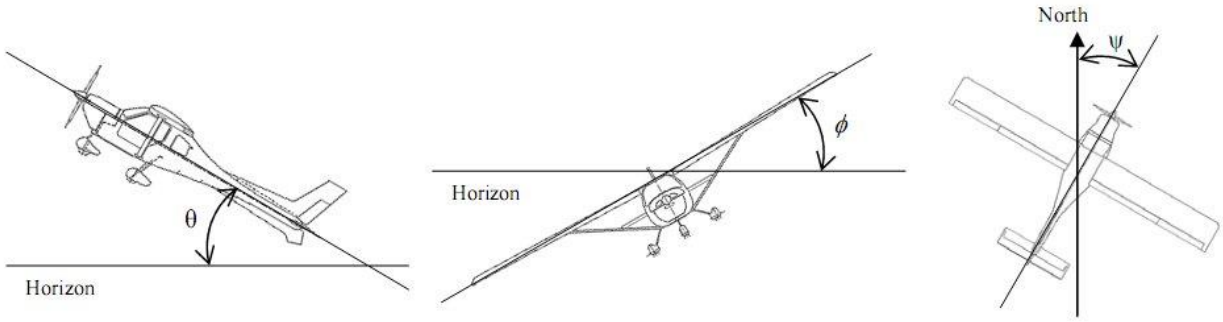

Figure 5 – Basic Illustration of Attitude Angles

The three Euler attitude parameters thus fully capture the attitude of the body axes relative to inertial axes.

3.2.2 Attitude Dynamics

Given the Euler attitude parameters above, the next step is to consider how the time rate of change of these parameters is related to other kinematic states. Intuitively, it is expected that the rate of change of attitude would be related in some way to the body angular rate coordinates of the aircraft (P, Q, R). With reference to the derivation on page 100 of [2], the Euler 3-2-1 attitude dynamics can be shown to be,

$$\begin{bmatrix} \dot{\Phi} \\ \dot{\Theta} \\ \dot{\Psi} \end{bmatrix} = \begin{bmatrix} 1 & \sin\Phi\tan\Theta & \cos\Phi\tan\Theta \\ 0 & \cos\Phi & -\sin\Phi \\ 0 & \sin\Phi\sec\Theta & \cos\Phi\sec\Theta \end{bmatrix} \begin{bmatrix} \mathrm{P} \\ \mathrm{Q} \\ \mathrm{R} \end{bmatrix} \qquad |\Theta| \neq \frac{\pi}{2} \tag{3.7}$$

The above equation describes how roll, pitch and yaw rates relate to time rates of changes of the roll, pitch and yaw angles. Note the singularity that occurs at ±90 deg pitch angles. At this orientation an ambiguity exists between roll and pitch angles which mathematically gives rise to the singularity. For conventional flight however, the pitch angle is far from ±90 deg at all times, thus allowing the singularity to be ignored.

3.2.3 Position Dynamics

All that remains is to derive the position dynamics i.e. how the north, east and down states change over time as a function of the aircraft's velocity. The straightforward kinematic relationship between position and velocity when both vectors are coordinated into inertial axes is shown below,

$$\begin{bmatrix} \dot{N} \\ \dot{E} \\ \dot{D} \end{bmatrix} = \begin{bmatrix} V_N \\ V_E \\ V_D \end{bmatrix} \tag{3.8}$$

where V_N, V_E and V_D are the north, east and down velocities respectively. However, the dynamics to this point have been derived as a function of the body axes velocity coordinates (U,V,W). Thus, if some means could be found to relate the coordinates of a vector in one axis system to the coordinates of the same vector in another axis system then the problem would be solved. Transformation matrices are capable of just this. Consider the single axis yaw rotation shown in Figure 6 below.

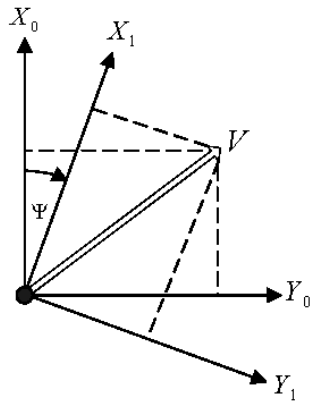

Figure 6 – Single Axis Yaw Rotation

Given the coordinates of vector $\boldsymbol{V}$ in the original axis system,

$$\mathbf{V_0} = \begin{bmatrix} x_0 \\ y_0 \\ z_0 \end{bmatrix} \tag{3.9}$$

then, through simple geometry it is straightforward to show that the coordinates of $\boldsymbol{V}$ in the rotated axis system are related to the coordinates of $\boldsymbol{V}$ in original axis system through the transformation matrix below,

$$\begin{bmatrix} x_1 \\ y_1 \\ z_1 \end{bmatrix} = \begin{bmatrix} \cos\Psi & \sin\Psi & 0 \\ -\sin\Psi & \cos\Psi & 0 \\ 0 & 0 & 1 \end{bmatrix} \begin{bmatrix} x_0 \\ y_0 \\ z_0 \end{bmatrix} \tag{3.10}$$

Similarly, the rotated axis system in Figure 6 could be rotated once more through the pitch angle to yield a transformation matrix of the form,

$$\begin{bmatrix} x_2 \\ y_2 \\ z_2 \end{bmatrix} = \begin{bmatrix} \cos\Theta & 0 & -\sin\Theta \\ 0 & 1 & 0 \\ \sin\Psi & 0 & \cos\Theta \end{bmatrix} \begin{bmatrix} x_1 \\ y_1 \\ z_1 \end{bmatrix} \tag{3.11}$$

And finally, the pitched axis system could be similarly rotated once more through the roll angle to yield a final transformation matrix of the form,

$$\begin{bmatrix} x_3 \\ y_3 \\ z_3 \end{bmatrix} = \begin{bmatrix} 1 & 0 & 0 \\ 0 & \cos\Phi & \sin\Phi \\ 0 & -\sin\Phi & \cos\Phi \end{bmatrix} \begin{bmatrix} x_2 \\ y_2 \\ z_2 \end{bmatrix} \tag{3.12}$$

Equations (3.10) to (3.12) can be multiplied together to relate the coordinates of vector $\boldsymbol{V}$ in the original axis system to the coordinates of the same vector in the axis system that has been yawed, pitched and rolled,

$$\begin{bmatrix} x_3 \\ y_3 \\ z_3 \end{bmatrix} = \begin{bmatrix} 1 & 0 & 0 \\ 0 & \cos\Phi & \sin\Phi \\ 0 & -\sin\Phi & \cos\Phi \end{bmatrix} \begin{bmatrix} \cos\Theta & 0 & -\sin\Theta \\ 0 & 1 & 0 \\ \sin\Psi & 0 & \cos\Theta \end{bmatrix} \begin{bmatrix} \cos\Psi & \sin\Psi & 0 \\ -\sin\Psi & \cos\Psi & 0 \\ 0 & 0 & 1 \end{bmatrix} \begin{bmatrix} x_0 \\ y_0 \\ z_0 \end{bmatrix} \tag{3.13}$$

This is of course exactly what is required to convert the coordinates of an inertially coordinated vectors to body axes and the transformation matrix shown below that performs the conversion is commonly referred to as the Direction Cosine Matrix (DCM),

$$\begin{bmatrix} x_B \\ y_B \\ z_B \end{bmatrix} = \begin{bmatrix} C_\Psi C_\Theta & S_\Psi C_\Theta & -S_\Theta \\ C_\Psi S_\Theta S_\Phi - S_\Psi C_\Phi & S_\Psi S_\Theta S_\Phi + C_\Psi C_\Phi & C_\Theta S_\Phi \\ C_\Psi S_\Theta C_\Phi + S_\Psi S_\Phi & S_\Psi S_\Theta C_\Phi - C_\Psi S_\Phi & C_\Theta C_\Phi \end{bmatrix} \begin{bmatrix} x_I \\ y_I \\ z_I \end{bmatrix} \qquad C_0 = \cos(\ ),\ S_0 = \sin(\ ) \tag{3.14}$$

For the position dynamics it was required however to be able to convert the body coordinates of the velocity vector to inertial coordinates. Thus the inverse of the DCM in equation (3.14) is required. It can be shown that the DCM is an orthogonal matrix and thus its inverse is simply its transpose. Thus,

$$\begin{bmatrix} V_N \\ V_E \\ V_D \end{bmatrix} = \begin{bmatrix} C_\Psi C_\Theta & C_\Psi S_\Theta S_\Phi - S_\Psi C_\Phi & C_\Psi S_\Theta C_\Phi + S_\Psi S_\Phi \\ S_\Psi C_\Theta & S_\Psi S_\Theta S_\Phi + C_\Psi C_\Phi & S_\Psi S_\Theta C_\Phi - C_\Psi S_\Phi \\ -S_\Theta & C_\Theta S_\Phi & C_\Theta C_\Phi \end{bmatrix} \begin{bmatrix} U \\ V \\ W \end{bmatrix} \qquad C_0 = \cos(\ ),\ S_0 = \sin(\ ) \tag{3.15}$$

And substituting into equation (3.8) the desired final result for the position dynamics is obtained,

$$\begin{bmatrix} \dot{N} \\ \dot{E} \\ \dot{D} \end{bmatrix} = \begin{bmatrix} C_\Psi C_\Theta & C_\Psi S_\Theta S_\Phi - S_\Psi C_\Phi & C_\Psi S_\Theta C_\Phi + S_\Psi S_\Phi \\ S_\Psi C_\Theta & S_\Psi S_\Theta S_\Phi + C_\Psi C_\Phi & S_\Psi S_\Theta C_\Phi - C_\Psi S_\Phi \\ -S_\Theta & C_\Theta S_\Phi & C_\Theta C_\Phi \end{bmatrix} \begin{bmatrix} U \\ V \\ W \end{bmatrix} \qquad C_0 = \cos(\ ),\ S_0 = \sin(\ ) \tag{3.16}$$

3.3 Summary

This section introduced the six degree of freedom equations of motion for a rigid body in their classic form. The equations of motion are summarised below for convenience. The only simplifying assumptions made in the dynamics are that the aircraft is symmetrical about the XZ-plane and that the cross product of inertia I_{xz} is zero.

$$X = m\left(\dot{U} - VR + WQ\right) \tag{3.17}$$

$$Y = m\left(\dot{V} + UR - WP\right) \tag{3.18}$$

$$Z = m\left(\dot{W} - UQ + VP\right) \tag{3.19}$$

$$L = \dot{P}I_{xx} + QR\left(I_{zz} - I_{yy}\right) \tag{3.20}$$

$$M = \dot{Q}I_{yy} + PR\left(I_{xx} - I_{zz}\right) \tag{3.21}$$

$$N = \dot{R}I_{zz} + PQ\left(I_{yy} - I_{xx}\right) \tag{3.22}$$

$$\begin{bmatrix} \dot{\Phi} \\ \dot{\Theta} \\ \dot{\Psi} \end{bmatrix} = \begin{bmatrix} 1 & \sin\Phi\tan\Theta & \cos\Phi\tan\Theta \\ 0 & \cos\Phi & -\sin\Phi \\ 0 & \sin\Phi\sec\Theta & \cos\Phi\sec\Theta \end{bmatrix} \begin{bmatrix} \mathrm{P} \\ \mathrm{Q} \\ \mathrm{R} \end{bmatrix} \qquad |\Theta| \neq \frac{\pi}{2} \tag{3.23}$$

$$\begin{bmatrix} \dot{N} \\ \dot{E} \\ \dot{D} \end{bmatrix} = \begin{bmatrix} C_\Psi C_\Theta & C_\Psi S_\Theta S_\Phi - S_\Psi C_\Phi & C_\Psi S_\Theta C_\Phi + S_\Psi S_\Phi \\ S_\Psi C_\Theta & S_\Psi S_\Theta S_\Phi + C_\Psi C_\Phi & S_\Psi S_\Theta C_\Phi - C_\Psi S_\Phi \\ -S_\Theta & C_\Theta S_\Phi & C_\Theta C_\Phi \end{bmatrix} \begin{bmatrix} U \\ V \\ W \end{bmatrix} \qquad C_0 = \cos(\ ),\ S_0 = \sin(\ ) \tag{3.24}$$

The 6DOF EOM are depicted graphically in Figure 7 below. The force and moment terms act as driving inputs to the dynamics. The kinetic equations of (3.17) to (3.22) relate these forces and moments to rates of change of the linear and angular velocity respectively. The kinematic equations of (3.23) and (3.24) in turn relate the linear and angular velocity to rates of change in attitude and position. Note that the equations of motion are applicable to any rigid body and thus, other that through justifying some of the assumptions made to this point, no aircraft specific dynamics have yet been modelled.

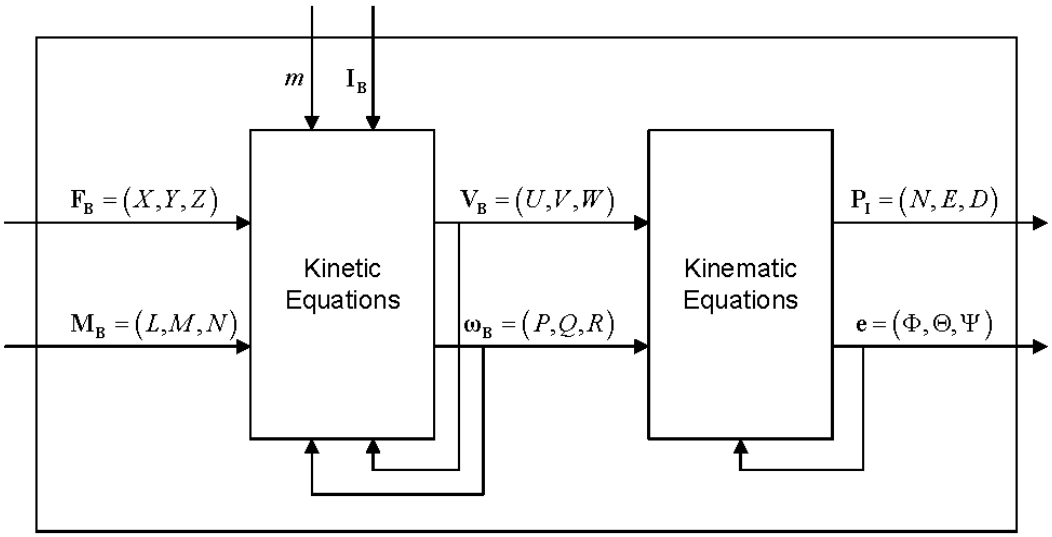

Figure 7 – Block Diagram Overview of 6DOF EOM

In the following section, the force and moment terms are expanded to model the forces and moments specifically produced by an aircraft.

4 Forces and Moments

With the general 6DOF EOM formulated, the focus shifts to determining the forces and moments that act on an aircraft as a function of its current state. For most aircraft there are 3 categories of forces and moments,

- Aerodynamic
- Thrust
- Gravitational

The total force and moment coordinates of the previous section can thus be expanded as follows,

$$X = X^A + X^T + X^G \tag{4.1}$$

$$Y = Y^A + Y^T + Y^G \tag{4.2}$$

$$Z = Z^A + Z^T + Z^G \tag{4.3}$$

$$L = L^A + L^T + L^G \tag{4.4}$$

$$M = M^A + M^T + M^G \tag{4.5}$$

$$N = N^A + N^T + N^G \tag{4.6}$$

where the superscripts A, T and G denote aerodynamic, thrust and gravitational force components respectively. The following subsections will address each of these categories in more detail.

4.1 Aerodynamic

The aerodynamic forces and moments are by far the most complex to model and introduce most of the uncertainty into the aircraft model. It can be shown from Bernoulli's equation and the Continuity principle for incompressible fluids (i.e. subsonic flight) [4] that aerodynamic forces and moments are proportional to the dynamic pressure experienced by the aircraft. The dynamic pressure (q) is defined below,

$$q = \frac{1}{2}\rho \bar{V}^2 \tag{4.7}$$

where ρ is the air density. Expanding the aerodynamic force and moment coordinates thus yields,

$$X^A = qSC_X \tag{4.8}$$

$$Y^A = qSC_Y \tag{4.9}$$

$$Z^A = qSC_Z \tag{4.10}$$

$$L^A = qSbC_l \tag{4.11}$$

$$M^A = qS\bar{c}C_m \tag{4.12}$$

$$N^A = qSbC_n \tag{4.13}$$

where S is the wing area, b is the wing span, $\bar{c}$ is the mean aerodynamic chord and $C_{(\cdot)}$ are the non-dimensional aerodynamic force and moment coefficients. These non-dimensional coefficients describe the aerodynamic properties of the specific airframe and are largely independent of the gross scale and flying speed of the aircraft (these factors have already been taken into account by the dynamic pressure and the scaling parameters). The coefficients are usually modelled in wind axes with the angle of sideslip assumed zero. Expanding the axial and normal force coefficients yields,

$$C_X = -C_D \cos\alpha + C_L \sin\alpha \tag{4.14}$$

$$C_Z = -C_L \cos\alpha - C_D \sin\alpha \tag{4.15}$$

where C_L and C_D are the lift and drag coefficients respectively. The remaining coefficients could also be transformed in a similar manner. However, with the angle of attack typically only a few degrees at most, the body and wind axis systems can be thought of as coinciding and thus the transformation tends only to unnecessarily complicate the results that follow. The transformation of equations (4.14) and (4.15) is necessary due to the large relative magnitude difference between the lift and drag coefficients that arises from typical aircraft lift to drag ratios (usually in excess of 10). Expanding the various coefficients for typical *subsonic, pre-stall* flight then yields,

$$C_D = C_{D_0} + \frac{C_L^2}{\pi A e} \tag{4.16}$$

$$C_y = C_{y_\beta}\beta + \frac{b}{2\bar{V}}C_{y_P}P + \frac{b}{2\bar{V}}C_{y_R}R + C_{y_{\delta_A}}\delta_A + C_{y_{\delta_R}}\delta_R \tag{4.17}$$

$$C_L = C_{L_0} + C_{L_\alpha}\alpha + \frac{\bar{c}}{2\bar{V}}C_{L_Q}Q + C_{L_{\delta_E}}\delta_E \tag{4.18}$$

$$C_l = C_{l_\beta}\beta + \frac{b}{2\bar{V}}C_{l_P}P + \frac{b}{2\bar{V}}C_{l_R}R + C_{l_{\delta_A}}\delta_A + C_{l_{\delta_R}}\delta_R \tag{4.19}$$

$$C_m = C_{m_0} + C_{m_\alpha}\alpha + \frac{\bar{c}}{2\bar{V}}C_{m_Q}Q + C_{m_{\delta_E}}\delta_E \tag{4.20}$$

$$C_n = C_{n_\beta}\beta + \frac{b}{2\bar{V}}C_{n_P}P + \frac{b}{2\bar{V}}C_{n_R}R + C_{n_{\delta_A}}\delta_A + C_{n_{\delta_R}}\delta_R \tag{4.21}$$

In the above equations, C_{D_0} is the parasitic drag coefficient, A the aspect ratio of the wing (ratio of its length to its breadth) and e the Oswald efficiency factor (typically between 0.8 and 0.95 for conventional subsonic aircraft). C_{L_0} and C_{m_0} are the static lift and pitching moment coefficients respectively. The terms of the form,

$$C_{A_B} \equiv \frac{\partial C_A}{\partial B'} \qquad (B' = nB \text{ where } n \text{ is the appropriate normalising coefficient of } B) \tag{4.22}$$

are the non-dimensional *stability and control derivatives*. The appropriate normalising coefficient for the incidence angles and the control deflection angles is 1 while for the pitch rate it is $\bar{c}/2\bar{V}$ and for the roll and yaw rates it is $b/2\bar{V}$.

Considering the model above, it is clear that the stability and control derivatives define the aerodynamic properties of a specific airframe. Thus the task of determining the aircraft aerodynamic model reduces to that of determining the various stability and control derivatives as well as the terms involved in the drag model. A number of methods exist with which to obtain these derivatives and are listed below,

- First principle methods based on empirical data
- Numerical methods of which there are a few categories
  - Basic vortex lattice codes such as Athena Vortex Lattice (AVL)
  - More complex panel codes such as C-marc
  - High fidelity Computational Fluid Dynamics (CFD) codes
- From wind tunnel data
- System Identification methods based on practical flight test data

First principle methods tend to provide a large amount of insight into the factors that contribute towards the various derivatives but typically however yield the least accurate results. Complex numerical method such as CFD tend to provide very good results but are often prohibitively expensive to use practically. Basic vortex lattice codes tend to provide a good compromise between complexity of use and accuracy of results for control system design purposes, especially for conventional autopilot designs. Wind tunnel data is also typically expensive to obtain but tends to yield very accurate results, especially for static derivatives. System identification techniques can yield accurate results but are complex to work with.

The following subsection provides insight into the physical origins and relative importance of the various derivatives.

4.1.1 Insight into Stability and Control Derivatives

The tables below provide insight into the stability and control derivatives used in the model of section 4.1. Before addressing the tables, it is important to understand the concept of induced angles of incidence.

4.1.1.1 Induced angles of incidence

Consider the airfoil shown in Figure 8 below.

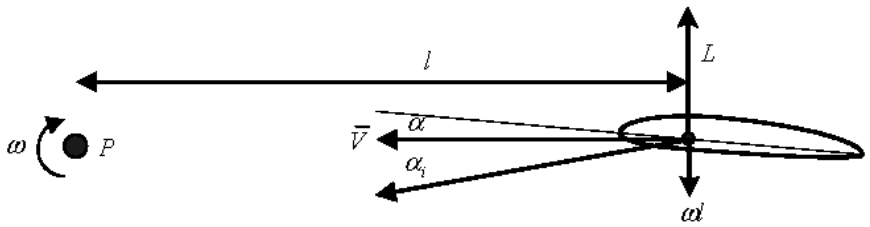

Figure 8 – Airfoil Illustrating Induced Angles of Incidence

The airfoil moves with a velocity $\bar{V}$ through the air-mass and experiences an angle of incidence α due to its physical orientation relative to the oncoming airflow. Ignoring any inherent lift due to airfoil camber or control surface deflections, the total lift force on the airfoil will be,

$$L = \frac{1}{2}\rho \bar{V}^2 S C_{L_\alpha} \alpha \tag{4.23}$$

Consider now the effect if the airfoil were to be rotated about point P, a distance l from the airfoil neutral point, with angular velocity ω. The local velocity vector at the airfoil would be the vector sum of the translational velocity $\bar{V}$ and the local tangential velocity ωl. Thus the *local* angle of attack would be increased by,

$$\alpha_i = \tan^{-1}\left(\frac{\omega l}{\bar{V}}\right) \approx \frac{\omega l}{\bar{V}} \tag{4.24}$$

referred to as an *induced angle of incidence*. The total lift can thus be written as follows,

$$\begin{aligned} L &= \frac{1}{2}\rho \bar{V}^2 S C_{L_\alpha} \left(\alpha + \alpha_i\right) \\ &= \frac{1}{2}\rho \bar{V}^2 S C_{L_\alpha} \left(\alpha + \frac{\omega l}{\bar{V}}\right) \\ &= qS\left(\left[C_{L_\alpha}\right]\alpha + \frac{l}{2\bar{V}}\left[2C_{L_\alpha}\right]\omega\right) \end{aligned} \tag{4.25}$$

Comparing equations (4.25) to equations (4.17) to (4.21), it should be clear that induced angles of incidence are the origin of all angular rate derivatives, as will be discussed in the tables of the following subsection.

4.1.1.2 Insight Tables

The tables below provide insight into the physical origins of the stability and control derivatives. Most of the information comes from Chapter 13 of [1].

DRAG DERIVATIVES	
C_{D_0}	Parasitic drag coefficient. Quantifies the aircraft's skin friction drag that is independent of the aircraft's angle of attack.
e	The Oswald efficiency factor. An empirically determined constant used in induced drag calculations. A typical value for this constant is 0.85.

LIFT DERIVATIVES	
C_{L_0}	Static lift coefficient. Quantifies the lift produced by the aircraft as a whole at zero angle of attack. This lift is due primarily to camber on the main wing but is also influenced by factors such as body shape. This coefficient strongly influences the angle of attack required to trim the aircraft.
C_{L_α}	The aircraft's lift curve slope. It quantifies the increase in lift coefficient as a function of angle of attack. This derivative has a theoretical maximum of 2π. It is one of the fundamental aircraft modelling parameters and is can be quite accurately obtained using either empirical or numerical methods.
C_{L_Q}	Quantifies the lift produced by the aircraft due to pitch rate motions. The lift produced is primarily as a result of the induced angle of incidence experienced by the tail-plane during pitch rate motions. The derivative can be quite accurately calculated using empirical or numerical methods. However, it typically has little to no significance on the aircraft dynamics.
$C_{L_{\delta_E}}$	Quantifies the lift force produced by elevator deflections. Few empirical methods exist to determine this control derivative and as such numerical methods are usually made use of. However, it is often has a negligible effect on the aircraft dynamics.

PITCHING MOMENT DERIVATIVES	
C_{m_0}	Static pitching moment coefficient. Quantifies the pitching moment produced by the aircraft as a whole at zero angle of attack. This static pitching moment is due primarily to the camber of the main wing, the setting angle of the tail-plane and the shape of the aircraft's fuselage. This coefficient strongly influences the elevator required to trim the aircraft during straight and level flight.
C_{m_α}	This very important parameter, often referred to as the pitch stiffness coefficient quantifies the degree of static stability of the aircraft. This is the aircraft's tendency to return towards its trim condition when perturbed in angle of attack. A negative coefficient implies a statically stable aircraft, while a positive coefficient implies a statically unstable aircraft. This coefficient is dependent on the distance between the aircraft's centre of mass and its neutral point (the point where the total angle of attack based aerodynamic force acts). Although empirical and numerical methods exist for determining the location of the neutral point, the accuracy is often questionable. Thus, for aircraft that are designed to be stable, a measure of safety margin is usually included by shifting the centre of mass forwards by an appropriate amount.
C_{m_Q}	Also, known as the *pitch damping* coefficient, quantifies the pitching moment produced by the aircraft due to pitch rate motions. This coefficient is related to the lift due to pitch rate coefficient through the normalised length to the tail-plane. The derivative can be quite accurately calculated using empirical or numerical methods and plays and important role in the aircraft dynamics.
$C_{m_{\delta_E}}$	Quantifies the pitching moment produced by elevator deflections. Few empirical methods exist to determine this important control derivative and as such numerical methods are usually made use of. The derivative directly influences eventual controller gains.

SIDE FORCE DERIVATIVES	
C_{y_β}	The side force due to sideslip derivative is contributed towards by the lateral lift of the fuselage and the angle of incidence on the fin during sideslip manoeuvres.
C_{y_P}	This derivative describes the side force produced due to roll rate perturbations. Due to the symmetry and streamlined nature of aircraft this derivative is most often negligibly small and thus has little influence on the aircraft dynamics.
C_{y_R}	Quantifies the side force produced by the aircraft due to yaw rate motions. The side force produced is primarily a result of the induced angle of incidence experienced by the fin during yaw rate motions. The derivative can be quite accurately calculated using empirical or numerical methods. However, it typically has very little significance on the aircraft dynamics.
$C_{y_{\delta_A}}$	Quantifies the side force produced by aileron deflections. Due to the orientation of the ailerons, this derivatives is usually very close to zero and has a negligible effect on the aircraft dynamics.
$C_{y_{\delta_R}}$	Quantifies the side force produced due to a rudder deflection. Few empirical methods exist to determine this control derivative and as such numerical methods are usually used to determine it. Its effect is usually quite small on the aircraft dynamics.

ROLL MOMENT DERIVATIVES	
C_{l_β}	This important lateral derivative describes the tendency of the aircraft to return towards wings level flight during sideslip motions. A large number of factors contribute towards the sign and magnitude of the derivative. Wing dihedral provides a stabilising effect by inducing a net differential angle of incidence across the wings during sideslip. Wing sweepback also provides s stabilising effect through airflow velocity induced differential lift across the wings. A high fin also makes stabilising contributions through the side force produced during sideslip. Finally, a high wing tends to have a stabilising effect due to the airflow pattern around the fuselage during sideslip. Because of the many factors that contribute towards the derivative, it is often very difficult to obtain accurately.
C_{l_P}	Also, known as the *roll damping* coefficient, this important derivative quantifies the roll moment produced by the aircraft due to roll rate motions. The coefficient is dominated by the differentially induced angle of incidence across the wing during roll rate motions. The induced angle of incidence on the fin also contribute towards the derivative although its effect is typically negligible. The derivative can be quite accurately calculated using empirical or numerical methods and plays and important role in the aircraft dynamics.
C_{l_R}	Quantifies the roll moment produced through yaw rate perturbations. The derivative is dominated by the differential lift induced across the wings during yaw rate perturbations and the above roll axis force on the fin induced through yaw rate motions. The derivative is an important one in describing the coupling between the roll and directional dynamics.
$C_{l_{\delta_A}}$	Quantifies the roll moment produced by aileron deflections. The important control derivative is usually obtained using numerical methods.
$C_{l_{\delta_R}}$	Quantifies the roll moment produced by rudder deflections. A typical high fin will produce an adverse roll moment. Numerical methods are usually made use of to determine this derivative.

YAW MOMENT DERIVATIVES	
C_{n_β}	This important lateral derivative describes the natural tendency of the aircraft to *weathercock* back into the airflow. It quantifies the degree of directional static stability of the aircraft, with a positive coefficient implying stability. The restoring moment is dominated by the angle of incidence induced force at the fin during sideslip manoeuvres. The derivative can be modelled well using both empirical and numerical methods.
C_{n_P}	Quantifies the yaw moment produced by roll rate perturbations. The major effect of roll rate is to induce differential lift across the wings. This differential lift is associated with a differential drag which in turn produces a yaw moment. This derivative couples the roll and directional modes of motion of the aircraft.
C_{n_R}	Also, known as the *yaw damping* coefficient, this important derivative quantifies the yaw moment produced by the aircraft due to yaw rate motions. This coefficient is contributed towards by induced angles of incidence on the fin and differential drag (due to local velocity perturbations) across the wings during yaw rate motions. The derivative can be quite accurately calculated using empirical or numerical methods and plays and important role in the aircraft dynamics.
$C_{n_{\delta_A}}$	Quantifies the *adverse yaw* moment produced as a result of an aileron deflection. Aileron deflections produce differential lift and thus differential drag across the wings. This differential drag produces a yaw moment that tends to yaw the nose of the aircraft into the opposite direction to that desired at the onset of a turn.
$C_{n_{\delta_R}}$	Quantifies the yaw moment due to rudder deflection. This control derivative is related to the side force due to rudder derivative through the normalised length to the fin. Numerical methods are usually made use of to determine this derivative.

4.2 Thrust

Although many complex propulsion models for the various types of aircraft engines exist, a simple first order lag model tends to suffice for most UAV applications. The first order lag model adequately captures the significantly band-limited nature of most propulsion sources and is provided below,

$$\dot{T} = -\frac{1}{\tau}T + \frac{1}{\tau}T_c \tag{4.26}$$

where T is the thrust magnitude, T_c the thrust command and τ the engine lag time constant. Assuming that the thrust vector lies along the body axes x-axis, then the following thrust model holds,

$$X^T = T \ , \ Y^T = Z^T = 0 \tag{4.27}$$

$$L^T = M^T = N^T = 0 \tag{4.28}$$

4.3 Gravitational

In a flat earth NED axis system, the gravitational acceleration vector is adequately modelled as providing a force equivalent to the aircraft's mass in the down direction. In inertial axes, the corresponding gravitational force coordinate vector is thus,

$$\mathbf{F}_{\mathbf{I}}^{\mathbf{G}} = \begin{bmatrix} 0 \\ 0 \\ mg \end{bmatrix} \tag{4.29}$$

Transforming this coordinate vector to body axes coordinates using the DCM of equation (3.14) yields the desired result,

$$\begin{bmatrix} X^G \\ Y^G \\ Z^G \end{bmatrix} = \begin{bmatrix} C_\Psi C_\Theta & S_\Psi C_\Theta & -S_\Theta \\ C_\Psi S_\Theta S_\Phi - S_\Psi C_\Phi & S_\Psi S_\Theta S_\Phi + C_\Psi C_\Phi & C_\Theta S_\Phi \\ C_\Psi S_\Theta C_\Phi + S_\Psi S_\Phi & S_\Psi S_\Theta C_\Phi - C_\Psi S_\Phi & C_\Theta C_\Phi \end{bmatrix} \begin{bmatrix} 0 \\ 0 \\ mg \end{bmatrix} = \begin{bmatrix} -\sin\Theta \\ \cos\Theta\sin\Phi \\ \cos\Theta\cos\Phi \end{bmatrix} mg \tag{4.30}$$

Finally, because in a uniform gravitational field the centre of gravity coincides with the centre of mass, the gravitational force produces no moment on the aircraft. Thus,

$$L^G = M^G = N^G = 0 \tag{4.31}$$

4.4 Summary

With the various components of the force and moment model derived, the aircraft model is completed as shown in Figure 9 below. On the right hand side is the six degree of freedom equations of motion block that models the dynamics of any rigid body given the forces and moments that act on it. On the left hand side is the force and moment block with the three categories of forces and moments that drive into the 6DOF block. The aircraft states feed back to the force and moment block which in turn determines the future of the states. The four control inputs (thrust command, aileron, elevator and rudder) are all that a pilot or control system has at its disposal to make the entire system behave as desired!

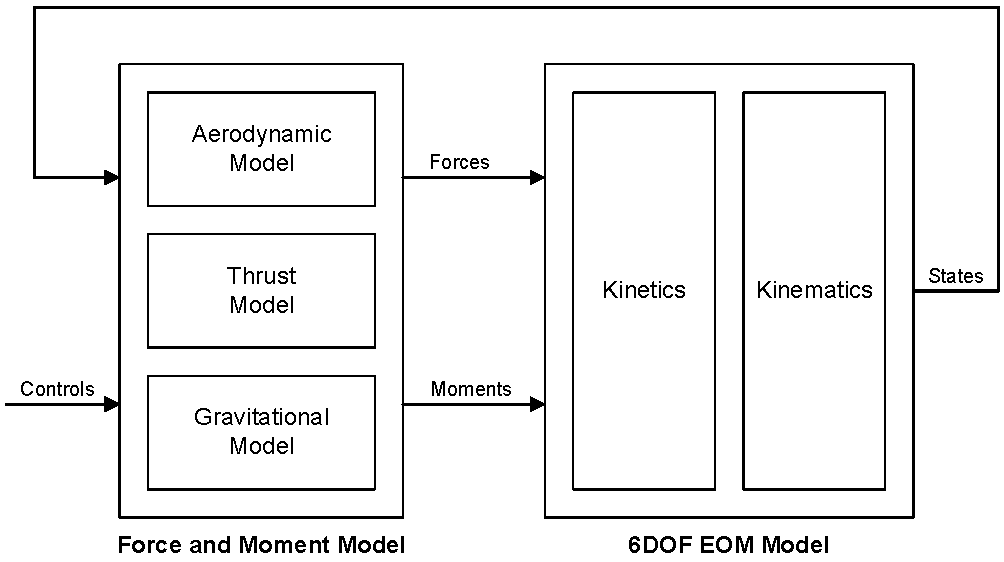

Figure 9 – Aircraft Model Block Diagram

5 Linearising the Aircraft Dynamics

The full nonlinear aircraft dynamics are useful for accurate simulation purposes but are difficult to deal with for control system design purposes. In their current form they provide very little insight into the aircraft dynamics and make determining stability and performance of a closed loop system difficult. We thus move to linearise the dynamics about a level flight trim condition so that we can make use of the many analysis and design tools available in the field of linear systems theory.

5.1 Defining and Calculating Trim Condition Variables

Although technically, the aircraft dynamics can be linearised about any equilibrium trajectory, the most common and useful of these trajectories is *straight and level flight*. During this static equilibrium flight condition, all force and moment coordinates on the aircraft must be exactly zero. Because the aircraft is symmetrical about its XZ-plane, and the trim condition is for symmetric (wings level) flight, all lateral motion and control variables $(V, P, R, \Phi, \delta_A, \delta_R)_T$ (where the subscript T means *at trim*) are exactly zero. Thus, the trim problem reduces to 2 dimensions, requiring the solution of $(U, W, Q, \Theta, \delta_E, T)_T$ or equivalently, $(\bar{V}, \alpha, Q, \Theta, \delta_E, T)_T$. Note that the variables $(\Psi, D)_T$ have been left out of the trim calculations since they can be set arbitrarily and the variables (N, E) are merely a consequence of the chosen and calculated trim variables.

Consider the trim force and moment diagram in Figure 10 below,

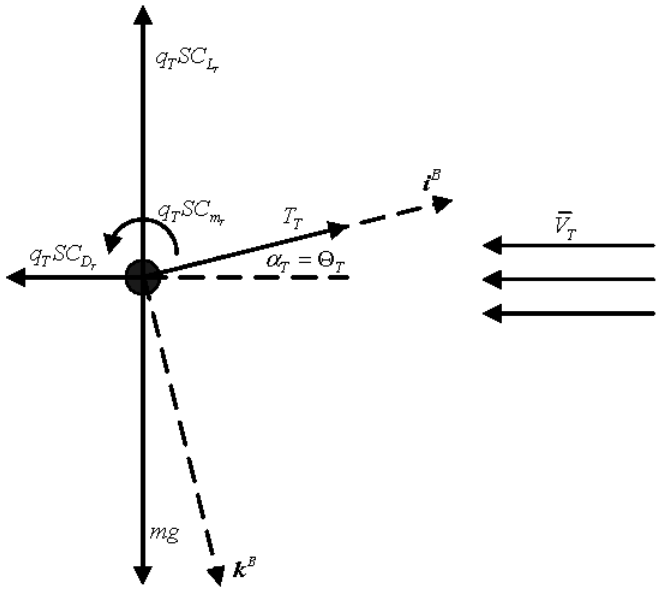

Figure 10 – Trim Force and Moment Diagram

In the above diagram,

$$q_T = \frac{1}{2}\rho \bar{V}_T^2 \tag{5.1}$$

and note that for straight and level flight trim,

$$\Theta_T = \alpha_T \tag{5.2}$$

It is common to specify the desired trim velocity $\bar{V}_T$, and thus q_T is known for a specific air density i.e. trim altitude. Considering the remaining longitudinal variables, equation (5.2) and the fact that for straight and level flight the pitch

rate at trim must be zero, the trim problem reduces to that of calculating $(\alpha, \delta_E, T)_T$. These three trim variables can be solved for using the three trim equations generated by balancing the forces along the x- and z-axes and the pitching moment about the centre of mass.

With reference to Figure 10 or equivalently equations (4.1), (4.3) and (4.5) with the appropriate substitutions, the forces in the body x- and z-axis directions and the pitching moment are constrained as follows at trim,

$$\left(-q_T S C_{D_T} \cos\alpha_T + q_T S C_{L_T} \sin\alpha_T\right) + T_T - mg\sin\Theta_T = 0 \tag{5.3}$$

$$\left(-qSC_{L_T} \cos\alpha_T - q_T S C_{D_T} \sin\alpha_T\right) + mg\cos\Theta_T = 0 \tag{5.4}$$

$$q_T S\bar{c} C_{m_T} = 0 \tag{5.5}$$

To solve the above simultaneous equations for the three variables of interest without making any simplifying assumptions requires the use of iterative numerical methods. However, by making two assumptions that hold well, a closed form solution for the trim states can be found. The assumptions are,

- The trim angle of attack (and thus pitch angle) is small
- The lift is an order of magnitude greater than the drag at trim

The above assumptions allow equations (5.4) and (5.5) to be simplified as follows,

$$-q_T S C_{L_T} + mg = 0 \tag{5.6}$$

$$q_T S\bar{c} C_{m_T} = 0 \tag{5.7}$$

Substituting for the lift and pitching moment coefficients from equations (4.18) and (4.20), and rearranging yields,

$$\begin{bmatrix} C_{L_0} \\ C_{m_0} \end{bmatrix} + \begin{bmatrix} C_{L_\alpha} & C_{L_{\delta_E}} \\ C_{m_\alpha} & C_{m_{\delta_E}} \end{bmatrix} \begin{bmatrix} \alpha_T \\ \delta_{E_T} \end{bmatrix} = \begin{bmatrix} \dfrac{mg}{q_T S} \\ 0 \end{bmatrix} \tag{5.8}$$

Changing the subject of the above formula, allows the trim angle of attack and trim elevator setting to be solved for,

$$\begin{bmatrix} \alpha_T \\ \delta_{E_T} \end{bmatrix} = \begin{bmatrix} C_{L_\alpha} & C_{L_{\delta_E}} \\ C_{m_\alpha} & C_{m_{\delta_E}} \end{bmatrix}^{-1} \begin{bmatrix} \dfrac{mg}{q_T S} - C_{L_0} \\ -C_{m_0} \end{bmatrix} \tag{5.9}$$

Substituting the result back into equation (5.3) allows the trim thrust to be solved for as follows,

$$T_T = q_T S C_{D_T} \cos\alpha_T - q_T S C_{L_T} \sin\alpha_T + mg\sin\alpha_T \tag{5.10}$$

where,

$$C_{D_T} = C_{D_0} + \frac{C_{L_T}^2}{\pi A e} \tag{5.11}$$

5.2 Linearising About Trim

With the trim condition defined and the trim variables calculated, the process of linearising the aircraft dynamics about trim can begin. To this end, equations (3.17) to (3.22) are rewritten below with the state derivatives on the left hand side and the roll and pitch angle dynamics from equation (3.23) are simply restated below,

$$\dot{U} = \frac{X}{m} + VR - WQ \tag{5.12}$$

$$\dot{V} = \frac{Y}{m} - UR + WP \tag{5.13}$$

$$\dot{W} = \frac{Z}{m} + UQ - VP \tag{5.14}$$

$$\dot{P} = \frac{L}{I_{xx}} - QR\frac{I_{zz} - I_{yy}}{I_{xx}} \tag{5.15}$$

$$\dot{Q} = \frac{M}{I_{yy}} - PR\frac{I_{xx} - I_{zz}}{I_{yy}} \tag{5.16}$$

$$\dot{R} = \frac{N}{I_{zz}} - PQ\frac{I_{yy} - I_{xx}}{I_{zz}} \tag{5.17}$$

$$\dot{\Phi} = P + Q\sin\Phi\tan\Theta + R\cos\Phi\tan\Theta \tag{5.18}$$

$$\dot{\Theta} = Q\cos\Phi - R\sin\Phi \tag{5.19}$$

All of the listed states form a coupled set of differential equations and thus constitute the primary dynamics of the aircraft. The dynamics governing the states Ψ, N, E and D are left out of the linearization process because they don't re-couple back into the above dynamics and thus don't form part of the fundamental aircraft dynamics. They are simply kinematic results of the primary aircraft dynamics states above. The dynamics of equations (5.12) to (5.19) can be displayed more concisely in the nonlinear state space form below,

$$\dot{\mathbf{x}} = \mathbf{f}\left(\mathbf{x}, \mathbf{u}\right) \tag{5.20}$$

where,

$$\mathbf{x} = \begin{bmatrix} U & V & W & P & Q & R & \Phi & \Theta \end{bmatrix}^T \tag{5.21}$$

$$\mathbf{u} = \begin{bmatrix} \delta_A & \delta_E & \delta_R & T \end{bmatrix}^T \tag{5.22}$$

and $\mathbf{f}$ is the vector function representing the respective dynamic equations. Now, writing each state and control as the sum of a trim value and a perturbation about trim yields,

$$\mathbf{x} = \mathbf{x}_T + \Delta\mathbf{x} \tag{5.23}$$

$$\mathbf{u} = \mathbf{u}_T + \Delta\mathbf{u} \tag{5.24}$$

where,

$$\Delta\mathbf{x} = \begin{bmatrix} u & v & w & p & q & r & \phi & \theta \end{bmatrix}^T \tag{5.25}$$

$$\Delta\mathbf{u} = \begin{bmatrix} \delta_a & \delta_e & \delta_r & \Delta T \end{bmatrix}^T \tag{5.26}$$

Expanding equation (5.20) in a Taylor series about the trim condition yields,

$$\dot{\mathbf{x}}_T + \Delta\dot{\mathbf{x}} = \mathbf{f}\left(\mathbf{x}_T + \Delta\mathbf{x}, \mathbf{u}_T + \Delta\mathbf{u}\right) = \mathbf{f}\left(\mathbf{x}_T, \mathbf{u}_T\right) + \left.\frac{\partial\mathbf{f}}{\partial\mathbf{x}}\right|_T \Delta\mathbf{x} + \left.\frac{\partial\mathbf{f}}{\partial\mathbf{u}}\right|_T \Delta\mathbf{u} + h.o.t. \tag{5.27}$$

Assuming that the deviations from trim are small, the higher order terms in the above equation can be ignored and the dynamics approximated by the linearised sensitivities about trim,

$$\Delta\dot{\mathbf{x}} \approx \mathbf{A_T}\Delta\mathbf{x} + \mathbf{B_T}\Delta\mathbf{u} \tag{5.28}$$

where,

$$\mathbf{A_T} = \left.\frac{\partial \mathbf{f}}{\partial \mathbf{x}}\right|_T \tag{5.29}$$

$$\mathbf{B_T} = \left.\frac{\partial \mathbf{f}}{\partial \mathbf{u}}\right|_T \tag{5.30}$$

and it has been noted that at the trim condition,

$$\dot{\mathbf{x}}_T = \mathbf{f}\left(\mathbf{x}_T, \mathbf{u}_T\right) = \mathbf{0} \tag{5.31}$$

The linearization problem thus becomes one of determining the vector partial derivatives of equations (5.29) and (5.30). Before this is done however, one commonly made assumption is employed to simplify the mathematics to follow.

5.2.1 Decoupling the Linear Dynamics

Write the state and control vectors as follows,

$$\mathbf{\Delta x} = \begin{bmatrix} \mathbf{\Delta x}_{Long} & \mathbf{\Delta x}_{Lat} \end{bmatrix}^T \tag{5.32}$$

$$\mathbf{\Delta u} = \begin{bmatrix} \mathbf{\Delta u}_{Long} & \mathbf{\Delta u}_{Lat} \end{bmatrix}^T \tag{5.33}$$

where,

$$\mathbf{\Delta x}_{Long} = \begin{bmatrix} u & w & q & \theta \end{bmatrix}^T \tag{5.34}$$

$$\mathbf{\Delta x}_{Lat} = \begin{bmatrix} v & p & r & \phi \end{bmatrix}^T \tag{5.35}$$

$$\mathbf{\Delta u}_{Long} = \begin{bmatrix} \delta_e & \Delta T \end{bmatrix}^T \tag{5.36}$$

$$\mathbf{\Delta u}_{Lat} = \begin{bmatrix} \delta_a & \delta_r \end{bmatrix}^T \tag{5.37}$$

so that the dynamics of equation (5.28) become,

$$\begin{bmatrix} \mathbf{\Delta \dot{x}}_{Long} \\ \mathbf{\Delta \dot{x}}_{Lat} \end{bmatrix} = \begin{bmatrix} \mathbf{A}_{\mathbf{T}_{11}} & \mathbf{A}_{\mathbf{T}_{12}} \\ \mathbf{A}_{\mathbf{T}_{21}} & \mathbf{A}_{\mathbf{T}_{22}} \end{bmatrix} \begin{bmatrix} \mathbf{\Delta x}_{Long} \\ \mathbf{\Delta x}_{Lat} \end{bmatrix} + \begin{bmatrix} \mathbf{B}_{\mathbf{T}_{11}} & \mathbf{B}_{\mathbf{T}_{12}} \\ \mathbf{B}_{\mathbf{T}_{21}} & \mathbf{B}_{\mathbf{T}_{22}} \end{bmatrix} \begin{bmatrix} \mathbf{\Delta u}_{Long} \\ \mathbf{\Delta u}_{Lat} \end{bmatrix} \tag{5.38}$$

Now, because aircraft are symmetrical about their XZ-plane, the following terms in the above dynamics will be exactly zero,

$$\mathbf{A}_{\mathbf{T}_{21}} = \mathbf{0} \tag{5.39}$$

$$\mathbf{B}_{\mathbf{T}_{21}} = \mathbf{0} \tag{5.40}$$

Furthermore, if the deviations from trim (particularly the roll angle) are small as required by the linearization assumption, then to a good approximation,

$$\mathbf{A}_{\mathbf{T}_{12}} \approx \mathbf{0} \tag{5.41}$$

$$\mathbf{B}_{\mathbf{T}_{12}} \approx \mathbf{0} \tag{5.42}$$

This assumption allows the linearised dynamics to be decoupled into *longitudinal* and *lateral* dynamics as shown below,

$$\mathbf{\Delta \dot{x}}_{Long} = \mathbf{A}_{\mathbf{T}_{11}} \mathbf{\Delta x}_{Long} + \mathbf{B}_{\mathbf{T}_{11}} \mathbf{\Delta u}_{Long} \tag{5.43}$$

$$\mathbf{\Delta \dot{x}}_{Lat} = \mathbf{A}_{\mathbf{T}_{22}} \mathbf{\Delta x}_{Lat} + \mathbf{B}_{\mathbf{T}_{22}} \mathbf{\Delta u}_{Lat} \tag{5.44}$$

The total linearization problem is now reduced to determining the partial derivatives that form the system and control matrices of the two decoupled linear systems above.

5.2.2 Linearising the Longitudinal Dynamics

From equation (5.43) the longitudinal dynamics are,

$$\Delta\dot{\mathbf{x}}_{Long} = \mathbf{A}_{\mathbf{T}_{11}}\Delta\mathbf{x}_{Long} + \mathbf{B}_{\mathbf{T}_{11}}\Delta\mathbf{u}_{Long} \tag{5.45}$$

which when expanded are,

$$\begin{bmatrix} \dot{u} \\ \dot{w} \\ \dot{q} \\ \dot{\theta} \end{bmatrix} = \begin{bmatrix} \frac{\partial \dot{U}}{\partial U} & \frac{\partial \dot{U}}{\partial W} & \frac{\partial \dot{U}}{\partial Q} & \frac{\partial \dot{U}}{\partial \Theta} \\ \frac{\partial \dot{W}}{\partial U} & \frac{\partial \dot{W}}{\partial W} & \frac{\partial \dot{W}}{\partial Q} & \frac{\partial \dot{W}}{\partial \Theta} \\ \frac{\partial \dot{Q}}{\partial U} & \frac{\partial \dot{Q}}{\partial W} & \frac{\partial \dot{Q}}{\partial Q} & \frac{\partial \dot{Q}}{\partial \Theta} \\ \frac{\partial \dot{\Theta}}{\partial U} & \frac{\partial \dot{\Theta}}{\partial W} & \frac{\partial \dot{\Theta}}{\partial Q} & \frac{\partial \dot{\Theta}}{\partial \Theta} \end{bmatrix} \begin{bmatrix} u \\ w \\ q \\ \theta \end{bmatrix} + \begin{bmatrix} \frac{\partial \dot{U}}{\partial \delta_E} & \frac{\partial \dot{U}}{\partial T} \\ \frac{\partial \dot{W}}{\partial \delta_E} & \frac{\partial \dot{W}}{\partial T} \\ \frac{\partial \dot{Q}}{\partial \delta_E} & \frac{\partial \dot{Q}}{\partial T} \\ \frac{\partial \dot{\Theta}}{\partial \delta_E} & \frac{\partial \dot{\Theta}}{\partial T} \end{bmatrix} \begin{bmatrix} \delta_e \\ \Delta T \end{bmatrix} \tag{5.46}$$

It is common to work with velocity magnitude and angle of attack perturbations $(\bar{v}, \alpha)$ in the state vector instead of axial and normal velocity perturbations (u, w) as are currently used. Considering equations (2.1) and (2.3), the following approximations can be made for the straight and level flight trim condition given that the angle of attack is small,

$$\bar{V} = \sqrt{U^2 + V^2 + W^2} \approx \sqrt{U^2} = U \tag{5.47}$$

$$W \approx U\alpha = (U_T + u)\alpha \approx U_T\alpha \approx V_T\alpha \tag{5.48}$$

Thus,

$$\dot{\bar{V}} \approx \dot{U} \tag{5.49}$$

$$\dot{W} \approx V_T\dot{\alpha} \tag{5.50}$$

Equation (5.46) can thus be written as follows,

$$\begin{bmatrix} \dot{\bar{v}} \\ \bar{V}_T\dot{\alpha} \\ \dot{q} \\ \dot{\theta} \end{bmatrix} = \begin{bmatrix} \frac{\partial \dot{U}}{\partial U} & \frac{\partial \dot{U}}{\partial W} & \frac{\partial \dot{U}}{\partial Q} & \frac{\partial \dot{U}}{\partial \Theta} \\ \frac{\partial \dot{W}}{\partial U} & \frac{\partial \dot{W}}{\partial W} & \frac{\partial \dot{W}}{\partial Q} & \frac{\partial \dot{W}}{\partial \Theta} \\ \frac{\partial \dot{Q}}{\partial U} & \frac{\partial \dot{Q}}{\partial W} & \frac{\partial \dot{Q}}{\partial Q} & \frac{\partial \dot{Q}}{\partial \Theta} \\ \frac{\partial \dot{\Theta}}{\partial U} & \frac{\partial \dot{\Theta}}{\partial W} & \frac{\partial \dot{\Theta}}{\partial Q} & \frac{\partial \dot{\Theta}}{\partial \Theta} \end{bmatrix} \begin{bmatrix} \dot{\bar{v}} \\ \bar{V}_T\alpha \\ q \\ \theta \end{bmatrix} + \begin{bmatrix} \frac{\partial \dot{U}}{\partial \delta_E} & \frac{\partial \dot{U}}{\partial T} \\ \frac{\partial \dot{W}}{\partial \delta_E} & \frac{\partial \dot{W}}{\partial T} \\ \frac{\partial \dot{Q}}{\partial \delta_E} & \frac{\partial \dot{Q}}{\partial T} \\ \frac{\partial \dot{\Theta}}{\partial \delta_E} & \frac{\partial \dot{\Theta}}{\partial T} \end{bmatrix} \begin{bmatrix} \delta_e \\ \Delta T \end{bmatrix} \tag{5.51}$$

So,

$$\begin{bmatrix}\dot{\bar{v}}\\ \dot{\alpha}\\ \dot{q}\\ \dot{\theta}\end{bmatrix}=\begin{bmatrix}\frac{\partial\dot{U}}{\partial U} & \bar{V}_T\frac{\partial\dot{U}}{\partial W} & \frac{\partial\dot{U}}{\partial Q} & \frac{\partial\dot{U}}{\partial\Theta}\\ \frac{1}{\bar{V}_T}\frac{\partial\dot{W}}{\partial U} & \frac{\partial\dot{W}}{\partial W} & \frac{1}{\bar{V}_T}\frac{\partial\dot{W}}{\partial Q} & \frac{1}{\bar{V}_T}\frac{\partial\dot{W}}{\partial\Theta}\\ \frac{\partial\dot{Q}}{\partial U} & \bar{V}_T\frac{\partial\dot{Q}}{\partial W} & \frac{\partial\dot{Q}}{\partial Q} & \frac{\partial\dot{Q}}{\partial\Theta}\\ \frac{\partial\dot{\Theta}}{\partial U} & \bar{V}_T\frac{\partial\dot{\Theta}}{\partial W} & \frac{\partial\dot{\Theta}}{\partial Q} & \frac{\partial\dot{\Theta}}{\partial\Theta}\end{bmatrix}\begin{bmatrix}\dot{\bar{v}}\\ \alpha\\ q\\ \theta\end{bmatrix}+\begin{bmatrix}\frac{\partial\dot{U}}{\partial\delta_E} & \frac{\partial\dot{U}}{\partial T}\\ \frac{1}{\bar{V}_T}\frac{\partial\dot{W}}{\partial\delta_E} & \frac{1}{\bar{V}_T}\frac{\partial\dot{W}}{\partial T}\\ \frac{\partial\dot{Q}}{\partial\delta_E} & \frac{\partial\dot{Q}}{\partial T}\\ \frac{\partial\dot{\Theta}}{\partial\delta_E} & \frac{\partial\dot{\Theta}}{\partial T}\end{bmatrix}\begin{bmatrix}\delta_e\\ \Delta T\end{bmatrix} \tag{5.52}$$

Finally, all of the above partial derivatives can be calculated by beginning with equations (5.12) to (5.19), performing the partial derivatives, and making use of the force and moment models of section 4. This lengthy process is not shown in the notes and only the end result is provided below,

$$\begin{bmatrix}\dot{\bar{v}}\\ \dot{\alpha}\\ \dot{q}\\ \dot{\theta}\end{bmatrix}=\begin{bmatrix}\frac{\rho V_T S C_{X_T}}{m} & \frac{q_T S}{m}\left(C_{L_\alpha}\alpha_T+C_{L_T}-\frac{2C_{L_T}C_{L_\alpha}}{\pi Ae}\right) & 0 & -g\cos\Theta_T\\ -\frac{\rho S C_{L_T}}{m} & -\frac{q_T S}{m\bar{V}_T}C_{L_\alpha} & 1-\frac{q_T S}{m\bar{V}_T}\frac{\bar{c}}{2\bar{V}_T}C_{L_Q} & -\frac{g}{\bar{V}_T}\sin\Theta_T\\ 0 & \frac{q_T S\bar{c}}{I_{yy}}C_{m_\alpha} & \frac{q_T S\bar{c}}{I_{yy}}\frac{\bar{c}}{2\bar{V}_T}C_{m_Q} & 0\\ 0 & 0 & 1 & 0\end{bmatrix}\begin{bmatrix}\dot{\bar{v}}\\ \alpha\\ q\\ \theta\end{bmatrix}+\begin{bmatrix}0 & \frac{1}{m}\\ -\frac{q_T S}{m\bar{V}_T}C_{L_{\delta_E}} & 0\\ \frac{q_T S\bar{c}}{I_{yy}}C_{m_{\delta_E}} & 0\\ 0 & 0\end{bmatrix}\begin{bmatrix}\delta_e\\ \Delta T\end{bmatrix} \tag{5.53}$$

Note that the some simplifying assumptions have been used in obtaining the above result. For more details on exactly how the terms in the above equation are obtained, see Chapter 4 of [2].

5.2.3 Linearising the Lateral Dynamics

From equation (5.44) the lateral dynamics are,

$$\Delta\dot{\mathbf{x}}_{Lat}=\mathbf{A}_{\mathbf{T}_{22}}\Delta\mathbf{x}_{Lat}+\mathbf{B}_{\mathbf{T}_{22}}\Delta\mathbf{u}_{Lat} \tag{5.54}$$

which when expanded are,

$$\begin{bmatrix}\dot{v}\\ \dot{p}\\ \dot{r}\\ \dot{\phi}\end{bmatrix}=\begin{bmatrix}\frac{\partial\dot{V}}{\partial V} & \frac{\partial\dot{V}}{\partial P} & \frac{\partial\dot{V}}{\partial R} & \frac{\partial\dot{V}}{\partial\Phi}\\ \frac{\partial\dot{P}}{\partial V} & \frac{\partial\dot{P}}{\partial P} & \frac{\partial\dot{P}}{\partial R} & \frac{\partial\dot{P}}{\partial\Phi}\\ \frac{\partial\dot{R}}{\partial V} & \frac{\partial\dot{R}}{\partial P} & \frac{\partial\dot{R}}{\partial R} & \frac{\partial\dot{R}}{\partial\Phi}\\ \frac{\partial\dot{\Phi}}{\partial V} & \frac{\partial\dot{\Phi}}{\partial P} & \frac{\partial\dot{\Phi}}{\partial R} & \frac{\partial\dot{\Phi}}{\partial\Phi}\end{bmatrix}\begin{bmatrix}v\\ p\\ r\\ \phi\end{bmatrix}+\begin{bmatrix}\frac{\partial\dot{V}}{\partial\delta_A} & \frac{\partial\dot{V}}{\partial\delta_R}\\ \frac{\partial\dot{P}}{\partial\delta_A} & \frac{\partial\dot{P}}{\partial\delta_R}\\ \frac{\partial\dot{R}}{\partial\delta_A} & \frac{\partial\dot{R}}{\partial\delta_R}\\ \frac{\partial\dot{\Phi}}{\partial\delta_A} & \frac{\partial\dot{\Phi}}{\partial\delta_R}\end{bmatrix}\begin{bmatrix}\delta_a\\ \delta_r\end{bmatrix} \tag{5.55}$$

It is common to work with angle of sideslip perturbations (β) instead of lateral velocity perturbations (v) as are used above. Considering equation (2.3), the following approximation can be made for a straight and level flight trim condition given that the angle of sideslip is small,

$$V=\bar{V}\sin\beta\approx\bar{V}\beta=\left(\bar{V}_T+\bar{v}\right)\beta\approx\bar{V}_T\beta \tag{5.56}$$

Thus,

$$\dot{V} \approx \bar{V}_T \dot{\beta} \tag{5.57}$$

Equation (5.55) can thus be written as follows,

$$\begin{bmatrix} V_T\dot{\beta} \\ \dot{p} \\ \dot{r} \\ \dot{\phi} \end{bmatrix} = \begin{bmatrix} \frac{\partial \dot{V}}{\partial V} & \frac{\partial \dot{V}}{\partial P} & \frac{\partial \dot{V}}{\partial R} & \frac{\partial \dot{V}}{\partial \Phi} \\ \frac{\partial \dot{P}}{\partial V} & \frac{\partial \dot{P}}{\partial P} & \frac{\partial \dot{P}}{\partial R} & \frac{\partial \dot{P}}{\partial \Phi} \\ \frac{\partial \dot{R}}{\partial V} & \frac{\partial \dot{R}}{\partial P} & \frac{\partial \dot{R}}{\partial R} & \frac{\partial \dot{R}}{\partial \Phi} \\ \frac{\partial \dot{\Phi}}{\partial V} & \frac{\partial \dot{\Phi}}{\partial P} & \frac{\partial \dot{\Phi}}{\partial R} & \frac{\partial \dot{\Phi}}{\partial \Phi} \end{bmatrix} \begin{bmatrix} V_T\beta \\ p \\ r \\ \phi \end{bmatrix} + \begin{bmatrix} \frac{\partial \dot{V}}{\partial \delta_A} & \frac{\partial \dot{V}}{\partial \delta_R} \\ \frac{\partial \dot{P}}{\partial \delta_A} & \frac{\partial \dot{P}}{\partial \delta_R} \\ \frac{\partial \dot{R}}{\partial \delta_A} & \frac{\partial \dot{R}}{\partial \delta_R} \\ \frac{\partial \dot{\Phi}}{\partial \delta_A} & \frac{\partial \dot{\Phi}}{\partial \delta_R} \end{bmatrix} \begin{bmatrix} \delta_a \\ \delta_r \end{bmatrix} \tag{5.58}$$

So,

$$\begin{bmatrix} \dot{\beta} \\ \dot{p} \\ \dot{r} \\ \dot{\phi} \end{bmatrix} = \begin{bmatrix} \frac{\partial \dot{V}}{\partial V} & \frac{1}{\bar{V}_T}\frac{\partial \dot{V}}{\partial P} & \frac{1}{\bar{V}_T}\frac{\partial \dot{V}}{\partial R} & \frac{1}{\bar{V}_T}\frac{\partial \dot{V}}{\partial \Phi} \\ \bar{V}_T\frac{\partial \dot{P}}{\partial V} & \frac{\partial \dot{P}}{\partial P} & \frac{\partial \dot{P}}{\partial R} & \frac{\partial \dot{P}}{\partial \Phi} \\ \bar{V}_T\frac{\partial \dot{R}}{\partial V} & \frac{\partial \dot{R}}{\partial P} & \frac{\partial \dot{R}}{\partial R} & \frac{\partial \dot{R}}{\partial \Phi} \\ \bar{V}_T\frac{\partial \dot{\Phi}}{\partial V} & \frac{\partial \dot{\Phi}}{\partial P} & \frac{\partial \dot{\Phi}}{\partial R} & \frac{\partial \dot{\Phi}}{\partial \Phi} \end{bmatrix} \begin{bmatrix} \beta \\ p \\ r \\ \phi \end{bmatrix} + \begin{bmatrix} \frac{1}{\bar{V}_T}\frac{\partial \dot{V}}{\partial \delta_A} & \frac{1}{\bar{V}_T}\frac{\partial \dot{V}}{\partial \delta_R} \\ \frac{\partial \dot{P}}{\partial \delta_A} & \frac{\partial \dot{P}}{\partial \delta_R} \\ \frac{\partial \dot{R}}{\partial \delta_A} & \frac{\partial \dot{R}}{\partial \delta_R} \\ \frac{\partial \dot{\Phi}}{\partial \delta_A} & \frac{\partial \dot{\Phi}}{\partial \delta_R} \end{bmatrix} \begin{bmatrix} \delta_a \\ \delta_r \end{bmatrix} \tag{5.59}$$

Finally, all of the above partial derivatives can be calculated by beginning with equations (5.12) to (5.19), performing the partial derivatives, and making use of the force and moment models of section 4. This lengthy process is not shown in the notes and only the end result is provided below,

$$\begin{bmatrix} \dot{\beta} \\ \dot{p} \\ \dot{r} \\ \dot{\phi} \end{bmatrix} = \begin{bmatrix} \frac{q_T S}{m\bar{V}_T}C_{y_\beta} & \frac{q_T S}{m\bar{V}_T}\frac{b}{2\bar{V}_T}C_{y_P} & \frac{q_T S}{m\bar{V}_T}C_{y_R} - 1 & \frac{g}{\bar{V}_T}\cos\Theta_T \\ \frac{q_T Sb}{I_{xx}}C_{l_\beta} & \frac{q_T Sb}{I_{xx}}\frac{b}{2\bar{V}_T}C_{l_P} & \frac{q_T Sb}{I_{xx}}\frac{b}{2\bar{V}_T}C_{l_R} & 0 \\ \frac{q_T Sb}{I_{zz}}C_{n_\beta} & \frac{q_T Sb}{I_{zz}}\frac{b}{2\bar{V}_T}C_{n_P} & \frac{q_T Sb}{I_{zz}}\frac{b}{2\bar{V}_T}C_{n_R} & 0 \\ 0 & 1 & \tan\Theta_T & 0 \end{bmatrix} \begin{bmatrix} \beta \\ p \\ r \\ \phi \end{bmatrix} + \begin{bmatrix} \frac{q_T S}{m\bar{V}_T}C_{y_{\delta_A}} & \frac{q_T S}{m\bar{V}_T}C_{y_{\delta_R}} \\ \frac{q_T Sb}{I_{xx}}C_{l_{\delta_A}} & \frac{q_T Sb}{I_{xx}}C_{l_{\delta_R}} \\ \frac{q_T Sb}{I_{zz}}C_{n_{\delta_A}} & \frac{q_T Sb}{I_{zz}}C_{n_{\delta_R}} \\ 0 & 0 \end{bmatrix} \begin{bmatrix} \delta_a \\ \delta_r \end{bmatrix} \tag{5.60}$$

For more details on exactly how the terms in the above equation are obtained, see Chapter 4 of [2].

5.3 Summary

This section investigated the linearization of the nonlinear aircraft dynamics about a straight and level flight trim condition. It began by investigating the straight and level flight trim condition further and derived the following equations that allow the remaining trim variables to be calculated,

$$\begin{bmatrix} \alpha_T \\ \delta_{E_T} \end{bmatrix} = \begin{bmatrix} C_{L_\alpha} & C_{L_{\delta_E}} \\ C_{m_\alpha} & C_{m_{\delta_E}} \end{bmatrix}^{-1} \begin{bmatrix} \frac{mg}{q_T S} - C_{L_0} \\ -C_{m_0} \end{bmatrix} \tag{5.61}$$

$$T_T = q_T S C_{D_T}\cos\alpha_T - q_T S C_{L_T}\sin\alpha_T + mg\sin\alpha_T \tag{5.62}$$

The equations of motion were then linearised and decoupled about the trim condition to yield the following two linear models,

$$\begin{bmatrix} \dot{\bar{v}} \\ \dot{\alpha} \\ \dot{q} \\ \dot{\theta} \end{bmatrix} = \begin{bmatrix} \frac{\rho V_T S C_{X_T}}{m} & \frac{q_T S}{m}\left(C_{L_\alpha}\alpha_T + C_{L_T} - \frac{2C_{L_T}C_{L_\alpha}}{\pi A e} \right) & 0 & -g\cos\Theta_T \\ -\frac{\rho S C_{L_T}}{m} & -\frac{q_T S}{m\bar{V}_T} C_{L_\alpha} & 1 - \frac{q_T S}{m\bar{V}_T}\frac{\bar{c}}{2\bar{V}_T} C_{L_Q} & -\frac{g}{\bar{V}_T}\sin\Theta_T \\ 0 & \frac{q_T S\bar{c}}{I_{yy}} C_{m_\alpha} & \frac{q_T S\bar{c}}{I_{yy}}\frac{\bar{c}}{2\bar{V}_T} C_{m_Q} & 0 \\ 0 & 0 & 1 & 0 \end{bmatrix} \begin{bmatrix} \dot{\bar{v}} \\ \alpha \\ q \\ \theta \end{bmatrix} + \begin{bmatrix} 0 & \frac{1}{m} \\ -\frac{q_T S}{m\bar{V}_T} C_{L_{\delta_E}} & 0 \\ \frac{q_T S\bar{c}}{I_{yy}} C_{m_{\delta_E}} & 0 \\ 0 & 0 \end{bmatrix} \begin{bmatrix} \delta_e \\ \Delta T \end{bmatrix} \tag{5.63}$$

$$\begin{bmatrix} \dot{\beta} \\ \dot{p} \\ \dot{r} \\ \dot{\phi} \end{bmatrix} = \begin{bmatrix} \frac{q_T S}{m\bar{V}_T} C_{y_\beta} & \frac{q_T S}{m\bar{V}_T}\frac{b}{2\bar{V}_T} C_{y_P} & \frac{q_T S}{m\bar{V}_T} C_{y_R} - 1 & \frac{g}{\bar{V}_T}\cos\Theta_T \\ \frac{q_T Sb}{I_{xx}} C_{l_\beta} & \frac{q_T Sb}{I_{xx}}\frac{b}{2\bar{V}_T} C_{l_P} & \frac{q_T Sb}{I_{xx}}\frac{b}{2\bar{V}_T} C_{l_R} & 0 \\ \frac{q_T Sb}{I_{zz}} C_{n_\beta} & \frac{q_T Sb}{I_{zz}}\frac{b}{2\bar{V}_T} C_{n_P} & \frac{q_T Sb}{I_{zz}}\frac{b}{2\bar{V}_T} C_{n_R} & 0 \\ 0 & 1 & \tan\Theta_T & 0 \end{bmatrix} \begin{bmatrix} \beta \\ p \\ r \\ \phi \end{bmatrix} + \begin{bmatrix} \frac{q_T S}{m\bar{V}_T} C_{y_{\delta_A}} & \frac{q_T S}{m\bar{V}_T} C_{y_{\delta_R}} \\ \frac{q_T Sb}{I_{xx}} C_{l_{\delta_A}} & \frac{q_T Sb}{I_{xx}} C_{l_{\delta_R}} \\ \frac{q_T Sb}{I_{zz}} C_{n_{\delta_A}} & \frac{q_T Sb}{I_{zz}} C_{n_{\delta_R}} \\ 0 & 0 \end{bmatrix} \begin{bmatrix} \delta_a \\ \delta_r \end{bmatrix} \tag{5.64}$$

In the next section, standard tools from linear systems theory are used to investigate the natural longitudinal and lateral dynamics of the aircraft.

6 Analysis of the Linearised Dynamics

In the previous section, the nonlinear aircraft model was linearised and decoupled about a level flight trim condition. This process resulted in the linear longitudinal and lateral dynamics. This section focuses on the analysis of these dynamics and presents insight into the aircraft's natural *modes of motion*. It also seeks to provide an understanding of the physical origins of the various modes of motion as well as provide insight as to which stability derivatives most dominantly influence the different modes. This level of insight is ultimately required for proper control system design.

To proceed with the analysis, a small part of linear systems theory is revisited in the subsection that follows to allow the reader to understand how the natural modes of motion of a dynamic system are obtained.

6.1 Determining the Natural Modes of Motion of a System

The reader will recall that the motion of a linear system is governed by the *poles* of the system. Often in linear systems analysis, the type of motion corresponding to a particular pole e.g. oscillating, decaying exponential, is referred to as a *mode of motion*. Thus, when we refer to obtaining the natural modes of motion of a system it is equivalent to us determining the open loop poles of a system. To this end, consider a state space system of the following form,

$$\dot{\mathbf{x}} = \mathbf{A}\mathbf{x} + \mathbf{B}\mathbf{u} \tag{6.1}$$

$$\mathbf{y} = \mathbf{C}\mathbf{x} \tag{6.2}$$

Note that both the longitudinal and lateral models of the previous section take on the form of equation (6.1). Equation (6.2) is referred to as an output equation, where the $\mathbf{C}$ matrix is set to extract the desired output state. Taking the Laplace transform of both equations yields,

$$s\mathbf{X}(s) = \mathbf{A}\mathbf{X}(s) + \mathbf{B}\mathbf{U}(s) \tag{6.3}$$

$$\mathbf{Y}(s) = \mathbf{C}\mathbf{X}(s) \tag{6.4}$$

Rearranging equation (6.3) and substituting for $\mathbf{X}(s)$ into equation (6.4) yields the transfer function,

$$\frac{\mathbf{Y}(s)}{\mathbf{U}(s)} = \mathbf{C}\left(s\mathbf{I} - \mathbf{A}\right)^{-1}\mathbf{B} = \frac{\mathbf{C}\text{adj}\left(s\mathbf{I} - \mathbf{A}\right)\mathbf{B}}{\det\left(s\mathbf{I} - \mathbf{A}\right)} \tag{6.5}$$

The poles of the system are where the transfer function goes to infinity, and are thus seen to be the values of s that satisfy the characteristic equation,

$$\det\left(s\mathbf{I} - \mathbf{A}\right) = 0 \tag{6.6}$$

However, this equation is the standard equation used in linear algebra to calculate the *eigenvalues* (in this case values of s) of a matrix $\mathbf{A}$. The poles of a system are thus seen to simply be the eigenvalues of the system matrix $\mathbf{A}$ and thus standard numerical routines, such as eig.m in MATLAB, can be used to obtain the poles of a system. Given the ability now to obtain the poles or natural modes of motion of a state space system, the following two sections investigate the classic natural modes for the longitudinal and lateral systems derived in section 5.

6.2 Longitudinal Modes of Motion

The poles of the longitudinal system can be obtained using equation (6.6) with the system matrix taken from equation (5.63). Figure 11 below provides a pole plot of the typical result of such a calculation.

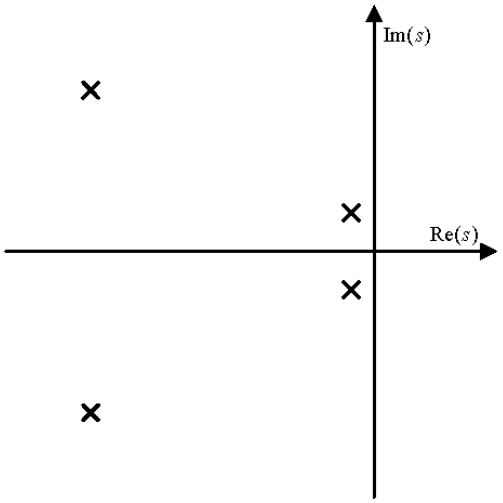

Figure 11 – Typical Longitudinal Poles

The figure illustrates that there are two complex pole pairs that typically govern the longitudinal modes of motion of an aircraft. These two classic modes of motion are discussed in the subsections that follow.

6.2.1 Short Period Mode

The higher frequency complex pole pair in Figure 11 is referred to as the *Short Period Mode*. For typical small to medium scale UAVs (2m to 5m wingspans), this mode of motion has a natural frequency between 3 and 10 rad/s and a good damping ratio of usually greater than 0.5. The mode describes the aircraft's tendency to realign itself with the velocity vector when disturbed. Consider the aircraft flying trimmed for straight and level flight. Now consider the effect of a small disturbance that instantaneously changes the aircraft's angle of attack. For statically stable aircraft, the restoring pitching moment, quantified by C_{m_α}, will cause the aircraft to rotate back towards its trim flight condition. The damping induced from the associated pitch rate motion, quantified by C_{m_Q}, will remove energy from the system and thus result in a stable mode of motion. For pure short period mode motions, the aircraft can thus be thought of as constrained to move only about its y-axis with aerodynamic spring and damping torques that tend to realign the aircraft with the oncoming airflow.

6.2.2 Phugoid Mode

The lower frequency complex pole pair in Figure 11 is referred to as the *Phugoid Mode*. Note that Figure 11 is not drawn to scale and this mode tends to have a natural frequency of less than 0.5 rad/s and poor damping. It is also not uncommon for the mode to be unstable. The Phugoid Mode is a largely kinematic mode of motion and describes the exchange of potential and kinetic energy when the aircraft is disturbed from trimmed flight. Consider an aircraft flying straight and level that experiences a sudden velocity magnitude perturbation. The extra airspeed results in extra lift which will cause the aircraft to pitch up and climb. As the aircraft gains potential energy, it looses kinetic energy and the speed correspondingly reduces. This in turn decreases the lift and the aircraft begins to pitch downwards and loose altitude. The process continues to repeat itself with the motion typically damped by the energy removed through aerodynamic drag.

6.3 Lateral Modes of Motion

The poles of the lateral system can be obtained using equation (6.6) with the system matrix taken from equation (5.64). Figure 12 below provides a pole plot of the typical result of such a calculation.

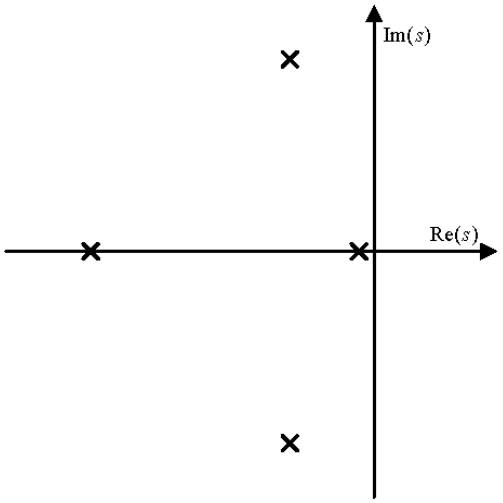

Figure 12 – Typical Lateral Poles

The figure illustrates the two real poles and a complex pole pair that typically govern the lateral dynamics of an aircraft. These three classic modes of motion are discussed in the subsections that follow.

6.3.1 Roll Mode

The higher frequency real pole in Figure 12 is referred to as the *Roll Mode*. For typical small to medium sized UAVs this mode of motion is between 5 and 15 rad/s. The mode describes the roll rate dynamics of an aircraft. When an aircraft experiences a roll moment disturbance, the roll rate will initially start to grow with the integral of the moment disturbance. However, the wing provides a natural roll damping, quantified by C_{l_p}, through the induced angles of incidence across its surface during roll rate perturbations. The damping roll moment will eventually build up to counter the roll moment disturbance and leave the aircraft moving at a constant roll rate. The typical speed of the Roll mode pole indicates that the associated dynamic response is very fast and the aircraft appears to always operate at constant roll rates when disturbance or control moments are applied about the roll axis e.g. aileron commands almost immediately set up a constant roll rate on the aircraft.

6.3.2 Dutch Roll Mode

The complex pole pair in Figure 12 is referred to as the *Dutch Roll Mode*. For most aircraft this mode of motion is of a similar frequency to the Short Period Mode frequency. However, it is typically very poorly naturally damped. The Dutch Roll Mode is almost the directional equivalent of the Short Period Mode. It describes the tendency of the aircraft to align itself with the oncoming airflow when disturbed laterally i.e. with a sideslip angle. Consider an aircraft operating about trim with a small sideslip perturbation. The fin will create a restoring yaw moment, quantified by C_{n_β}, to move the nose of the aircraft back into the wind. The associated yaw rate, quantified by C_{n_R}, will provide damping during the motion. The aircraft will thus potentially oscillate back towards its stable trim condition. However, an additional complication that arises with the Dutch Roll Mode that is not present in the Short Period Mode is the fact that the wing is also moved backwards and forwards through the air during the yaw rate motion. The differential velocity experienced by the wing will result in differential lift and drag, quantified at least partially by C_{l_R} and C_{n_R} respectively. The differential lift will result in roll rate perturbations which in turn will cause differential lift and drag perturbations through C_{l_p} and C_{n_p}. The differential drag perturbations will serve to damp the yaw rate motions further. The net effect is that the aircraft oscillates in both yaw and roll and when viewed from the back, along the x-axis, tends to trace out ellipses in the sky.

6.3.3 Spiral Mode

The lower frequency pole in Figure 11 is referred to as the *Spiral Mode*. Note that Figure 12 is not drawn to scale and this mode tends to have a very low natural frequency. It is also very common for the mode to be slightly unstable. Like the Phugoid Mode, the Spiral Mode is a largely kinematic mode of motion and describes the tendency of the aircraft to restore itself to wings level flight or diverge from wings level flight when laterally disturbed i.e. in roll angle. Consider

an aircraft disturbed in roll angle from straight an level trim flight. Any sideslip induced by the turn will tend to either worsen or relieve the roll angle disturbance depending on the sign of C_{l_β}. It should be remembered from section 4 that factors such as dihedral, wing sweep, high/low wing and high/low fin all contribute towards the sign of C_{l_β}. The roll angle will also start to induce a turn and thus create differential lift across the wings, quantified by C_{l_R}, which will tend to amplify the roll disturbance. Thus, it can be seen that the a number of factors play a role in determining the exact frequency and stability of the Spiral Mode.

6.4 Summary

This section investigated the natural modes of motion of conventional aircraft. It was seen that longitudinally the following modes typically exist,

- Short Period Mode
- Phugoid Mode

and laterally, the following modes typically exist,

- Roll Mode
- Dutch Roll Mode
- Spiral Mode

A brief explanation yielding physical insight into the various modes was provided.

7 Classic Control Systems for Aircraft

The purpose of this section is to provide a brief overview of the classic types of controllers used on aircraft. These controllers are typically designed based on the linearised aircraft dynamics derived in section 5 and analysed in section 6. As such, the control system overview will be divided into longitudinal and lateral controllers.

7.1 Longitudinal Controllers

Classic longitudinal aircraft controllers adopt a successive loop closure approach, where feedback control loop after feedback control loop is closed, with each loop abstracting the aircraft further from the outer loop. This type of control strategy tends to work well in practice and often yields simple, easy to tune controllers. The subsections that follow describe the typical controllers encountered, from the inside (fastest) loops to the outside (slowest) loops.

7.1.1 Pitch Rate Damper

In section 6.2.1 the Short Period Mode was discussed. There is was seen that this mode of motion typically has a high frequency and is adequately damped. However, to provide further damping with respect to inertial space it is customary to design a pitch rate damper. As shown in Figure 13 this type of controller feeds pitch rate back to elevator. It has the effect of artificially increasing the aircraft's natural pitch damping and thus tends to increase the damping of the short period mode. The pitch rate measurement is usually obtained directly from a pitch rate gyroscope. This control loop is largely for wind gust disturbance rejection purposes. Note that the aircraft continues to present the elevator as a control input for the next control loop.

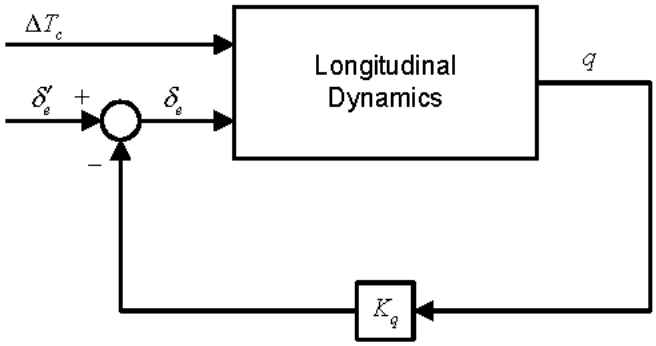

Figure 13 – Pitch Rate Damper

7.1.2 Airspeed and Climb Rate Controller

With the pitch rate damper in place, the next controller to be implemented is the Multiple-Input-Multiple-Output (MIMO) airspeed and climb rate controller. As shown in Figure 14, this controller makes use of the elevator and thrust actuators to control the airspeed and climb rate of the aircraft. The tight coupling between the airspeed and climb rate dynamics usually forces pure MIMO controller design techniques to be used. Linear Quadratic Regulator (LQR) theory is often used for this purpose. Integrator states are usually appended to the errors in airspeed and climb rate to ensure unity DC gain of the closed loop system. The airspeed and climb rate are either obtained from an estimator or can be directly measured through differential pressure and the differentiation of absolute pressure. Note that the climb rate output equations can be shown to be,

$$\dot{h} = -\dot{D} = U_T\theta - w \tag{7.1}$$

by linearising and decoupling the down velocity from equation (3.24).

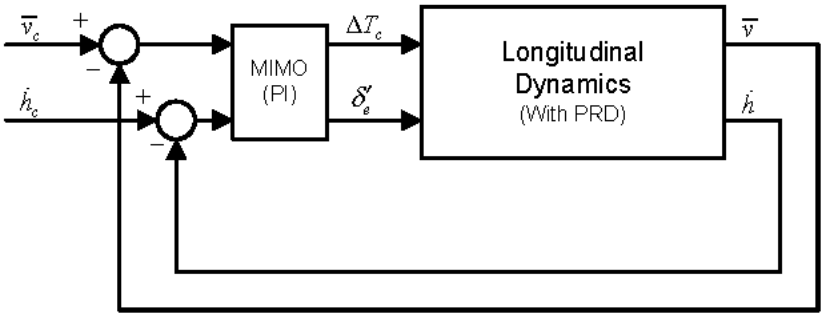

Figure 14 – Airspeed and Climb Rate Controller

7.1.3 Altitude Controller

With the airspeed and climb rate controller in place a final altitude control loop can be implemented as shown in Figure 15 below. The controller interfaces directly with the climb rate command of the airspeed and climb rate controllers. This has the effect of commanding a positive climb rate when the aircraft is below its desired altitude and a negative climb rate when the aircraft is above its altitude. The altitude is typically obtained from either barometric pressure, GPS or some type of relative sensor such as an ultrasonic range finder or radio altimeter.

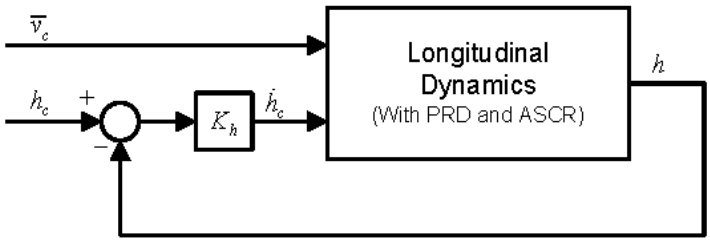

Figure 15 – Altitude Controller

7.2 Lateral Controllers

Classical lateral controllers also tend to adopt a successive loop closure control architecture. The subsections that follow discuss these classic controllers from the inside (fastest) loops to the outside (slowest) loops.

7.2.1 Dutch Roll Damper

It was seen in section 6.3.2 that the Dutch Roll Mode is typically lightly damped. The purpose of the Dutch Roll damper is to add artificial damping to this mode of motion and as such stop the natural elliptical motion of the tail when disturbed. In its simplest form, the Dutch Roll damper feeds yaw rate back to the rudder actuator. The yaw rate is typically obtained directly from a yaw rate gyroscope. This feedback has the effect of adding artificial yaw damping to the aircraft which would be sufficient if not for one drawback. When the aircraft turns it will experience constant yaw rates as the heading changes over time. Direct feedback of yaw rate for Dutch Roll damping would thus result in the rudder attempting to fight constant turns of the aircraft. This is of course undesirable and the problem is overcome by adapting the controller as shown in Figure 16. There it is seen that the yaw rate signal is first fed through a high pass (or washout) filter before being multiplied by the feedback gain and fed to the rudder. This has the effect of providing damping when high frequency yaw rate perturbations are experienced while at the same time providing no feedback in the steady state such as during constant turns. The filter cut-off frequency needs to be carefully chosen so as to allow Dutch Roll Mode motions to pass through while at the same time sufficiently blocking steady state yaw rates.

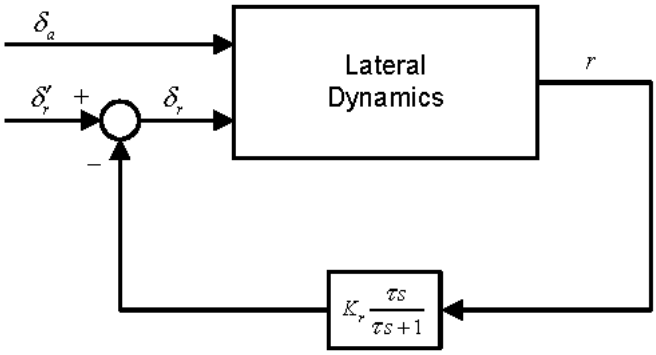

Figure 16 – Dutch Roll Damper

7.2.2 Roll Angle Controller

With the Dutch Roll damper in place, the next classic lateral controller is the roll angle controller. As shown in Figure 17 below, this controller makes use of the ailerons to regulate the roll angle of the aircraft. Roll angle is notoriously difficult to obtain on a dynamic platform and is one of the main reasons complex estimation algorithms are required on UAVs. However, assuming that a roll angle is available for feedback, a Proportional-Integral (PI) type controller is usually designed to regulate the roll angle with zero steady state error.

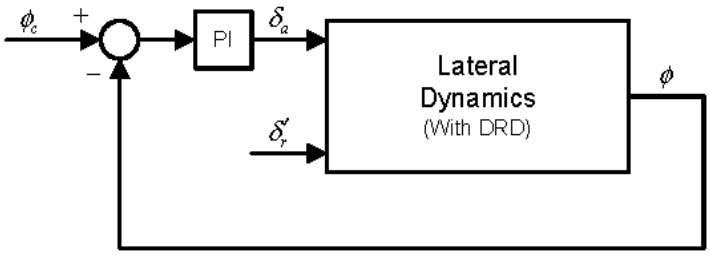

Figure 17 – Roll Angle Controller

7.2.3 Heading Controller

Finally, with a roll angle controller in place, a heading controller is usually designed to allow the aircraft to track a desired heading. As shown in Figure 18 this controller interfaces with the roll angle command of the previous controller. If the actual heading differs from the desired heading, a roll angle will be commanded to reduce this error to zero. Care needs to be taken with this controller to ensure that large roll angles are not commanded and that the shortest path is taken to reach particular heading.

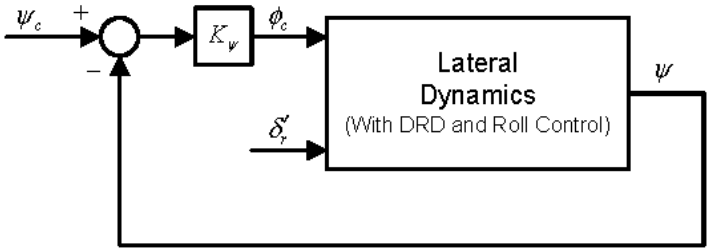

Figure 18 – Heading Controller

7.3 Summary

This section introduced the classic controllers used to regulate the motion of an aircraft. Longitudinally it was seen that the following controllers are used,

- Pitch Rate Damper
- Airspeed and Climb Rate Controller
- Altitude Controller

and laterally it was seen that the following controllers are used,

- Dutch Roll Damper
- Roll Angle Controller
- Heading Angle Controller

A number of variations on the above controllers exist as well as completely different control architectures. The purpose of this section was merely to provide a flavour of the classic controllers used.

8 Design of Longitudinal Controllers

This section presents the detailed design procedure for each of the longitudinal controllers. The following feedback control loops are designed and closed successively, from the fastest inner control loop to the slowest outer control loop:

- Pitch Rate Damper
- Airspeed and Climb Rate Controller
- Altitude Controller

After an inner control loop has been designed and closed, its closed loop model is determined and it then serves as the plant for the design of the next control loop.

8.1 Design of the Pitch Rate Damper

The control architecture of the pitch rate damper is shown in the block diagram of Figure 19.

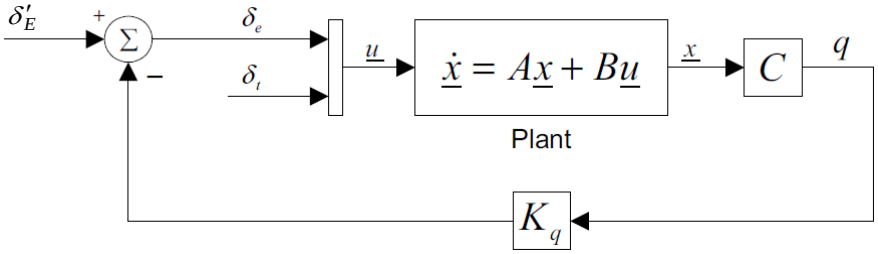

Figure 19 – Pitch Rate Damper Block Diagram

The pitch rate damper feeds back the aircraft's pitch rate via a proportional gain K_q to the elevator δ_E to provide additional artificial pitch rate damping. The plant is the longitudinal dynamics of the aircraft in state space form represented by equation (5.63). The output matrix $\mathbf{C}_q$ extracts the pitch rate state from the state vector, and represents an angular rate sensor, e.g. a rate gyroscope, that measures the angular rate about the aircraft's pitch axis. The pitch rate damper continues to present the elevator as a control input δ'_E for the next control loop.

Important note: Since a positive elevator deflection causes a negative pitching moment, the feedback gain Kq should have a negative value to produce a negative feedback loop.

The design of the pitch rate damper consists of determining an appropriate value for the proportional feedback gain K_q.

The transfer function from elevator to pitch rate is obtained from the state space model through

$$\frac{q(s)}{\delta_E(s)} = \mathbf{C}_q (s\mathbf{I} - \mathbf{A}_{long})^{-1} \mathbf{B}_{\delta_E} \tag{8.1}$$

where $\mathbf{A}_{long}$ is the longitudinal system matrix A from equation (5.63), $\mathbf{B}_{\delta_E}$ is the first column of the longitudinal input matrix B from equation (5.63), and $\mathbf{C}_q$ is the output matrix that extracts the pitch rate q from the longitudinal state vector $\mathbf{x}_{long}$:

$$\mathbf{A}_{long} = \begin{bmatrix} \frac{\rho \bar{V}_T S C_{X_T}}{m} & \frac{q_T S}{m}\left(C_{L_\alpha}\alpha_T + C_{L_T} - \frac{2C_{L_T}C_{L_\alpha}}{\pi A e} \right) & 0 & g\cos\Theta_T \\ -\frac{\rho S C_{L_T}}{m} & -\frac{q_T S}{m\bar{V}_T} C_{L_\alpha} & 1 - \frac{q_T S}{m\bar{V}_T}\frac{\bar{c}}{2\bar{V}_T} C_{L_Q} & -\frac{g}{\bar{V}_T}\sin\Theta_T \\ 0 & \frac{q_T S \bar{c}}{I_{yy}} C_{m_\alpha} & \frac{q_T S \bar{c}}{I_{yy}}\frac{\bar{c}}{2\bar{V}_T} C_{m_Q} & 0 \\ 0 & 0 & 1 & 0 \end{bmatrix} \tag{8.2}$$

$$\mathbf{B}_{\delta_E} = \begin{bmatrix} 0 \\ -\dfrac{q_T S}{m\bar{V}_T} C_{L_{\delta_E}} \\ \dfrac{q_T S\bar{c}}{I_{yy}} C_{m_{\delta_E}} \\ 0 \end{bmatrix} \tag{8.3}$$

$$\mathbf{C}_q = \begin{bmatrix} 0 & 0 & 1 & 0 \end{bmatrix} \tag{8.4}$$

The root locus of the pitch rate damper with respect to the feedback gain K_q is shown in Figure 20. The two poles with large movement are the short period mode poles while the phugoid mode poles are barely visible near the origin.

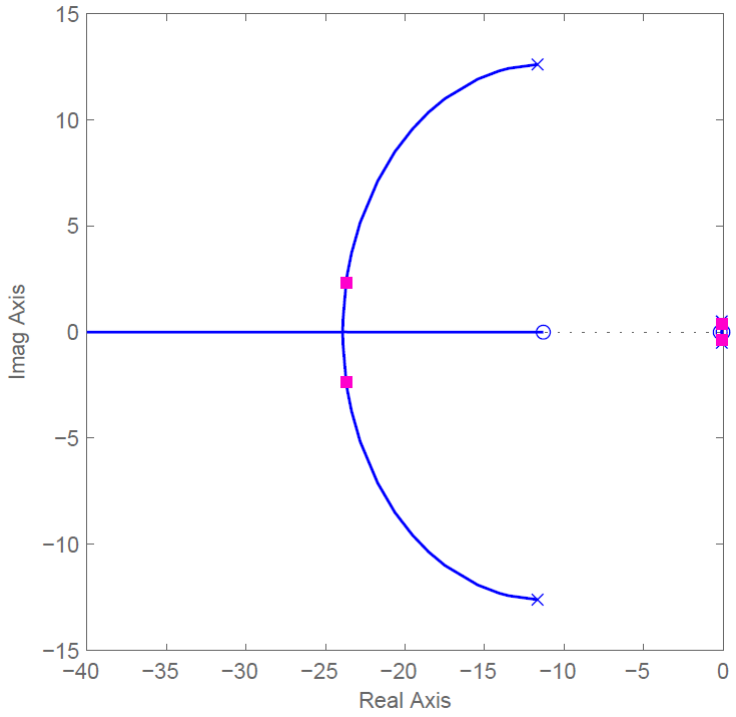

Figure 20 – Pitch Rate Damper Root Locus

It is desired to choose the pitch rate damper feedback gain as high as possible, so as to provide maximum artificial damping. However, if the feedback gain is made too high then the bandwidth of the system begins to increase and unmodeled dynamics can be excited. These can include dynamics due to structural resonant modes as well as nonlinear actuator effects such as slew rate and saturation. The feedback gain should therefore be chosen to increases the short period mode damping to at least optimally damped (damping ratio > 0.7), but without exciting unmodeled dynamics.

After adding the pitch rate damper, the closed loop system that encapsulates the longitudinal dynamics with the pitch rate damper can be expressed in state space form as

$$\dot{\mathbf{x}}_{long} = \left[\mathbf{A}_{long} - \mathbf{B}_{long}\begin{bmatrix} K_q & 0 \end{bmatrix}^T \mathbf{C}_q\right]\mathbf{x}_{long} + \mathbf{B}_{long}\mathbf{u}_{long} \tag{8.5}$$

The closed loop model of the longitudinal dynamics with pitch rate damper will serve as the plant for the airspeed and climb rate controller, which is the next feedback control loop. We will therefore write it in a more compact form as

$$\dot{\mathbf{x}}_{long} = \mathbf{A}_{PRD}\mathbf{x}_{long} + \mathbf{B}_{long}\mathbf{u}'_{long} \tag{8.6}$$

with

$$\mathbf{A}_{PRD} = \left[\mathbf{A}_{long} - \mathbf{B}_{long}\begin{bmatrix} K_q & 0 \end{bmatrix}^T \mathbf{C}_q\right] \tag{8.7}$$

$$\mathbf{x}_{long} = \begin{bmatrix} \bar{v} & \alpha & q & \theta \end{bmatrix}^T \tag{8.8}$$

$$\mathbf{u}'_{long} = \begin{bmatrix} \delta'_e & \delta_T \end{bmatrix}^T \tag{8.9}$$

$$\delta_e = K_q q + \delta'_e \tag{8.10}$$

8.2 Airspeed and Climb Rate Controller

The control architecture for the airspeed climb rate controller is shown in Figure 21.

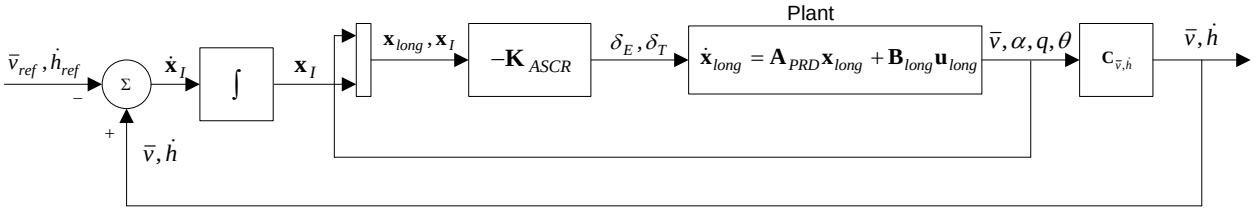

Figure 21 – Airspeed and Climb Rate Controller Block Diagram

The airspeed and climb rate controller uses full state feedback to control both the airspeed and the climb rate by commanding both the elevator and the throttle actuators, using knowledge of the full longitudinal dynamics model and its cross coupling effects. The full longitudinal state vector is fed back and two integrator states are added, one for airspeed and one for climb rate, to ensure that they follow the airspeed reference and climb rate reference with zero steady state error. The plant is the longitudinal dynamics with pitch rate damper given by equation (8.6). The output matrix $\mathbf{C}_{\bar{v},\dot{h}}$ extracts the airspeed $\bar{v}$ and the climb rate $\dot{h}$ from the longitudinal state vector $\mathbf{x}_{long}$. The airspeed error and the climb rate errors (the difference measured outputs and the references) are fed into integrators to obtain the airspeed and climb rate errors integrated over time, which are represented by the integrated error vector $\mathbf{x}_I$. The longitudinal state vector $\mathbf{x}_{long}$, augmented with the integrated error vector $\mathbf{x}_I$, is then used for full state feedback. The airspeed and climb rate controller presents the airspeed reference and the climb rate reference as control inputs for the next control loop.

Full state feedback requires a state estimator that estimates of the full state vector from the available sensor measurements represented by the output vector. For the purposes of the controller design, we will assume that such an estimator can be implemented, and that all of the longitudinal states are available for feedback.

The longitudinal dynamics with pitch rate damper is augmented with the two integrator states for airspeed error and climb rate error as follows. The integrator dynamics are

$$\dot{\mathbf{x}}_I = \mathbf{y} - \mathbf{r} = \mathbf{C}_{\bar{v},\dot{h}}\mathbf{x} - \mathbf{r} \tag{8.11}$$

with

$$\mathbf{x}_I = \begin{bmatrix} \int (\bar{v} - \bar{v}_{ref})dt & \int (\dot{h} - \dot{h}_{ref})dt \end{bmatrix}^T \tag{8.12}$$

$$\mathbf{y} = \begin{bmatrix} \bar{v} & \dot{h} \end{bmatrix}^T \tag{8.13}$$

$$\mathbf{r}_{\bar{v},\dot{h}} = \begin{bmatrix} \bar{v}_{ref} & \dot{h}_{ref} \end{bmatrix}^T \tag{8.14}$$

$$\mathbf{C}_{\bar{v},\dot{h}} = \begin{bmatrix} 1 & 0 & 0 & 0 \\ 0 & -\bar{V}_T & 0 & \bar{V}_T \end{bmatrix} \tag{8.15}$$

where $\mathbf{x}_I$ is the integration error state vector containing the airspeed and climb rate errors integrated over time, $\mathbf{y}$ is the output vector containing the airspeed and climb rate measurements, and $\mathbf{r}_{\bar{v},\dot{h}}$ is the reference vector containing the

airspeed and climb rate references. The output matrix $\mathbf{C}_{\bar{v},\dot{h}}$ extracts the airspeed $\bar{v}$ directly from the state vector $\mathbf{x}_{long}$ and the climb rate $\dot{h}$ indirectly through the following equation

$$\dot{h} = \bar{V}_T(\theta - \alpha) \tag{8.16}$$

where $\bar{V}_T$ is the trim airspeed, and $(\theta - \alpha)$ is the flight path angle, i.e. the "pitch angle" of the aircraft's velocity vector.

The state space model of the longitudinal dynamics augmented with the integrator states is then given by

$$\begin{bmatrix} \dot{\mathbf{x}}_{long} \\ \dot{\mathbf{x}}_I \end{bmatrix} = \begin{bmatrix} \mathbf{A}_{PRD} & \mathbf{0}_{4x2} \\ \mathbf{C}_{\bar{v},\dot{h}} & \mathbf{0}_{2x2} \end{bmatrix} \begin{bmatrix} \mathbf{x}_{long} \\ \mathbf{x}_I \end{bmatrix} + \begin{bmatrix} \mathbf{B}_{long} \\ \mathbf{0}_{2x2} \end{bmatrix} \mathbf{u}_{long} + \begin{bmatrix} \mathbf{0}_{4x2} \\ -\mathbf{I}_{2x2} \end{bmatrix} \mathbf{r}_{\bar{v},\dot{h}} \tag{8.17}$$

The full state feedback control law is given by

$$\mathbf{u} = -\mathbf{K}_{ASCR} \begin{bmatrix} \dot{\mathbf{x}} \\ \dot{\mathbf{x}}_I \end{bmatrix} \tag{8.18}$$

The optimal control gain $\mathbf{K}_{ASCR}$ is calculated by LQR optimisation algorithm that minimises the cost function

$$J = \int_0^\infty (\mathbf{x}^T \mathbf{Q} \mathbf{x} + \mathbf{u}^T \mathbf{R} \mathbf{u}) dt \tag{8.19}$$

where the state weighting matrix **Q** and the input weighting matrix **R** are both diagonal matrices that have to be chosen by the designer. The direct solution for the optimal control gain can be calculated with Matlab using

$$\text{K = lqr(A,B,Q,R)} \tag{8.20}$$

Bryson's rule suggests that the designer initially chooses the diagonal matrices **Q** and **R** such that

$$\begin{aligned} \mathbf{Q} &= diag\left[\frac{1}{\max(\bar{v})^2} \quad \frac{1}{\max(\alpha)^2} \quad \frac{1}{\max(q)^2} \quad \frac{1}{\max(\theta)^2} \right] \\ \mathbf{R} &= diag\left[\frac{1}{\max(\delta_E)^2} \quad \frac{1}{\max(\delta_T)^2} \right] \end{aligned} \tag{8.21}$$

The designer should then iteratively modify the weighting matrices to achieve an acceptable trade-off between performance and control effort. The following guidelines for modifying the weighting matrices may be helpful:

- Increasing the overall weight of the state weighting matrix **Q** relative to the input weighting matrix **R**, i.e. multiplying the whole **Q** matrix with a scalar value with a magnitude greater than one, should result in faster response at the expense of more control effort.
- Decreasing the overall weight of the state weighting matrix **Q** relative to the input weighting matrix **R**, i.e. multiplying the whole **Q** matrix with a scalar value with a magnitude less than one, should result in less control effort at the expense of slower response.
- Within the **Q** matrix, placing more weight on the airspeed state relative to the angle of attack and pitch angle states, should result in better airspeed tracking performance at the expense of worse climb rate tracking performance.
- Within the **Q** matrix, placing more weight on the angle of attack and pitch angle states relative to the airspeed state, should result in better climb rate tracking performance at the expense of worse airspeed tracking performance.
- Within the **Q** matrix, the pitch rate state should be assigned a light weight relative to the angle of attack and pitch angle states, to give the controller enough pitch rate authority to regulate the climb rate.
- Within the **R** matrix, the thrust input should be assigned a heavier weight relative to the elevator actuator, to discourage the controller from using it aggressively. Remember that the thrust actuator has a real pole which has not been included in the plant dynamics.

Once an acceptable gain matrix $\mathbf{K}_{ASCR}$ has been found, the closed loop system that encapsulates the longitudinal dynamics with the pitch rate damper and the airspeed climb rate controller can be expressed in state space form as

$$\begin{bmatrix} \dot{\mathbf{x}}_{long} \\ \dot{\mathbf{x}}_I \end{bmatrix} = \left(\begin{bmatrix} \mathbf{A}_{PRD} & \mathbf{0}_{4x2} \\ \mathbf{C}_{\bar{v},\dot{h}} & \mathbf{0}_{2x2} \end{bmatrix} - \begin{bmatrix} \mathbf{B}_{PRD} \\ \mathbf{0}_{2x2} \end{bmatrix} \mathbf{K}_{ASCR} \right) \begin{bmatrix} \mathbf{x}_{long} \\ \mathbf{x}_I \end{bmatrix} + \begin{bmatrix} \mathbf{0}_{4x2} \\ -\mathbf{I}_{2x2} \end{bmatrix} \mathbf{r}_{\bar{v},\dot{h}} \tag{8.22}$$

The closed loop model of the longitudinal dynamics with pitch rate damper and airspeed climb rate controller will serve as the plant for the altitude controller, which is the next feedback control loop. We will therefore write it in a more compact form as

$$\begin{bmatrix} \dot{\mathbf{x}}_{long} \\ \dot{\mathbf{x}}_I \end{bmatrix} = \mathbf{A}_{ASCR} \begin{bmatrix} \mathbf{x}_{long} \\ \mathbf{x}_I \end{bmatrix} + \mathbf{B}_{ASCR} \begin{bmatrix} \bar{v}_{ref} \\ \dot{h}_{ref} \end{bmatrix} \tag{8.23}$$

with

$$\mathbf{A}_{ASCR} = \begin{bmatrix} \mathbf{A}_{PRD} & \mathbf{0}_{4x2} \\ \mathbf{C}_{\bar{v},\dot{h}} & \mathbf{0}_{2x2} \end{bmatrix} - \begin{bmatrix} \mathbf{B}_{PRD} \\ \mathbf{0}_{2x2} \end{bmatrix} \mathbf{K}_{ASCR} \tag{8.24}$$

$$\mathbf{B}_{ASCR} = \begin{bmatrix} \mathbf{0}_{4x2} \\ -\mathbf{I}_{2x2} \end{bmatrix} \tag{8.25}$$

8.3 Altitude Controller

The control architecture for the altitude controller is shown in block diagram form in Figure 22.

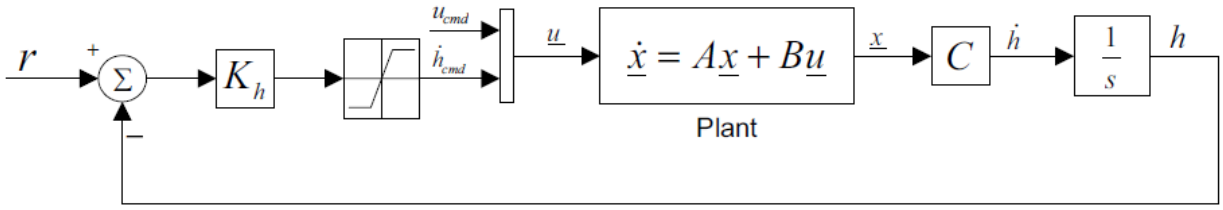

Figure 22 – Altitude Controller Block Diagram

The altitude controller generates a climb rate command $\dot{h}_{ref}$ proportional to the altitude error (the difference between the altitude reference h_{ref} and the altitude measurement h). The natural integration from climb rate to altitude makes the system type 1, which means it should be able to follow a constant altitude reference with zero error at steady state. Before the climb rate command is fed to the climb rate controller, it is sent through a saturation block to ensure that it does not command climb rate signals that exceed the climb rate limitations of the aircraft. This block automatically ensures that the aircraft enters a constant climb rate when large altitude step commands are issued.

The plant is the longitudinal dynamics with the pitch rate damper and the airspeed and climb rate controller given by equation (8.23), but augmented with an altitude state. The output matrix $\mathbf{C}_{\dot{h}}$ extracts the climb rate $\dot{h}$ from the state vector, and feeds it to a natural integrator to become the altitude state *h*, which is typically measured by a barometric pressure sensor, or GPS. The altitude controller presents the altitude reference input as a control input to the next control loop.

The design of the altitude controller consists of determining an appropriate value for the proportional gain K_h. First, the state space model of the airspeed and climb rate control dynamics is augmented with the altitude state by

$$\begin{bmatrix} \dot{\mathbf{x}}_{ASCR} \\ \dot{h} \end{bmatrix} = \begin{bmatrix} \mathbf{A}_{ASCR} & \mathbf{0}_{6x1} \\ \mathbf{C}_{\dot{h}} & 0 \end{bmatrix} \begin{bmatrix} \mathbf{x}_{ASCR} \\ h \end{bmatrix} + \begin{bmatrix} \mathbf{B}_{\dot{h}_{ref}} \\ 0 \end{bmatrix} \dot{h}_{ref} \tag{8.26}$$

with

$$\mathbf{x}_{ASCR} = \begin{bmatrix} \mathbf{x}_{long} & \mathbf{x}_I \end{bmatrix}^T \tag{8.27}$$

$$\mathbf{C}_{\dot{h}} = \begin{bmatrix} 0 & -\overline{V}_T & 0 & \overline{V}_T & \mathbf{0}_{1x2} \end{bmatrix} \tag{8.28}$$

$$\mathbf{B}_{\dot{h}_{ref}} = \begin{bmatrix} \mathbf{0}_{1x5} & -1 \end{bmatrix}^T \tag{8.29}$$

where $\mathbf{x}_{ASCR}$ is the longitudinal state vector augmented with the airspeed and climb rate error integrals, $\mathbf{B}_{CR}$ is the second column of the airspeed and climb rate controller input matrix $\mathbf{B}_{ASCR}$, and $\mathbf{C}_{\dot{h}}$ is the output matrix that extracts the climb rate $\dot{h}$ from the state vector.

The transfer function from climb rate reference to altitude is obtained from the state space model through

$$\frac{h(s)}{\dot{h}_{ref}(s)} = \frac{1}{s} \mathbf{C}_{\dot{h}} (s\mathbf{I} - \mathbf{A}_{ASCR})^{-1} \mathbf{B}_{\dot{h}_{ref}} \tag{8.30}$$

The root locus of the altitude controller with respect to the proportional gain K_h is shown in Figure 23 and Figure 24. Figure 23 shows that the two branches of the root locus that originate at the open-loop poles near the origin move into the right half-plane for large gain values. For large values of gain, the closed-loop altitude controller will therefore become unstable. However, zooming in on the root locus brances near the origin, as shown in Figure 24, reveals that the closed-loop poles remain in the lef-half plane for small gain values. For small values of gain, the closed-loop altitude controller should therefore be stable. The proportional gain should therefore be selected so that the closed-loop poles near the origin remain stable, and have an acceptable damping ratio and speed of response.

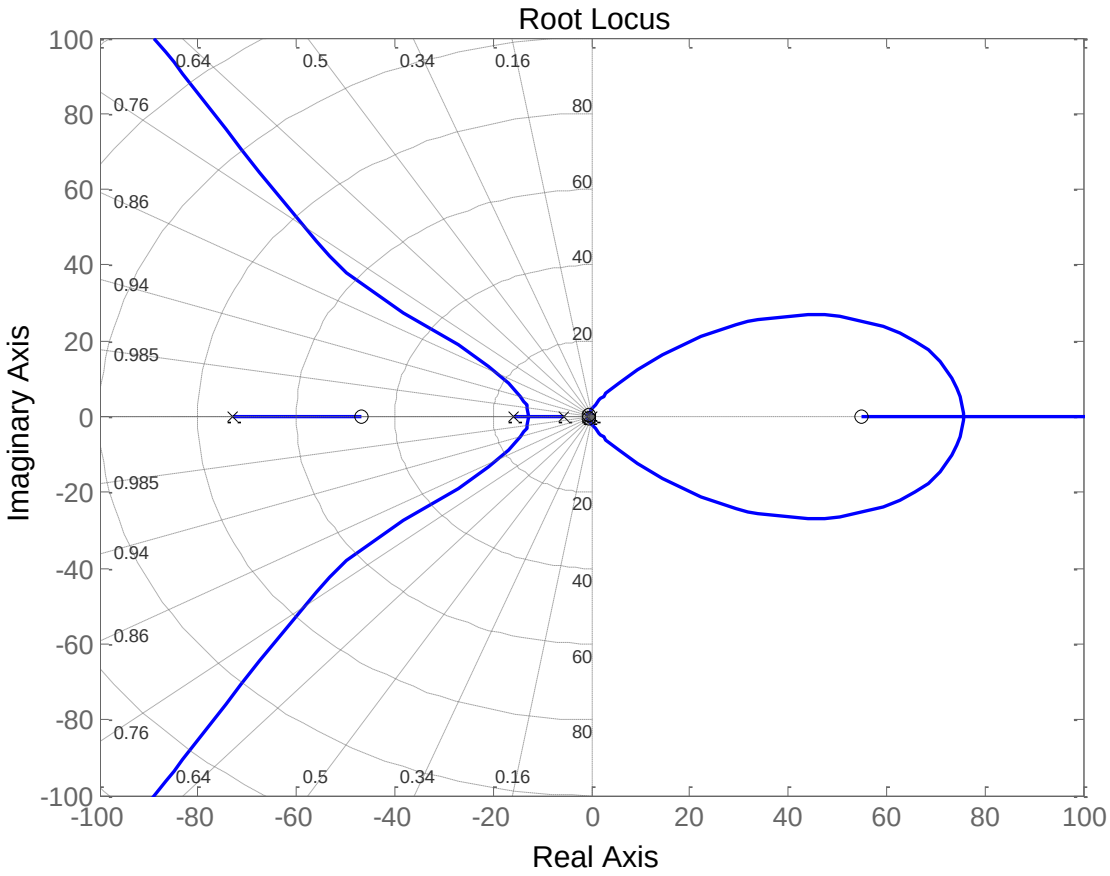

Figure 23 – Altitude Controller Root Locus

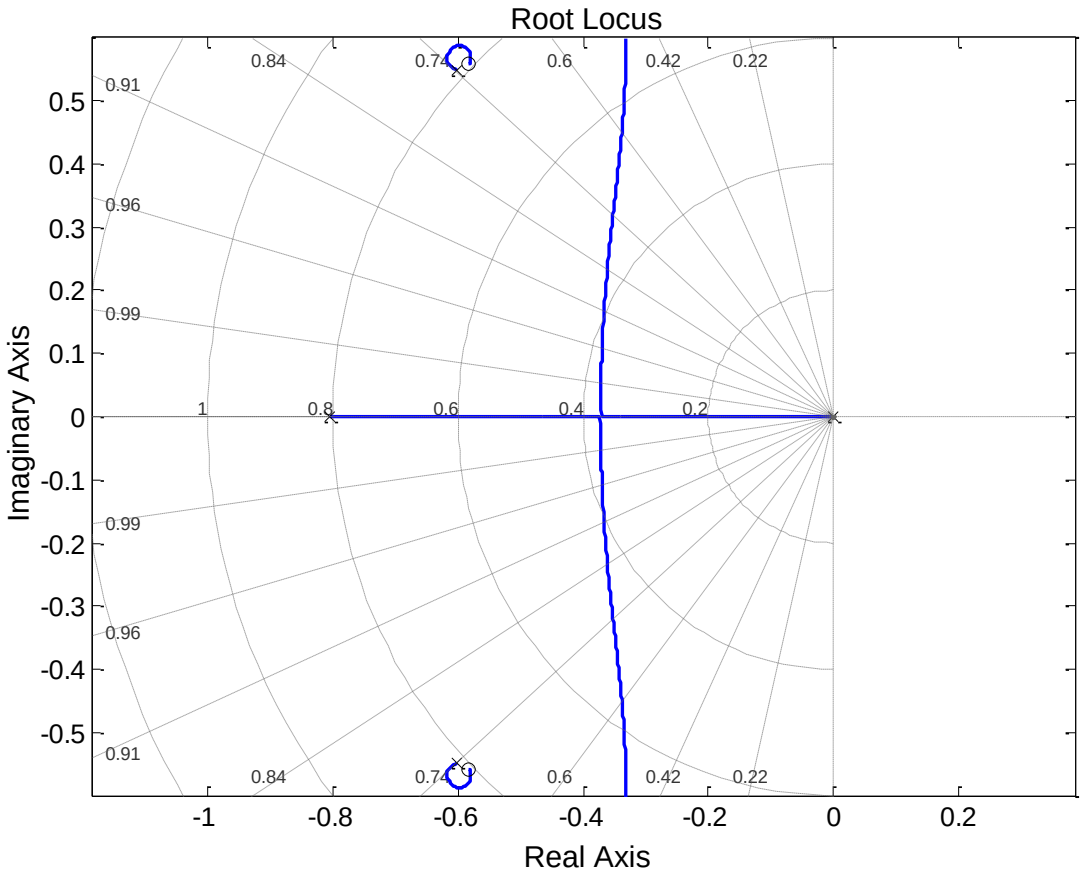

Figure 24 – Altitude Controller Root Locus (Zoomed In)

After adding the altitude controller, the encapsulated closed loop dynamics of the aircraft with the altitude controller included, is given in state space form as

$$\begin{bmatrix} \dot{\mathbf{x}}_{ASCR} \\ \dot{h} \end{bmatrix} = \begin{bmatrix} \mathbf{A}_{ASCR} & -\mathbf{B}_{ASCR}\begin{bmatrix} 0 \\ K_h \end{bmatrix} \\ \mathbf{C}_{\dot{h}} & 0 \end{bmatrix} \begin{bmatrix} \mathbf{x}_{ASCR} \\ h \end{bmatrix} + \begin{bmatrix} \mathbf{B}_{ASCR}\begin{bmatrix} 1 & 0 \\ 0 & K_h \end{bmatrix} \\ \mathbf{0}_{1x2} \end{bmatrix} \begin{bmatrix} \bar{v}_{ref} \\ h_{ref} \end{bmatrix} \tag{8.31}$$

The encapsulated dynamics of the aircraft with pitch rate damper, airspeed and climb rate controller, and altitude controller, presents an airspeed reference and an altitude reference as control inputs to the next control loop.

9 Design of Lateral Controllers

This section presents the detailed design procedure for each of the lateral controllers. The following feedback control loops are designed and closed successively, from the fastest inner control loop to the slowest outer control loop:

- Dutch Roll Damper
- Roll Angle Controller
- Heading Controller

As with the lateral controllers, after an inner control loop has been designed and closed, its closed loop model is determined and it then serves as the plant for the design of the next control loop.

9.1 Dutch Roll Damper

The control architecture of the dutch roll damper is shown in the block diagram of Figure 25.

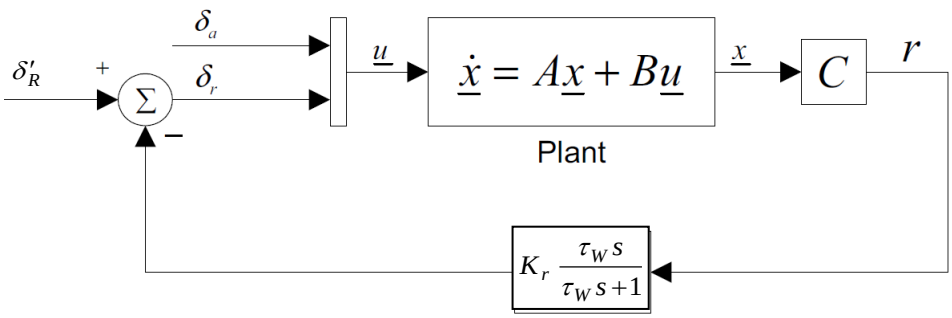

Figure 25 – Dutch Roll Damper Block Diagram

The dutch roll damper feeds back the aircraft's yaw rate via a proportional gain K_r to the rudder δ_R to provide additional artificial yaw rate damping. The yaw rate signal must however be high pass filtered before it is fed to the rudder so that the damper does not counter constant turn rate motions. The plant is the lateral dynamics of the aircraft in state space form represented by equation (5.64). The output matrix $\mathbf{C}_r$ extracts the yaw rate state from the state vector, and represents an angular rate sensor, e.g. a rate gyroscope, that measures the angular rate about the aircraft's yaw axis. The dutch roll damper continues to present the rudder as a control input δ'_R for the next control loop.

The design of the dutch roll damper consists of choosing values for the washout filter cutoff frequency $1/\tau_W$ and the proportional feedback gain K_r.

Important note: Since a positive rudder deflection causes a negative yawing moment, the feedback gain K_r should have a negative value to produce a negative feedback loop.

The transfer function from elevator to pitch rate is obtained from the state space model through

$$\frac{r(s)}{\delta_R(s)} = \mathbf{C}_r(s\mathbf{I} - \mathbf{A}_{lat})^{-1}\mathbf{B}_{\delta_R} \tag{9.1}$$

where $\mathbf{A}_{lat}$ is the lateral system matrix A from equation (5.64), $\mathbf{B}_{\delta_R}$ is the second column of the lateral input matrix B from equation (5.64), and $\mathbf{C}_r$ is the output matrix that extracts the yaw rate r from the longitudinal state vector $\mathbf{x}_{lat}$:

$$\mathbf{A}_{lat} = \begin{bmatrix} \frac{q_T S}{m\bar{V}_T} C_{y_\beta} & \frac{q_T S}{m\bar{V}_T}\frac{b}{2\bar{V}_T} C_{y_P} & \frac{q_T S}{m\bar{V}_T} C_{y_R} - 1 & \frac{g}{\bar{V}_T}\cos\Theta_T \\ \frac{q_T Sb}{I_{xx}} C_{l_\beta} & \frac{q_T S}{I_{xx}}\frac{b}{2\bar{V}_T} C_{l_P} & \frac{q_T Sb}{I_{xx}}\frac{b}{2\bar{V}_T} C_{l_R} & 0 \\ \frac{q_T Sb}{I_{zz}} C_{n_\beta} & \frac{q_T S}{I_{zz}}\frac{b}{2\bar{V}_T} C_{n_P} & \frac{q_T Sb}{I_{zz}}\frac{b}{2\bar{V}_T} C_{n_R} & 0 \\ 0 & 1 & \tan\Theta_T & 0 \end{bmatrix} \tag{9.2}$$

$$\mathbf{B}_{\delta_R} = \begin{bmatrix} \frac{q_T S}{m\bar{V}_T} C_{y_{\delta_R}} & \frac{q_T Sb}{I_{xx}} C_{l_{\delta_R}} & \frac{q_T Sb}{I_{zz}} C_{n_{\delta_R}} & 0 \end{bmatrix}^T \tag{9.3}$$

$$\mathbf{C}_r = \begin{bmatrix} 0 & 0 & 1 & 0 \end{bmatrix} \tag{9.4}$$

Choosing the washout filter cutoff frequency is an iterative process. However, it must be chosen low enough to ensure the frequency of the dutch roll mode lies within its passband (without too much phase error), but high enough so as not to interfere with constant turn rate motions. A washout filter cutoff frequency equal to a quarter of the natural frequency of the dutch roll mode is suggested as a good starting point.

With the filter dynamics included, the root locus plot with respect to the filter feedback gain K_r is plotted as shown in Figure 26.

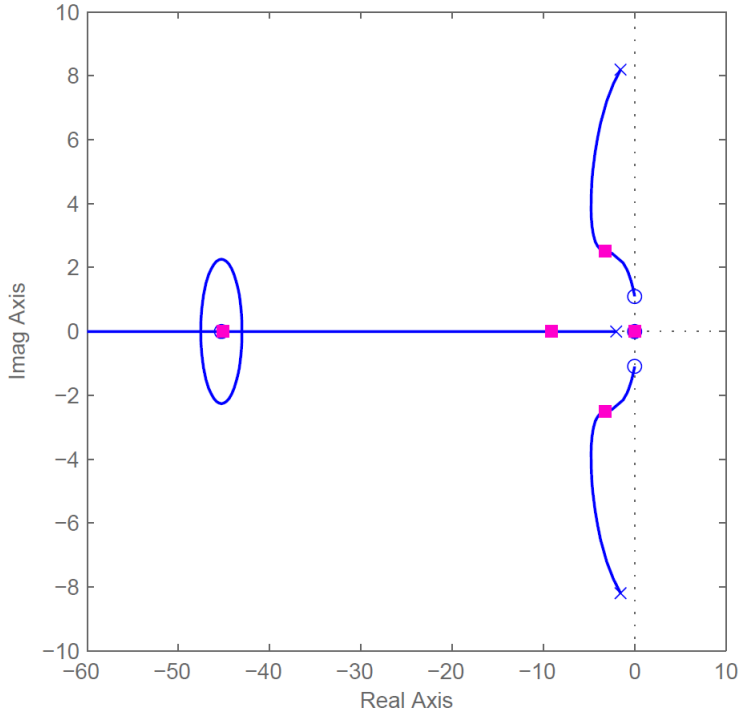

Figure 26 – Dutch Roll Mode Root Locus.

The filter gain is chosen to provide maximum damping of the dutch roll mode for the cutoff frequency chosen. The complete washout filter with the feedback gain included is stated below,

$$D_{DRD}(s) = K_r \frac{\tau_W s}{\tau_W s + 1} \tag{9.5}$$

After adding the dutch roll damper, the closed loop system that encapsulates the lateral dynamics augmented with the dutch roll damper can be expressed in state space form as

$$\begin{bmatrix}\dot{\mathbf{x}}_{lat}\\ \dot{x}_W\end{bmatrix}=\begin{bmatrix}\mathbf{A}_{lat}-\mathbf{B}_{\delta_R}D_W\mathbf{C}_r & -\mathbf{B}_{\delta_R}C_W\\ B_W\mathbf{C}_r & A_W\end{bmatrix}\begin{bmatrix}\mathbf{x}_{lat}\\ x_W\end{bmatrix}+\begin{bmatrix}\mathbf{B}_{lat}\\ 0\end{bmatrix}\mathbf{u}_{lat} \tag{9.6}$$

where A_W, B_W, C_W, and D_W are the state space matrices of the washout filter (9.4).

$$\begin{aligned}\dot{x}_W &= \left[-\frac{1}{\tau_W}\right]x_W+[K_r]u_{washout}\\ y_{washout} &= \left[-\frac{1}{\tau_W}\right]x_W+[K_r]u_{washout}\end{aligned} \tag{9.7}$$

that is, $A_W=-\frac{1}{\tau_W}$, $B_W=K_r$, $C_W=-\frac{1}{\tau_W}$ and $D_W=K_r$.

The closed loop model of the lateral dynamics with dutch roll damper will serve as the plant for the roll angle controller, which is the next feedback control loop. We will therefore write it in a more compact form as

$$\dot{\mathbf{x}}_{DRD}=\mathbf{A}_{DRD}\mathbf{x}_{DRD}+\mathbf{B}_{DRD}\mathbf{u}_{lat} \tag{9.8}$$

with

$$\mathbf{A}_{DRD}=\begin{bmatrix}\mathbf{A}_{lat}-\mathbf{B}_{\delta_R}D_W\mathbf{C}_r & -\mathbf{B}_{\delta_R}C_W\\ B_W\mathbf{C}_r & A_W\end{bmatrix} \tag{9.9}$$

$$\mathbf{B}_{DRD}=\begin{bmatrix}\mathbf{B}_{lat}\\ 0\end{bmatrix} \tag{9.10}$$

$$\mathbf{x}_{DRD}=[\beta \quad p \quad r \quad \phi \quad x_W]^T \tag{9.11}$$

$$\mathbf{u}_{lat}=[\delta_A \quad \delta_R']^T \tag{9.12}$$

9.2 Roll Angle Controller

The control architecture of the roll angle controller is shown in the block diagram of Figure 27

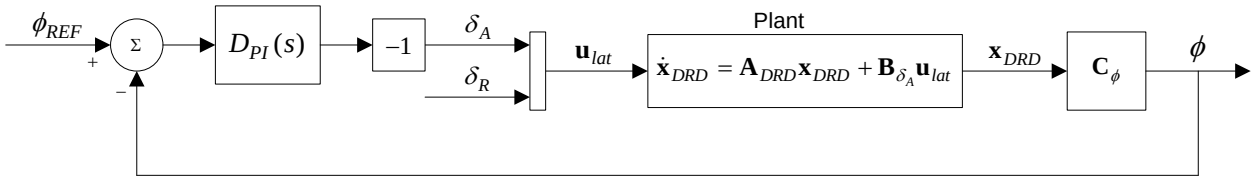

Figure 27 – Roll Angle Controller Block Diagram

The roll angle controller is a PI controller that generates an aileron command δ_A proportional to weighted sum of the roll angle error and the time integral of the roll angle error. The integral term in the PI controller makes the system type 1, which means it should be able to follow a constant roll angle reference with zero error at steady state.

The plant is the lateral dynamics with the dutch roll damper given by equation (9.8). The output matrix $\mathbf{C}_\phi$ extracts the roll angle from the lateral state vector. The roll angle controller presents the roll angle reference input as a control input to the next control loop.

The design of the roll angle controller consists of designing the PI controller to place the closed-loop poles at locations with acceptable speed of response and damping.

Important note: Since a positive aileron deflection causes a negative rolling moment, the output of the PI controller should be multiplied by -1 to produce a negative feedback loop.

The transfer function from aileron to roll angle is obtained from the state space model through

$$\frac{\phi(s)}{\delta_A(s)} = \mathbf{C}_\phi (s\mathbf{I} - \mathbf{A}_{DRD})^{-1} \mathbf{B}_{\delta_A} \tag{9.13}$$

where $\mathbf{A}_{DRD}$ is the system matrix A of the lateral dynamics with dutch roll damper from equation (9.9), $\mathbf{B}_{\delta_A}$ is the first column of the lateral input matrix B from equation (5.64), and $\mathbf{C}_\phi$ is the output matrix that extracts the roll angle ϕ from the augmented lateral state vector $\mathbf{x}_{DRD}$:

$$\mathbf{A}_{DRD} = \begin{bmatrix} \mathbf{A}_{lat} - \mathbf{B}_{\delta_R} D_W \mathbf{C}_r & -\mathbf{B}_{\delta_R} C_W \\ B_W C_r & A_W \end{bmatrix} \tag{9.14}$$

$$\mathbf{B}_{\delta_A} = \begin{bmatrix} \frac{q_T S}{m\bar{V}_T} C_{y_{\delta_A}} & \frac{q_T Sb}{I_{xx}} C_{l_{\delta_A}} & \frac{q_T Sb}{I_{zz}} C_{n_{\delta_A}} & 0 \end{bmatrix}^T \tag{9.15}$$

$$\mathbf{C}_\phi = \begin{bmatrix} 0 & 0 & 0 & 1 & 0 \end{bmatrix} \tag{9.16}$$

The PI controller transfer function is given by

$$D_{PI}(s) = \frac{-\delta_A(s)}{\phi_{error}(s)} = K\frac{s+z}{s} = (K_P + \frac{K_I}{s}) \tag{9.17}$$

After adding the integrator and the zero of the PI controller to the plant transfer function, the root locus will look similar to Figure 28.

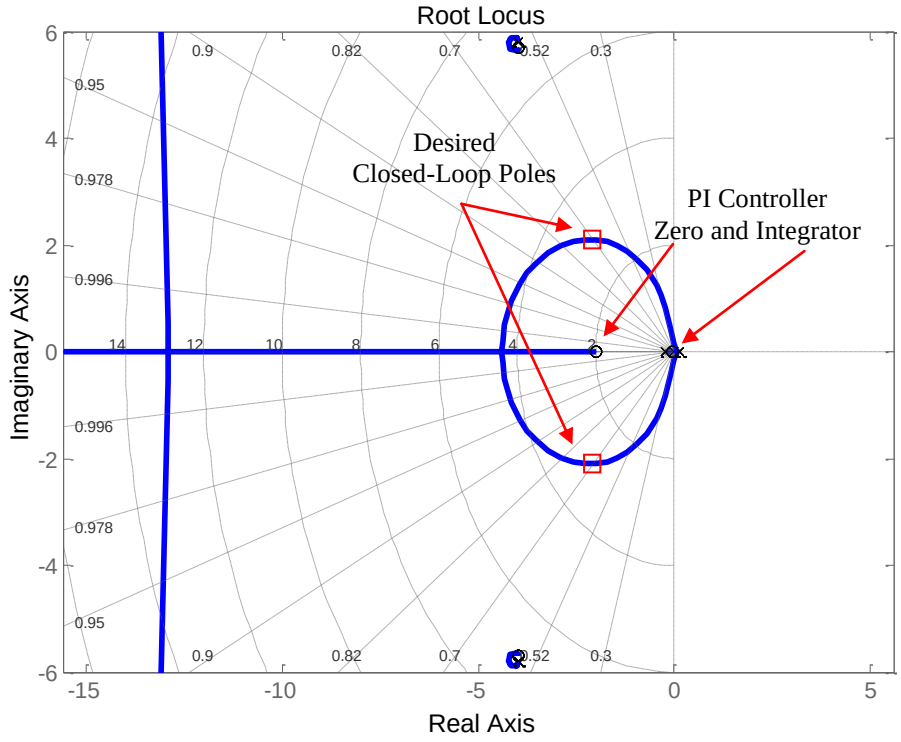

Figure 28 – Roll Angle PI Controller Root Locus

The location of the PI controller zero may be adjusted until the dominant branches of the root locus pass through closed-loop pole locations that have optimal damping and a fast enough natural frequency. The PI controller gain should then be calculated to move the closed-loop poles to the desired location.

After adding the PI controller (with its output multiplied by -1), the closed loop system that encapsulates the lateral dynamics with the dutch roll damper and roll angle controller can be expressed in state space form as

$$\begin{bmatrix} \dot{\mathbf{x}}_{DRD} \\ \dot{x}_I \end{bmatrix} = \begin{bmatrix} \mathbf{A}_{DRD} + \mathbf{B}_{\delta_A} K_P \mathbf{C}_\phi & -\mathbf{B}_{\delta_A} K_I \\ -\mathbf{C}_\phi & 0 \end{bmatrix} \begin{bmatrix} \mathbf{x}_{DRD} \\ x_I \end{bmatrix} + \begin{bmatrix} -K_P \mathbf{B}_{\delta_A} \\ 1 \end{bmatrix} \phi_{ref} \tag{9.18}$$

The closed loop model of the lateral dynamics with dutch roll damper and roll angle controller will serve as the plant for the heading controller, which is the next feedback control loop. We will therefore write it in a more compact form as

$$\dot{\mathbf{x}}_{RAC} = \mathbf{A}_{RAC} \mathbf{x}_{RAC} + \mathbf{B}_{RAC} \phi_{REF} \tag{9.19}$$

with

$$\mathbf{A}_{RAC} = \begin{bmatrix} \mathbf{A}_{DRD} + \mathbf{B}_{\delta_A} K_P \mathbf{C}_\phi & -\mathbf{B}_{\delta_A} K_I \\ -\mathbf{C}_\phi & 0 \end{bmatrix} \tag{9.20}$$

$$\mathbf{B}_{RAC} = \begin{bmatrix} -K_P \mathbf{B}_{\delta_A} \\ 1 \end{bmatrix} \tag{9.21}$$

$$\mathbf{x}_{RAC} = \begin{bmatrix} \beta & p & r & \phi & x_W & x_I \end{bmatrix}^T \tag{9.22}$$

9.3 Heading Controller

The control architecture of the heading controller is shown in the block diagram of Figure 29.

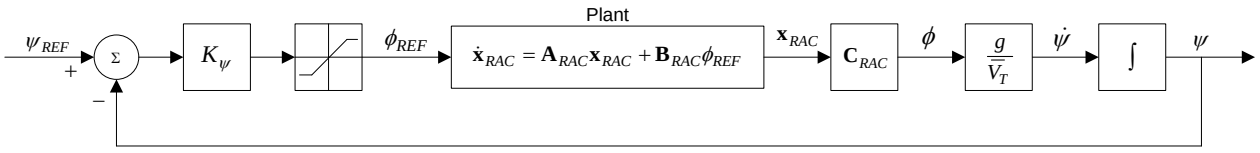

Figure 29 – Heading Controller Block Diagram

The heading controller generates a roll angle command ϕ_{ref} proportional to the heading error (the difference between the heading reference ψ_{ref} and the heading measurement ψ). The roll angle command produces a heading rate that is proportional to the roll angle of the aircraft.

Consider the diagram in Figure 30, where the aircraft is shown in a steady, constant altitude, banked turn.

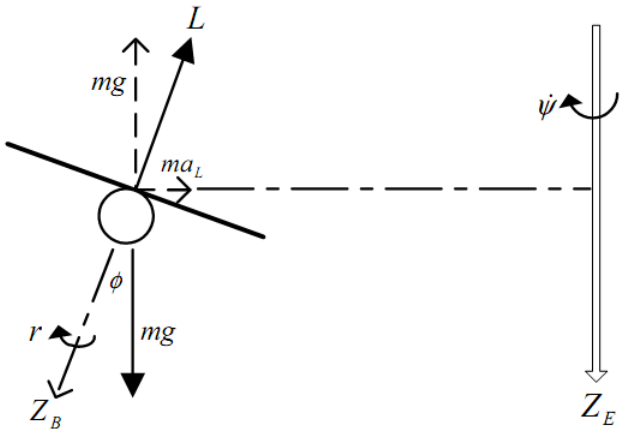

Figure 30 – Aircraft in steady banked turn

During the turn, the lift vector is responsible for countering the weight of the aircraft and for providing the necessary centripetal acceleration for the turn. Thus the lateral acceleration can be written as

$$a_L = \overline{V}_T \dot{\psi} = g \tan\phi \tag{9.23}$$

For small bank angles, $\tan\phi \approx \phi$ and equation (9.23) may be simplified to

$$\dot{\psi} = \frac{g}{\overline{V}_T}\phi \tag{9.24}$$

The natural integration from heading rate to heading makes the system type 1, which means it should be able to follow a constant heading reference with zero error at steady state. Before the roll angle command is fed to the roll angle controller, it is sent through a saturation block to ensure that it does not command roll angle signals that exceed the roll angle limitations of the aircraft. This block automatically ensures that the aircraft enters a constant roll angle when large heading step commands are issued.

The plant is the lateral dynamics with the pitch rate damper and the roll angle controller given by equation (9.19), but augmented with a heading state. The output matrix $\mathbf{C}_{RAC}$ extracts the roll angle ϕ from the state vector, which is then multiplied by $g/\overline{V}_T$ to obtain the heading rate $\dot{\psi}$, which in turn is fed to a natural integrator to become the heading state ψ. The heading is typically obtained from the horizontal velocity measured by a GPS. The heading controller presents the heading reference input as a control input to the next control loop.

The design of the heading controller consists of determining an appropriate value for the proportional gain K_ψ. First, the state space model of the roll angle control dynamics is augmented with the heading state by

$$\begin{bmatrix} \dot{\mathbf{x}}_{RAC} \\ \dot{\psi} \end{bmatrix} = \begin{bmatrix} \mathbf{A}_{RAC} & 0 \\ \mathbf{C}_{\dot{\psi}} & 0 \end{bmatrix} \begin{bmatrix} \mathbf{x}_{RAC} \\ \psi \end{bmatrix} + \begin{bmatrix} \mathbf{B}_{RAC} \\ 0 \end{bmatrix} \phi_{ref} \tag{9.25}$$

with

$$\mathbf{C}_{\dot{\psi}} = \begin{bmatrix} \mathbf{0}_{1x3} & \frac{g}{\bar{V}_T} & \mathbf{0}_{1x2} \end{bmatrix} \tag{9.26}$$

The transfer function from roll angle reference to heading is obtained from the state space model through

$$\frac{\psi(s)}{\phi_{ref}(s)} = \frac{1}{s} \mathbf{C}_{\dot{\psi}} (s\mathbf{I} - \mathbf{A}_{RAC})^{-1} \mathbf{B}_{RAC} \tag{9.27}$$

The root locus of the heading controller with respect to the proportional gain K_ψ is shown in Figure 31 and Figure 32 (zoomed in). The proportional gain is selected to place the dominant closed loop pole on the real axis with a response that is fast enough without using excessive roll angle commands.

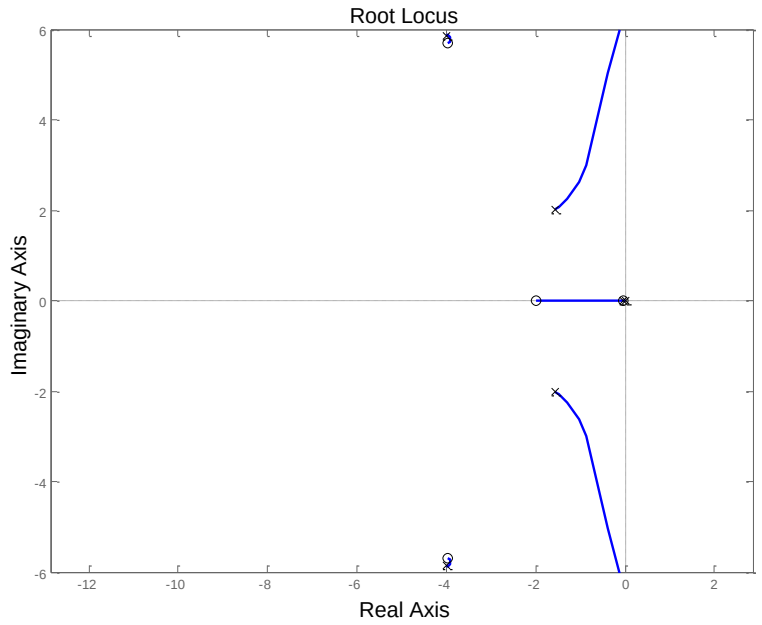

Figure 31 – Heading Controller Root Locus

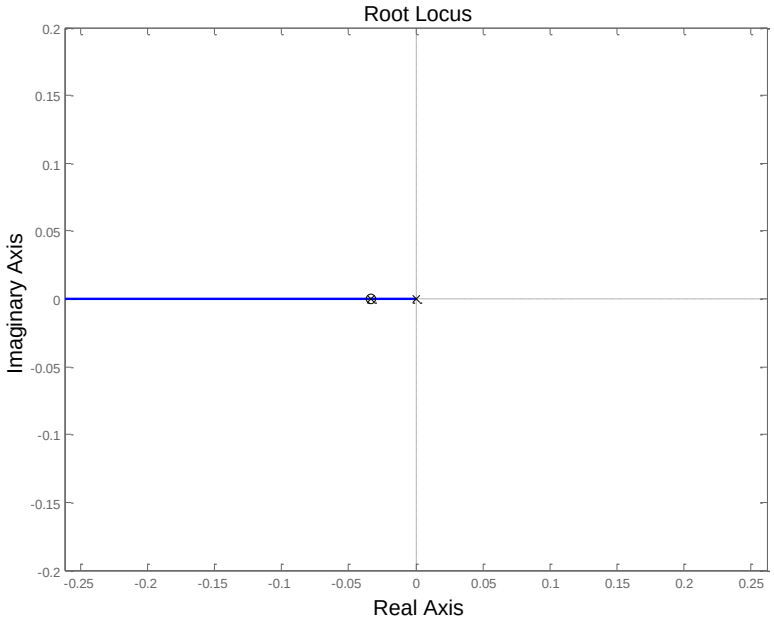

Figure 32 – Heading Controller Root Locus (Zoomed In)

After adding the heading controller, the encapsulated closed loop dynamics of the aircraft with the heading controller included, is given in state space form as

$$\begin{bmatrix} \dot{\mathbf{x}}_{RAC} \\ \dot{\psi} \end{bmatrix} = \begin{bmatrix} \mathbf{A}_{RAC} & -\mathbf{B}_{RAC} K_{\psi} \\ \mathbf{C}_{\dot{\psi}} & 0 \end{bmatrix} \begin{bmatrix} \mathbf{x}_{RAC} \\ \psi \end{bmatrix} + \begin{bmatrix} \mathbf{B}_{RAC} K_{\psi} \\ 0 \end{bmatrix} \psi_{ref} \tag{9.28}$$

The closed loop model of the heading controller will serve as the plant for the guidance controller, which is the next feedback control loop. We will therefore write it in a more compact form as

$$\dot{\mathbf{x}}_{HC} = \mathbf{A}_{HC} \mathbf{x}_{HC} + \mathbf{B}_{HC} \psi_{REF} \tag{9.29}$$

with

$$\mathbf{A}_{HC} = \begin{bmatrix} \mathbf{A}_{RAC} & -\mathbf{B}_{RAC} K_{\psi} \\ \mathbf{C}_{\dot{\psi}} & 0 \end{bmatrix} \tag{9.30}$$

$$\mathbf{B}_{HC} = \begin{bmatrix} \mathbf{B}_{RAC} K_{\psi} \\ 0 \end{bmatrix} \tag{9.31}$$

$$\mathbf{x}_{RAC} = \begin{bmatrix} \beta & p & r & \phi & x_w & x_I & \psi \end{bmatrix}^T \tag{9.32}$$

10 Guidance and Waypoint Navigation

This section presents the implementation of a guidance controller that controls the aircraft to navigate a flight path plan consisting of a set of waypoints.

10.1 Guidance

The flight path that we wish the aircraft to follow is defined as a series of straight-line path segments between predefined waypoints. Each waypoint is a set of North and East coordinates on a map. We will call the straight-line segment between two consecutive waypoints the ground track.

The purpose of the guidance controller is to guide the aircraft onto the ground track by controlling the cross-track position error to zero. Given the source waypoint and the destination waypoint, the heading and length of the ground track is calculated from the diagram in Figure 33.

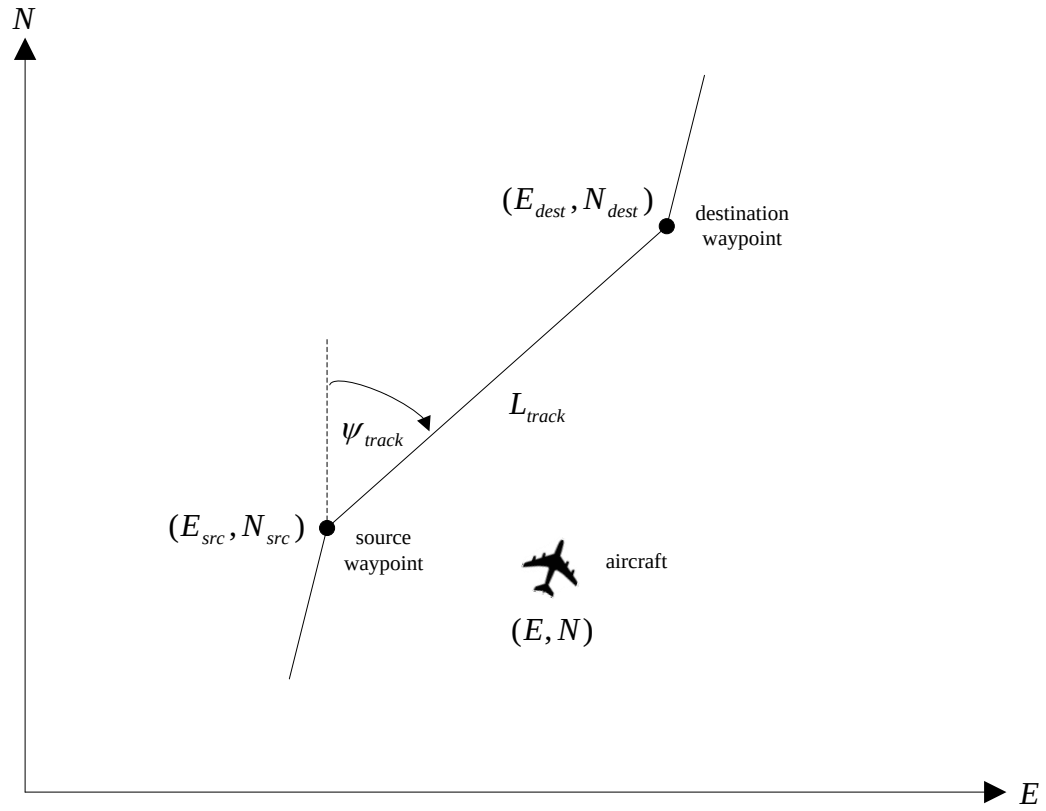

Figure 33 - Ground track between source waypoint and destination waypoint.

The track heading ψ_{track} (relative to north) and the track length L_{track} is calculated with

$$\tan\psi_{track} = \frac{E_{\text{dest}} - E_{\text{src}}}{N_{\text{dest}} - N_{\text{src}}} \tag{10.1}$$

$$L_{track} = \sqrt{(N_{\text{dest}} - N_{\text{src}})^2 + (E_{\text{dest}} - E_{\text{src}})^2} \tag{10.2}$$

The aircraft's cross track error y and its in-track distance x from the source waypoint is shown in Figure 34. The cross track error is the perpendicular distance from the aircraft's position to the ground track. The in-track distance along the track, is the distance of the aircraft's projection onto the track, from the source waypoint.

An elegant way of calculating the cross-track error and the in-track distance, is to define an auxiliary guidance axis system as shown in Figure 35.

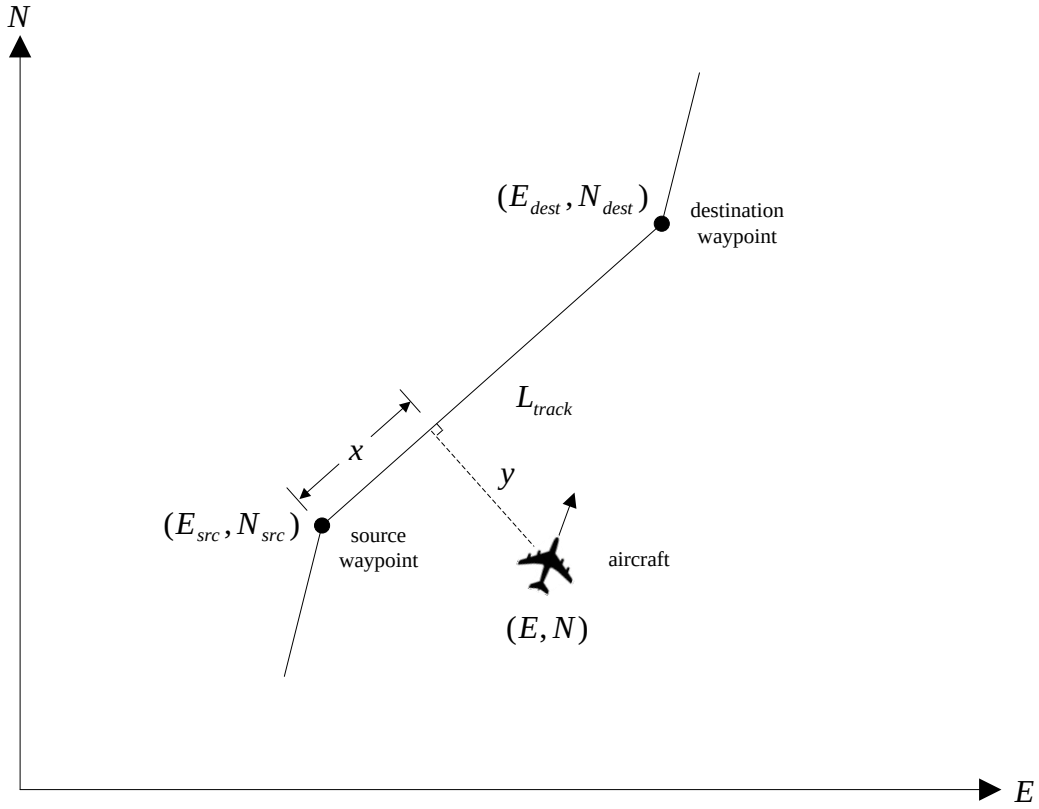

Figure 34 – Cross-track error and in-track distance along track.

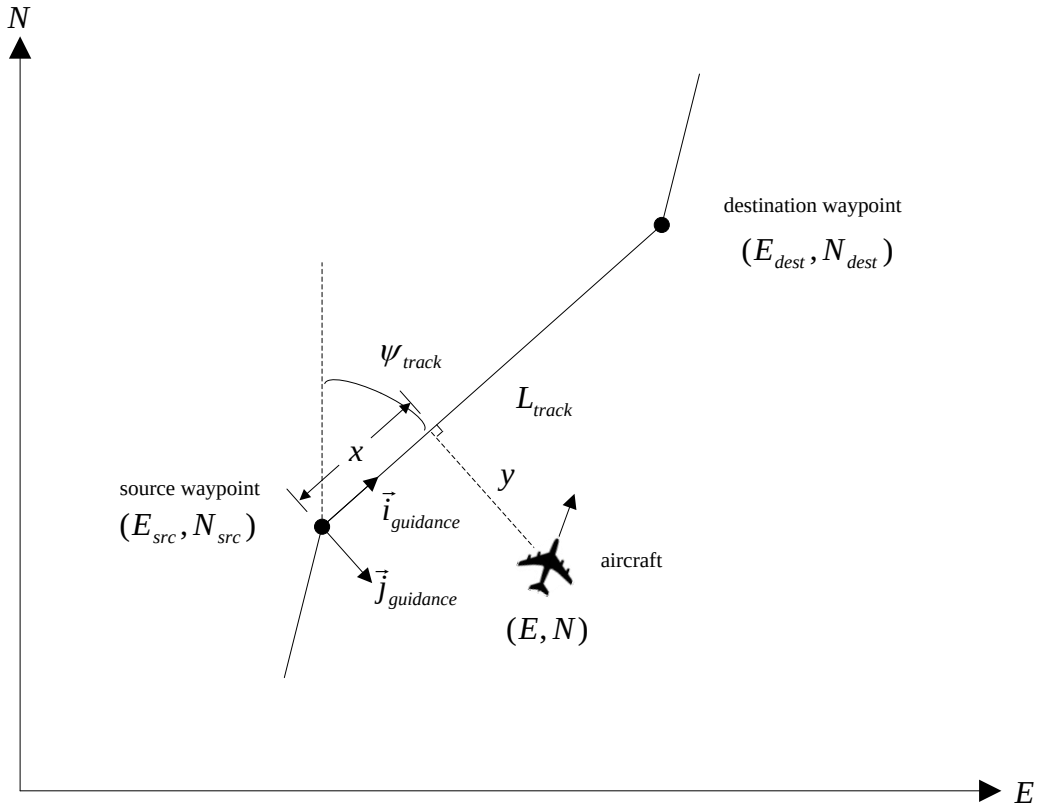

Figure 35 – Guidance Axis System

The origin of the guidance axis system is at the location of the source waypoint, it's x-axis is parallel to the ground track and pointing in the direction of the destination waypoint, its y-axis is perpendicular to the ground track, and its's z-axis coincides with the down axis of the NED axis system. The guidance axis system is obtained by rotating the NED axis system through the track heading angle ψ_{track}, and by moving its origin to the location of the source waypoint.

To obtain the cross-track error and the in-track distance, the aircraft position is first transformed from the NED axes to the guidance axes. The cross-track error is then simply the y-component in the guidance axis system, and the in-track distance is simply the x-component in the guidance axis system.

The aircraft's position is transformed from the NED axis system to the guidance axis system with the following equation

$$\begin{bmatrix} x \\ y \end{bmatrix} = \begin{bmatrix} \cos\psi_{track} & \sin\psi_{track} \\ -\sin\psi_{track} & \cos\psi_{track} \end{bmatrix} \begin{bmatrix} N - N_{\text{src}} \\ E - E_{\text{src}} \end{bmatrix} \tag{10.3}$$

The aircraft is following the ground track when the aircraft heading equals the ground track heading, and the cross track error is zero. The aircraft has reached the destination waypoint when its in-track distance equals the length of the ground track.

A guidance controller is required to control the cross track error to zero, and a waypoint scheduler is required to select the next destination waypoint when the current waypoint is reached.

10.2 Guidance Controller

The control architecture of the guidance controller is shown in Figure 36.

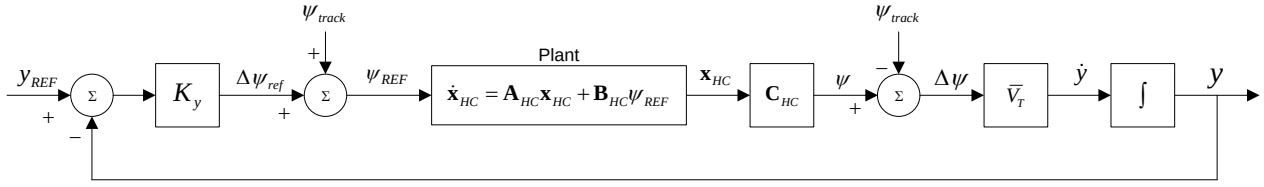

Figure 36 – Guidance Controller Block Diagram

The guidance controller generates a heading command ψ_{ref} proportional to the cross track error. The heading command produces a rate of change in the cross track error that is proportional to the heading of the aircraft relative to the ground track heading $\psi - \psi_{track}$, and the ground speed of the aircraft $\bar{V}_{ground}$.

Consider the diagrams in Figure 37 and Figure 38, which shows the aircraft flying at a constant heading relative to the ground track. The rate of change of the cross track error is the projection of the aircraft ground speed into the cross track axis, which is represented by the following equation

$$\dot{y} = \bar{V}\sin(\psi - \psi_{track}) \tag{10.4}$$

For small heading angles relative to the ground track heading, $\sin(\psi - \psi_{track}) \approx (\psi - \psi_{track})$ and equation (10.4) may be simplified to

$$\dot{y} = \bar{V}(\psi - \psi_{track}) \tag{10.5}$$

The natural integration from the cross track error rate to the cross track error makes the system type 1, which means it should be able to follow a ground track reference with zero error at steady state.

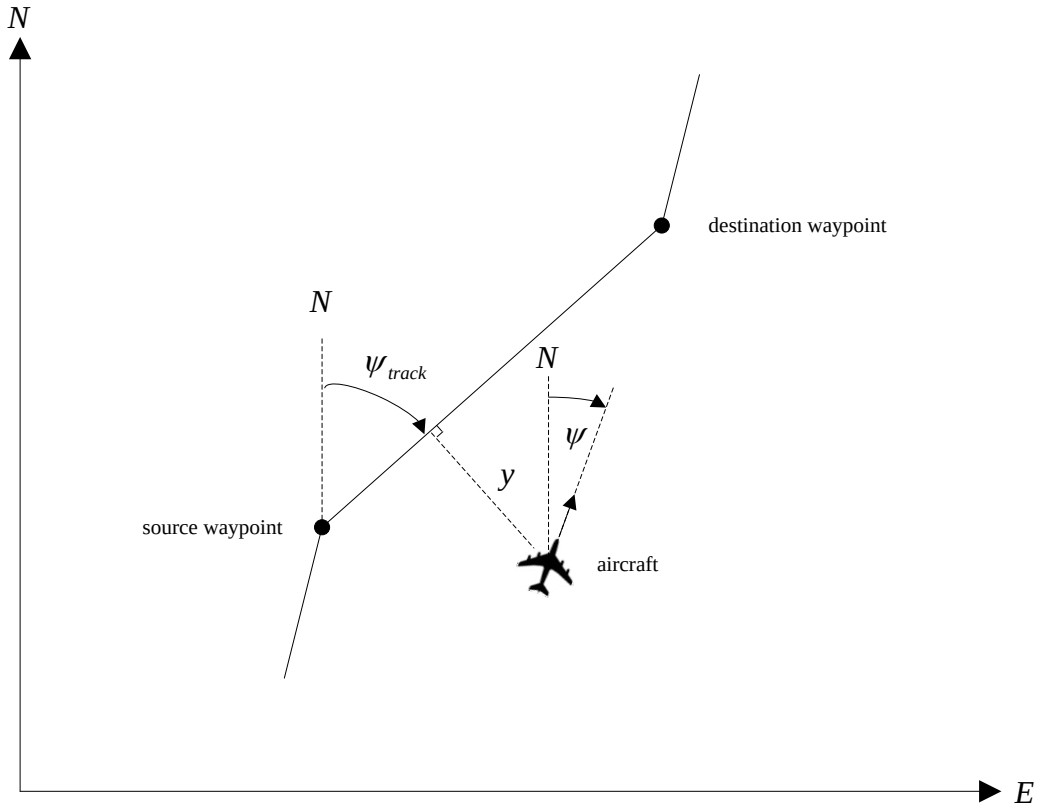

Figure 37 – Aircraft heading, ground track heading, and cross-track error

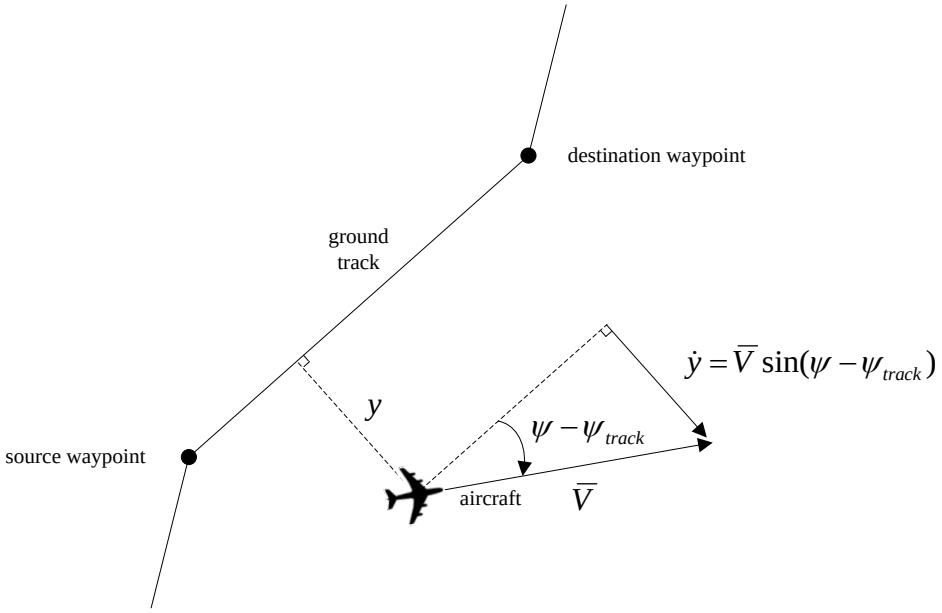

Figure 38 – Cross track error rate

The plant is the lateral dynamics with the pitch rate damper, roll angle controller, and heading controller given by equation (9.29), but augmented with a cross track error state. The output matrix $\mathbf{C}_{\psi}$ extracts the heading angle ψ from the state vector. The track heading ψ_{track} is then subtracted, and the result is multiplied with the ground speed $\overline{V}$ to obtain the cross track error rate $\dot{y}$, which in turn is fed to a natural integrator to become the cross track error state y. In practice, the cross track error is obtained from the GPS latitude and longitude transformed to NED axes, and then transformed to the guidance axes.

The guidance controller produces a heading command $\Delta\psi$ relative to the ground track heading ψ_{track}.Since the eading controller expects a heading reference relative to north, the ground track heading must be added to the relative heading command before sending it to the heading controller.

$$\psi_{ref} = \Delta\psi + \psi_{track} \tag{10.6}$$

The guidance controller expects the waypoint scheduler to supply it with a destination waypoint and a source waypoint from which it extracts the track heading ψ_{track} and the cross track error y.

The design of the guidance controller consists of determining an appropriate value for the proportional gain K_y. First, the state space model of the heading control dynamics is augmented with the cross track error state by

$$\begin{bmatrix} \dot{\mathbf{x}}_{HC} \\ \dot{y} \end{bmatrix} = \begin{bmatrix} \mathbf{A}_{HC} & 0 \\ \mathbf{C}_{\dot{y}} & 0 \end{bmatrix} \begin{bmatrix} \mathbf{x}_{HC} \\ y \end{bmatrix} + \begin{bmatrix} \mathbf{B}_{HC} \\ 0 \end{bmatrix} \psi_{ref} + \begin{bmatrix} \mathbf{0}_{7x1} \\ -1 \end{bmatrix} \psi_{track} \tag{10.7}$$

with

$$\mathbf{C}_{\dot{y}} = \begin{bmatrix} \mathbf{0}_{1x6} & \bar{V}_T \end{bmatrix} \tag{10.8}$$

The transfer function from heading angle reference (relative to the track heading) to the cross track error is obtained from the state space model through

$$\frac{y(s)}{\Delta\psi_{ref}(s)} = \frac{1}{s}\mathbf{C}_{\dot{y}}(s\mathbf{I} - \mathbf{A}_{HC})^{-1}\mathbf{B}_{HC} \tag{10.9}$$

The root locus of the guidance controller with respect to the proportional gain K_y is shown in Figure 39 and Figure 40 (zoomed in). The proportional gain is selected to place the dominant closed loop pole on the real axis with a response that is an order of magnitude slower than the closed-loop poles of the heading angle controller, to ensure time-scale separation.

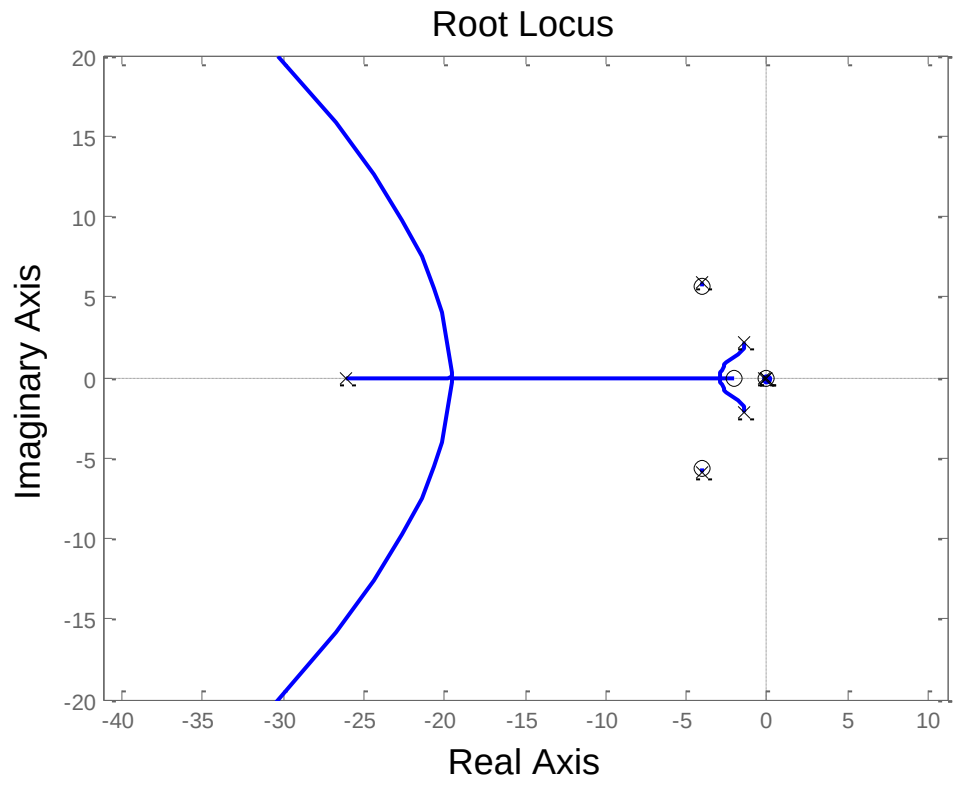

Figure 39 – Guidance Controller Root Locus

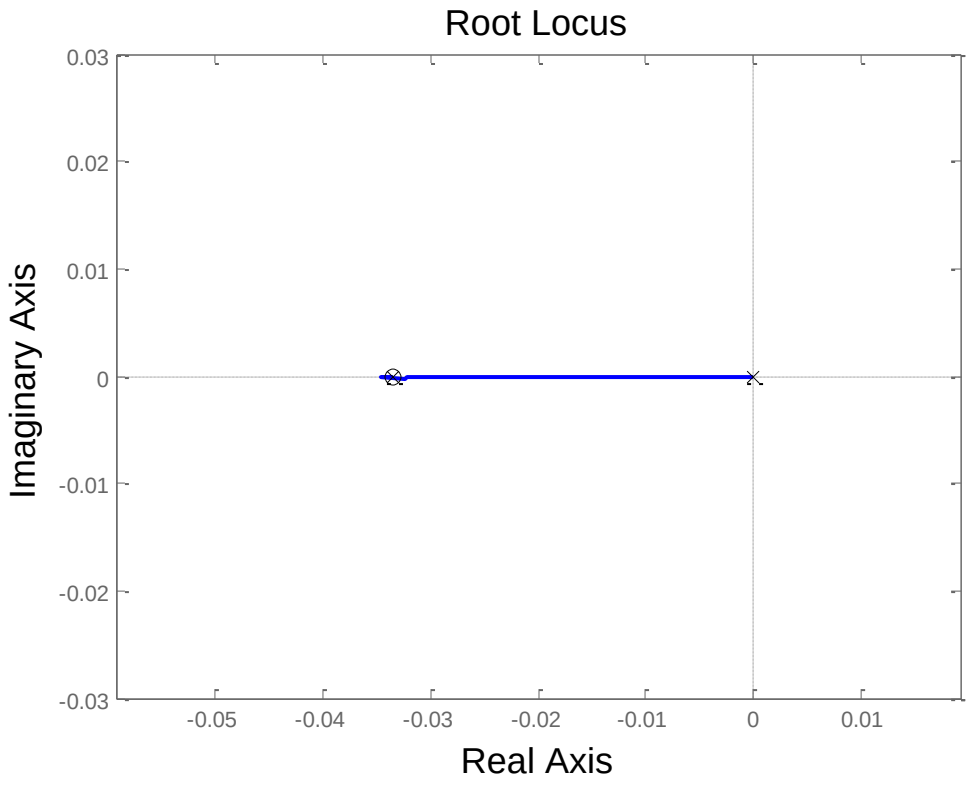

Figure 40 – Guidance Controller Root Locus (Zoomed In)

After adding the guidance controller, the encapsulated closed loop dynamics of the aircraft with the guidance controller included, is given in state space form as

$$\begin{bmatrix} \dot{\mathbf{x}}_{HC} \\ \dot{y} \end{bmatrix} = \begin{bmatrix} \mathbf{A}_{HC} & -\mathbf{B}_{HC} K_y \\ \mathbf{C}_{\dot{y}} & 0 \end{bmatrix} \begin{bmatrix} \mathbf{x}_{HC} \\ y \end{bmatrix} \tag{10.10}$$

The closed-loop dynamics does not present a reference input, since the ground track reference is implicit in the cross-track error state.

10.3 Waypoint Scheduler

A waypoint scheduler is used to schedule the next straight-line segment to be followed once the aircraft has reached the end of the current straight-line segment. The waypoint scheduler uses the in-track distance x to determine when the current destination waypoint has been reached. When the in-track distance x from the source waypoint is greater than the length of the straight line segment L_{track}, then the destination waypoint has been reached. The next waypoint in the waypoint list must then become the destination waypoint, and the current destination waypoint must become the source waypoint.

11 Aircraft State Estimation

Up to this point, our flight controllers have assumed that the aircraft state vector (position, velocity, attitude, angular rates) is available for feedback. In practice, the aircraft state vector is not directly available for measurement, but has to be estimated from sensor measurements.

The following sensors are typically available on unmanned aerial vehicles:

- GPS
- Accelerometers, Gyroscopes
- Magnetometer
- Pressure sensors (absolute pressure, pitot sensor)

An extended Kalman filter (EKF) is used to estimate the state vector from these sensors measurements, and from mathematical models of the aircraft environment (gravity vector, magnetic field vector).

11.1 Kinematic State Estimator

The block diagram of the kinematic state estimator is shown in Figure 41.

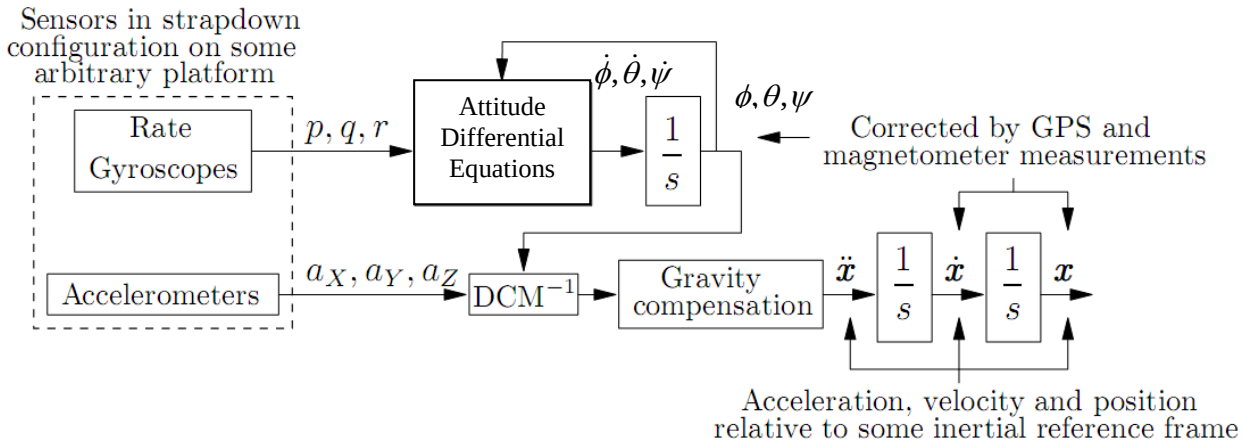

Figure 41 – Kinematic State Estimator Block Diagram (Simplified)

The kinematic state estimator estimates the vehicle's attitude, velocity and position by propagating a kinematic dynamic model based on three-axis accelerometer and gyroscope measurements, and correcting the propagated states using sensor measurements from the GPS sensor, three-axis acceleratometers and magnetometer.

The vehicle is equipped with rate gyroscopes and accelerometers in a strapdown configuration. The strapdown term indicates that the various sensors are fixed to the platform and rotates and translates along with it. The measured angular velocity with respect to some inertial reference frame serve as inputs to attitude differential equations, which are then integrated to obtain the vehicle's attitude. Next, the accelerometer measurements are coordinated in the inertial reference frame using the inverse direction cosine matrix (which is obtained from the quaternion attitude). After compensating for gravity, the accelerations are integrated twice to obtain the platform's velocity and displacement with respect to the inertial reference frame.

The attitude, velocity and position states are therefore obtained by numerically integrating the gyroscope and accelerometer sensor measurements from some initial state. However, due to errors in the initial condition, biases in the gyroscope and accelerometer measurements, and numerical integration errors, the propagated state estimate tends to drift away from the actual state over time. The GPS and magnetometer measurements, which provide direct and indirect measurements of the attitude, velocity and position, are therefore used to correct the state estimates.

An extended Kalman filter (EKF) is used to combine the state propagation from the gyroscope and accelerometer measuements with the corrections from the GPS and magnetometer measurements in an optimal way.

The advantage of the kinematic state estimator is that it does not require knowledge of the vehicle's kinetic model, such as knowledge of the aerodynamic forces and moments, and is therefore vehicle independent.

The kinematic state estimator is an extended Kalman filter that iteratively estimates the following state estimate vector

$$\hat{\mathbf{x}} = \begin{bmatrix} \hat{N} & \hat{E} & \hat{D} & \hat{v}_N & \hat{v}_E & \hat{v}_D & \hat{\phi} & \hat{\theta} & \hat{\psi} \end{bmatrix}^T \tag{11.1}$$

where $\hat{N}$, $\hat{E}$, $\hat{D}$ and $\hat{v}_N$, $\hat{v}_E$, $\hat{v}_D$ are the position and velocity estimates of the vehicle in inertial axes, and $\hat{\phi}$, $\hat{\theta}$, $\hat{\psi}$ is the attitude estimate of the vehicle expressed as roll, pitch and yaw.

Execution

At each sampling instant the kinematic state estimator executes the following steps sequentially:

1. Read sensors
    a. Three-axis accelerometer measurements in body axes
    b. Three-axis gyroscope measurements in body axes
    c. GPS latitude, longitude and altitude in inertial axes
    d. Three-axis magnetometer measurements in body axes
2. Propagate position and velocity estimates in inertial axes by numerically integrating the acceleration measurements obtained from the three-axis accelerometers. (The attitude estimate from the previous sampling instant is used to transform the body axes accelerometer measurements to inertial axes.)
3. Correct the position and velocity estimate using the measured position obtained from the GPS sensor.
4. Propagate the attitude estimate by numerically integrating the angular rate measurements obtained from the three-axis gyroscopes. (The attitude estimate from the previous sampling instant is used to transform the body axes gyroscope measurements to roll rate, pitch rate and yaw rate.)
5. Propagate the attitude estimate error covariance matrix.
6. Calculate the Kalman filter gain to be used for the measurement correction.
7. Calculate measured gravity and geomagnetic field vectors in body axes from sensor measurements
8. Calculate reference gravity and geomagnetic field vectors in inertial axes from onboard gravity and geomagnetic field models
9. Calculate the "measured" attitude from the measured vectors in body axes and the reference vectors in inertial axes using either the TRIAD method or the Tilt/Heading method.
10. Correct the attitude estimate using the attitude obtained from the gravity and geomagnetic field vectors.
11. Correct the attitude state error covariance matrix.
12. Wait for the next sampling instant, then repeat

Step 1: Read Sensors

At the start of each new sampling instant, sensor measurements are obtained from the accelerometers, gyroscopes, GPS and magnetometer.

The GPS gives the position measurement as a latitude, longitude and altitude above mean sea level (MSL). The position measurement is converted to a NED position with

$$\begin{aligned} N_{meas} &= (Lat_{GPS} - Lat_{Runway})R_{Earth} \\ E_{meas} &= (Lon_{GPS} - Lon_{Runway})R_{Earth}\cos(Lat_{GPS}) \\ D_{meas} &= -(h_{GPS} - h_{Runway}) \end{aligned} \tag{11.2}$$

where N_{meas}, E_{meas}, D_{meas} is the measured NED position of the vehicle, Lat_{GPS}, Lon_{GPS}, h_{GPS} are the GPS latitude, longitude and altitude of the vehicle, Lat_{Runway}, Lon_{Runway}, h_{Runway} are the latitude, longitude and altitude corresponding to the origin of the NED axis system, and R_{Earth} is the radius of the Earth at the equator.

Step 2: Propagate Position and Velocity Estimate

The vehicle position and velocity estimates are propagated in the inertial axes by numerically integrating the acceleration measurements obtained from the three-axis accelerometers. (The attitude estimate from the previous sampling instant is used to transform the body axes accelerometer measurements to inertial axes.)

First, the accelerometer measurements are transformed from body axes to inertial axes using the estimated direction cosine matrix calculated from the attitude estimate at the previous sampling instant

$$D\hat{C}M_{I\to B} = \begin{bmatrix} \cos\hat{\psi}\cos\hat{\theta} & \sin\hat{\psi}\cos\hat{\theta} & -\sin\hat{\theta} \\ \cos\hat{\psi}\sin\hat{\theta}\sin\hat{\phi} - \sin\hat{\psi}\cos\hat{\phi} & \sin\hat{\psi}\sin\hat{\theta}\sin\hat{\phi} + \cos\hat{\psi}\cos\hat{\phi} & \cos\hat{\theta}\sin\hat{\phi} \\ \cos\hat{\psi}\sin\hat{\theta}\cos\hat{\phi} + \sin\hat{\psi}\sin\hat{\phi} & \sin\hat{\psi}\sin\hat{\theta}\cos\hat{\phi} + \cos\hat{\psi}\sin\hat{\phi} & \cos\hat{\theta}\cos\hat{\phi} \end{bmatrix} \tag{11.3}$$

where $\hat{\phi}$, $\hat{\theta}$, $\hat{\psi}$ are the roll, pitch and yaw estimates from the previous sampling instant, and $D\hat{C}M_{I\to B}$ is the estimated direction cosine matrix that transforms vectors from inertial axes to body axes.

The acceleration of the vehicle in inertial axes equals the raw accelerometer measurements in inertial axes minus gravitational acceleration. (The accelerometers on a stationary vehicle will measure an apparent acceleration of 9.8 m/s upward due to gravity.)

$$\begin{bmatrix} a_N \\ a_E \\ a_D \end{bmatrix} = D\hat{C}M^T_{I\to B}\begin{bmatrix} a^B_{x,meas} \\ a^B_{y,meas} \\ a^B_{z,meas} \end{bmatrix} + \begin{bmatrix} 0 \\ 0 \\ g \end{bmatrix} \tag{11.4}$$

where a_N, a_E, a_D, is the acceleration of the vehicle in inertial axes, $a^B_{x,meas}$, $a^B_{y,meas}$, $a^B_{z,meas}$ are the raw accelerometer measurements in body axes, and g is gravitational acceleration.

The position estimate is propagated forward in time by numerically integrating the velocity estimate at the previous sampling instant

$$\begin{bmatrix} \overline{N}(k) \\ \overline{E}(k) \\ \overline{D}(k) \end{bmatrix} = \begin{bmatrix} \hat{N}(k-1) \\ \hat{E}(k-1) \\ \hat{D}(k-1) \end{bmatrix} + \begin{bmatrix} \hat{v}_N(k-1) \\ \hat{v}_E(k-1) \\ \hat{v}_D(k-1) \end{bmatrix}\Delta T \tag{11.5}$$

where $\overline{N}(k)$, $\overline{E}(k)$, $\overline{D}(k)$ is the position estimate propagated to the current sampling instant, $\hat{N}(k-1)$, $\hat{E}(k-1)$, $\hat{D}(k-1)$ and $\hat{v}_N(k-1)$, $\hat{v}_E(k-1)$, $\hat{v}_D(k-1)$ are the position and velocity estimates from the previous sampling instant, and ΔT is the sampling period.

The velocity estimate is propagated forward in time by numerically integrating the acceleratometer measurements transformed to inertial axes and corrected for gravity

$$\begin{bmatrix} \overline{v}_N(k) \\ \overline{v}_E(k) \\ \overline{v}_D(k) \end{bmatrix} = \begin{bmatrix} \hat{v}_N(k-1) \\ \hat{v}_E(k-1) \\ \hat{v}_D(k-1) \end{bmatrix} + \begin{bmatrix} a_N \\ a_E \\ a_D \end{bmatrix}\Delta T \tag{11.6}$$

where $\overline{v}_N(k)$, $\overline{v}_E(k)$, $\overline{v}_D(k)$ is the velocity estimate propagated to the current sampling instant, $\hat{v}_N(k-1)$, $\hat{v}_E(k-1)$, $\hat{v}_D(k-1)$ is the velocity estimates from the previous sampling instant, and ΔT is the sampling period.

Step 3: Correct Position and Velocity Estimates based on Sensor Measurements

The propagated position and velocity estimates are corrected after receiving the measured position from the GPS sensor.

$$\begin{aligned}
\hat{N}(k) &= \bar{N}(k) + L_{11}\left[N_{meas} - \bar{N}(k)\right] + L_{12}\left[v_{N,meas} - \bar{v}_N(k)\right] \\
\hat{E}(k) &= \bar{E}(k) + L_{21}\left[E_{meas} - \bar{E}(k)\right] + L_{22}\left[v_{E,meas} - \bar{v}_E(k)\right] \\
\hat{D}(k) &= \bar{D}(k) + L_{31}\left[D_{meas} - \bar{D}(k)\right] + L_{32}\left[v_{D,meas} - \bar{v}_D(k)\right] \\
\hat{v}_N(k) &= \bar{v}_N(k) + L_{41}\left[N_{meas} - \bar{N}(k)\right] + L_{42}\left[v_{N,meas} - \bar{v}_N(k)\right] \\
\hat{v}_E(k) &= \bar{v}_E(k) + L_{51}\left[E_{meas} - \bar{E}(k)\right] + L_{52}\left[v_{E,meas} - \hat{v}_E(k)\right] \\
\hat{v}_D(k) &= \bar{v}_D(k) + L_{61}\left[D_{meas} - \bar{D}(k)\right] + L_{62}\left[v_{D,meas} - \bar{v}_D(k)\right]
\end{aligned} \tag{11.7}$$

The position and velocity estimates are corrected separately using fixed Kalman filter gains, and the state error covariance matrices are neither propagated nor corrected.

Step 4: Propagate Attitude Estimate

The attitude estimate is propagated by numerically integrating the angular rate measurements obtained from the three-axis gyroscopes. (The attitude estimate from the previous sampling instant is used to transform the body axes gyroscope measurements to roll rate, pitch rate and yaw rate.)

First, the roll rate, pitch rate and yaw rate are calculated from the gyroscope measurements in body axes using the attitude state estimate from the previous time instant, with

$$\begin{bmatrix} \dot{\phi}_{meas} \\ \dot{\theta}_{meas} \\ \dot{\psi}_{meas} \end{bmatrix} = \begin{bmatrix} 1 & \sin\hat{\phi}(k-1)\tan\hat{\theta}(k-1) & \cos\hat{\phi}(k-1)\tan\hat{\theta}(k-1) \\ 0 & \cos\hat{\phi}(k-1) & -\sin\hat{\theta}(k-1) \\ 0 & \sin\hat{\phi}(k-1)\sec\hat{\theta}(k-1) & \cos\hat{\phi}(k-1)\sec\hat{\theta}(k-1) \end{bmatrix} \begin{bmatrix} P_{gyro} \\ Q_{gyro} \\ R_{gyro} \end{bmatrix} \tag{11.8}$$

The attitude estimate is propagated forward in time by numerically integrating the roll rate, pitch rate and yaw rate obtained from the equation (11.8)

$$\begin{bmatrix} \bar{\phi}(k) \\ \bar{\theta}(k) \\ \bar{\psi}(k) \end{bmatrix} = \begin{bmatrix} \hat{\phi}(k-1) \\ \hat{\theta}(k-1) \\ \bar{\psi}(k-1) \end{bmatrix} + \begin{bmatrix} \dot{\phi}_{meas} \\ \dot{\theta}_{meas} \\ \dot{\psi}_{meas} \end{bmatrix} \Delta T \tag{11.9}$$

where $\bar{\phi}(k)$, $\bar{\theta}(k)$, $\psi(k)$ is the attitude estimate propagated to the current sampling instant, $\hat{\phi}(k-1)$, $\hat{\theta}(k-1)$, $\hat{\psi}(k-1)$ is the attitude estimate from the previous sampling instant, and ΔT is the sampling period.

Step 5: Propagate Attitude Estimation Error Covariance Matrix

After propagating the attitude estimated itself, the attitude estimation error covariance matrix must also be propagated, since it will be used to calculate the Kalman filter gain

$$\mathbf{M}(k) = \mathbf{A}_d \mathbf{P}(k-1)\mathbf{A}_d^T + \mathbf{B}_d \mathbf{Q} \mathbf{B}_d^T \tag{11.10}$$

where $\mathbf{M}(k)$ is the attitude estimation error covariance matrix propagated to this sampling instant, $\mathbf{P}(k-1)$ is the corrected attitude estimation error from the previous sampling instant, $\mathbf{A}_d$ and $\mathbf{B}_d$ are the discrete state transition matrix and the discrete input matrix respectively, and $\mathbf{Q}$ is the process noise covariance matrix.

The discrete state transition matrix $\mathbf{A}_d$ and the discrete input matrix $\mathbf{B}_d$ have been derived as

$$
\begin{aligned}
A_{11} &= 1 + \Delta T \cos\hat{\phi}(k-1)\tan\hat{\theta}(k-1)Q_{gyro} - \Delta T \sin\hat{\phi}(k-1)\tan\hat{\theta}(k-1)R_{gyro} \\
A_{12} &= \sin\hat{\phi}(k-1)/\cos^2\hat{\theta}(k-1)Q_{gyro} - \Delta T \cos\hat{\phi}(k-1)\cos^2\hat{\theta}(k-1)R_{gyro} \\
A_{13} &= 0 \\
A_{21} &= -\Delta T \sin\hat{\phi}(k-1)Q_{gyro} - \Delta T \cos\hat{\phi}(k-1)R_{gyro} \\
A_{22} &= 1 \\
A_{23} &= 0 \\
A_{31} &= \Delta T \cos\hat{\phi}(k-1)/\cos\hat{\theta}(k-1)Q_{gyro} - \Delta T \sin\hat{\phi}(k-1)\cos\hat{\theta}(k-1)R_{gyro} \\
A_{32} &= \Delta T \sin\hat{\phi}(k-1)\tan\hat{\theta}(k-1)/\cos\hat{\theta}(k-1)Q_{gyro} + \Delta T \cos\hat{\phi}(k-1)\tan\hat{\theta}(k-1)/\cos\hat{\theta}(k-1)R_{gyro} \\
A_{33} &= 1
\end{aligned}
\tag{11.11}
$$

and

$$
B_d = \begin{bmatrix} 1 & \sin\hat{\phi}(k-1)\tan\hat{\theta}(k-1) & \cos\hat{\phi}(k-1)\tan\hat{\theta}(k-1) \\ 0 & \cos\hat{\phi}(k-1) & -\sin\hat{\theta}(k-1) \\ 0 & \sin\hat{\phi}(k-1)\sec\hat{\theta}(k-1) & \cos\hat{\phi}(k-1)\sec\hat{\theta}(k-1) \end{bmatrix} \Delta T \tag{11.12}
$$

Step 6: Calculate the Kalman filter gain

The Kalman filter gain is calculated using

$$
\mathbf{L}(k) = \mathbf{M}(k)\mathbf{H}^T(k)\left[\mathbf{H}(k)\mathbf{M}(k)\mathbf{H}^T(k) + \mathbf{R}\right]^{-1} \tag{11.13}
$$

where $\mathbf{L}(k)$ is the Kalman filter gain, $\mathbf{H}(k)$ is the output matrix, and $\mathbf{R}$ is the measurement noise covariance matrix. Since the output vector is the "measured" roll, pitch, and yaw, the output matrix $\mathbf{H}(k)$ is simply the identity matrix

$$
\mathbf{H} = \mathbf{I}_{3x3} \tag{11.14}
$$

Step 7: Calculate Measured Gravity and Magnetic Field Vectors in Body Axes

In order to determine the attitude of the vehicle, the gravity and magnetic field vectors must be known in both body axes and inertial axes. The measured gravity and magnetic field vectors in body axes are obtained from the sensor measurements.

The measured gravity vector in body axes is calculated by subtracting the specific acceleration measured by the accelerometers from the total acceleration measured by the GPS.

The total acceleration measured by the GPS is calculated by numerically differentiating the velocity in inertial axes

$$
\mathbf{a}^I_{total,meas} = \frac{\hat{\mathbf{v}}_{NED}(k) - \hat{\mathbf{v}}_{NED}(k-1)}{\Delta T} \tag{11.15}
$$

The total acceleration is transformed to body axes using the estimated direction cosine matrix from the previous sampling instant

$$
\mathbf{a}^B_{total,meas} = D\hat{C}M_{I\to B}\mathbf{a}^I_{total,meas} \tag{11.16}
$$

Finally, the measured gravity vector in body axes is calculated by subtracting the subtracting the specific acceleration measured by the accelerometers from the total acceleration

$$\mathbf{g}_{meas}^{B} = \mathbf{a}_{total,meas}^{B} - \mathbf{a}_{specific,meas}^{B} \tag{11.17}$$

The measured magnetic field vector in body axes is obtained directly from the magnetometer sensor

$$\mathbf{m}_{meas}^{B} = \begin{bmatrix} m_x^B & m_y^B & m_z^B \end{bmatrix}^T \tag{11.18}$$

The measured gravity and geomagnetic field vectors in body axes are now available for determining the attitude in the next steps.

Step 8: Obtain Reference Gravity and Magnetic Field Vectors

The reference gravity and magnetic field vectors in inertial axes are obtained from mathematical models of the Earth's gravity field and of the geomagnetic field, and are typically functions of the latitude, longitude and altitude of the vehicle.

$$\begin{aligned} \mathbf{g}_{ref}^{I} &= \begin{bmatrix} g_N(lat, lon, alt) & g_E(lat, lon, alt) & g_D(lat, lon, alt) \end{bmatrix}^T \\ &\approx \begin{bmatrix} 0 & 0 & g \end{bmatrix}^T \end{aligned} \tag{11.19}$$

$$\mathbf{m}_{ref}^{I} = \begin{bmatrix} m_N(lat, lon, alt) & m_E(lat, lon, alt) & m_D(lat, lon, alt) \end{bmatrix}^T \tag{11.20}$$

When operating the vehicle over short distances, it is often sufficient to assume that the reference gravity vector and the reference magnetic field vector in inertial axes are constant. In this case, the latitude, longitude and altitude of the runway is used to calculate the constant reference vectors.

The reference gravity and geomagnetic field vectors in inertial axes are now available for determining the attitude in the next steps.

Step 9: Calculate the "Measured" Attitude from the Measured Vectors and Reference Vectors

The "measured" attitude is calculated from the measured gravity and geomagnetic field vectors in body axes and the reference gravity and geomagnetic field vectors in inertial axes, using either the TRIAD method, or the Tilt/Heading method.

TRIAD Method

The TRIAD algorithm calculates the direction cosine matrix that represents the attitude of the body axes relative to the reference axes, using two measured vectors in body axes and their corresponding modelled vectors in inertial axes.

Given two measured vectors $\mathbf{g}_{meas}^{B}$ and $\mathbf{m}_{meas}^{B}$ in body axes, and two corresponding reference vectors $\mathbf{g}_{ref}^{I}$ and $\mathbf{m}_{ref}^{I}$ in inertial axes, the objective is to determine the direction cosine matrix $DCM_{I\to B}$ that satisfies

$$\mathbf{g}_{meas}^{B} = DCM_{I\to B}\mathbf{g}_{ref}^{I} \tag{11.21}$$

$$\mathbf{m}_{meas}^{B} = DCM_{I\to B}\mathbf{m}_{ref}^{I} \tag{11.22}$$

The TRIAD algorithm is summarised in three steps:

1. Construct a TRIAD of orthonormal vectors $\mathbf{s}_1$, $\mathbf{s}_2$ and $\mathbf{s}_3$ in body axes from the measured vectors $\mathbf{g}^B_{meas}$ and $\mathbf{m}^B_{meas}$.

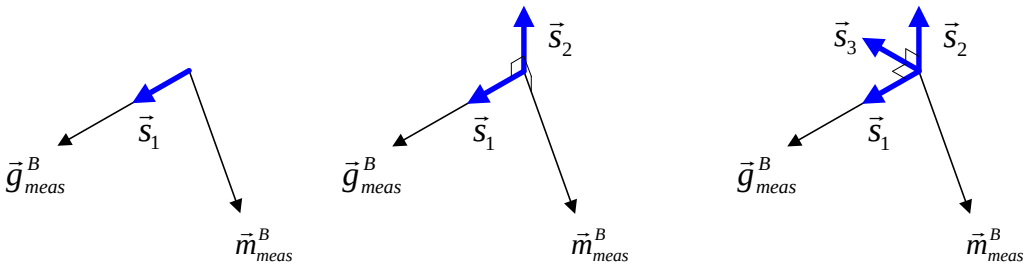

Figure 42 – Constructing the body axes TRIAD.

$$\begin{aligned}\mathbf{s}_1 &= \frac{\mathbf{g}^B_{meas}}{\left\|\mathbf{g}^B_{meas}\right\|}\\ \mathbf{s}_2 &= \frac{\mathbf{s}_1 \times \mathbf{m}^B_{meas}}{\left\|\mathbf{s}_1 \times \mathbf{m}^B_{meas}\right\|}\\ \mathbf{s}_3 &= \frac{\mathbf{s}_1 \times \mathbf{s}_2}{\left\|\mathbf{s}_1 \times \mathbf{s}_2\right\|}\end{aligned} \tag{11.23}$$

2. Construct a TRIAD of orthonormal vectors $\mathbf{r}_1$, $\mathbf{r}_2$ and $\mathbf{r}_3$ in inertial axes from the reference vectors $\mathbf{g}^I_{ref}$ and $\mathbf{m}^I_{ref}$.

$$\begin{aligned}\mathbf{r}_1 &= \frac{\mathbf{g}^I_{ref}}{\left\|\mathbf{g}^I_{ref}\right\|}\\ \mathbf{r}_2 &= \frac{\mathbf{r}_1 \times \mathbf{m}^I_{ref}}{\left\|\mathbf{r}_1 \times \mathbf{m}^I_{ref}\right\|}\\ \mathbf{r}_3 &= \frac{\mathbf{r}_1 \times \mathbf{r}_2}{\left\|\mathbf{r}_1 \times \mathbf{r}_2\right\|}\end{aligned} \tag{11.24}$$

3. Calculate the direction cosine matrix that transforms the inertial TRIAD $\mathbf{r}_1$, $\mathbf{r}_2$ and $\mathbf{r}_3$ to the body TRIAD $\mathbf{s}_1$, $\mathbf{s}_2$ and $\mathbf{s}_3$

$$\begin{aligned}\begin{bmatrix}\mathbf{s}_1 & \mathbf{s}_2 & \mathbf{s}_3\end{bmatrix} &= DCM_{I\to B}\begin{bmatrix}\mathbf{r}_1 & \mathbf{r}_2 & \mathbf{r}_3\end{bmatrix}\\ DCM_{I\to B} &= \begin{bmatrix}\mathbf{s}_1 & \mathbf{s}_2 & \mathbf{s}_3\end{bmatrix}\begin{bmatrix}\mathbf{r}_1 & \mathbf{r}_2 & \mathbf{r}_3\end{bmatrix}^{-1}\end{aligned} \tag{11.25}$$

Once the direction cosine matrix has been determined, the measured roll, pitch and yaw can be calculated with

$$\begin{aligned}\phi_{meas} &= \arctan\frac{DCM_{23}^{I\to B}}{DCM_{33}^{I\to B}}\\ \theta_{meas} &= -\arcsin DCM_{13}^{I\to B}\\ \psi_{meas} &= \arctan\frac{DCM_{12}^{I\to B}}{DCM_{11}^{I\to B}}\end{aligned} \tag{11.26}$$

The measured roll, pitch and yaw ϕ_{meas}, θ_{meas}, ψ_{meas} will be used to perform the attitude estimate correction.

Tilt / Heading Method

Since the TRIAD method is numerically intensive, an alternate method is called the Tilt / Heading method is sometimes used. The tilt/heading method is based on the premise that the roll and pitch angles of the vehicle can be determined from the tilt of the gravity vector, and the yaw angle of the vehicle can be determined from the magnetometer heading.

The roll and pitch angles are calculated from the measured gravity vector in body axes

$$\begin{aligned}\phi_{meas} &= \arctan\frac{g_y^B}{g_z^B}\\ \theta_{meas} &= \arctan\left(\frac{-g_x^B}{\sqrt{(g_y^B)^2+(g_z^B)^2}}\right)\end{aligned} \tag{11.27}$$

The yaw angle is calculated by comparing the magnetometer measurements in body axes with the known magnetic field reference in inertial axes. However, the effect of the vehicle's tilt must be removed, and the axial and lateral components of the measured vector must be projected into the same plane as the North and East components of the reference vector, as follows

$$\begin{aligned}\begin{bmatrix}m_x''\\ m_y''\\ m_z''\end{bmatrix} &= \mathbf{T}_\theta^{-1}\mathbf{T}_\phi^{-1}\begin{bmatrix}m_x^B\\ m_y^B\\ m_z^B\end{bmatrix}\\ \begin{bmatrix}m_x''\\ m_y''\\ m_z''\end{bmatrix} &= \begin{bmatrix}\cos\theta & \sin\theta\sin\phi & \sin\theta\cos\phi\\ 0 & \cos\phi & -\sin\phi\\ -\sin\theta & \cos\theta\sin\phi & \cos\theta\cos\phi\end{bmatrix}\begin{bmatrix}m_x^B\\ m_y^B\\ m_z^B\end{bmatrix}\end{aligned} \tag{11.28}$$

The yaw angle can then be calculated using

$$\psi_{meas} = \arctan\left(\frac{m_x''}{m_y''}\right) - \arctan\left(\frac{m_N^I}{m_E^I}\right) \tag{11.29}$$

The measured roll, pitch and yaw ϕ_{meas}, θ_{meas}, ψ_{meas} will be used to perform the attitude estimate correction.

Step 10: Correct Attitude Estimate based on Sensor Measurements

The propagated attitude estimate is corrected using the measured roll, pitch and yaw obtained from either the TRIAD method or the Tilt / Heading method. The Kalman filter gain $\mathbf{L}(k)$, which was calculated in a previous step, is used to perform the correction.

$$\begin{bmatrix} \hat{\phi}(k) \\ \hat{\theta}(k) \\ \hat{\psi}(k) \end{bmatrix} = \begin{bmatrix} \bar{\phi}(k) \\ \bar{\theta}(k) \\ \bar{\psi}(k) \end{bmatrix} + \mathbf{L}(k) \begin{bmatrix} \phi_{meas} - \bar{\phi}(k) \\ \theta_{meas} - \bar{\theta}(k) \\ \psi_{meas} - \bar{\psi}(k) \end{bmatrix} \tag{11.30}$$

Step 11: Correct Attitude Estimation Error Covariance Matrix

The attitude estimation error covariance matrix is updated to reflect the correction based on the sensor measurements with

$$\mathbf{P}(k) = \left[\mathbf{I} - \mathbf{L}(k)\mathbf{H}(k)\right]\mathbf{M}(k)\left[\mathbf{I} - \mathbf{L}(k)\mathbf{H}(k)\right]^T + \mathbf{L}(k)\mathbf{R}\mathbf{L}^T(k) \tag{11.31}$$

where $\mathbf{P}(k)$ is the corrected attitude estimation error covariance matrix, $\mathbf{L}(k)$ is the Kalman filter gain, $\mathbf{M}(k)$ is the propagated attitude estimation error covariance matrix, and $\mathbf{H}(k)$ is the output matrix, and $\mathbf{R}$ is the measurement noise covariance matrix.

The corrected attitude estimation error covariance matrix $\mathbf{P}(k)$ will be used for the next iteration of the kinematic state estimator.

Appendix A – Example Aircraft Data

The example aircraft is a CAP 232 0.90 size, off-the-shelf Radio Controlled (RC) aerobatic aircraft fitted with a GMS 1.20 cubic inch methanol engine. The parameters for this UAV were extracted from [5] where they were obtained using AVL. The parameters are listed below and are applicable to a 30 m/s straight and level flight trim condition.

Inertia:

$$m = 5.0 \text{ kg} \tag{8.1}$$

$$I_{xx} = 0.200 \text{ kgm}^2 \tag{8.2}$$

$$I_{yy} = 0.360 \text{ kgm}^2 \tag{8.3}$$

$$I_{zz} = 0.525 \text{ kgm}^2 \tag{8.4}$$

Geometry:

$$\bar{c} = 0.30 \text{ m} \tag{8.5}$$

$$b = 1.73 \text{ m} \tag{8.6}$$

$$S = 0.50 \text{ m}^2 \tag{8.7}$$

$$A = 5.97 \tag{8.8}$$

Aerodynamic:

$$e = 0.85 \qquad C_{D_0} = 0.0200 \tag{8.9}$$

$$C_{L_0} = 0.0 \qquad C_{L_\alpha} = 5.1309 \qquad C_{L_Q} = 7.7330 \qquad C_{L_{\delta_E}} = 0.7126 \tag{8.10}$$

$$C_{m_0} = 0.0 \qquad C_{m_\alpha} = -0.2954 \qquad C_{m_Q} = -10.281 \qquad C_{m_{\delta_E}} = -1.5852 \tag{8.11}$$

$$C_{Y_\beta} = -0.2777 \qquad C_{Y_P} = 0.0102 \qquad C_{Y_R} = 0.2122 \qquad C_{Y_{\delta_A}} = -0.0077 \qquad C_{Y_{\delta_R}} = 0.2303 \tag{8.12}$$

$$C_{l_\beta} = -0.0331 \qquad C_{l_P} = -0.4248 \qquad C_{l_R} = 0.0450 \qquad C_{l_{\delta_A}} = -0.3731 \qquad C_{l_{\delta_R}} = 0.0080 \tag{8.13}$$

$$C_{n_\beta} = 0.0860 \qquad C_{n_P} = -0.0251 \qquad C_{n_R} = -0.1250 \qquad C_{n_{\delta_A}} = -0.0065 \qquad C_{n_{\delta_R}} = -0.1129 \tag{8.14}$$

Propulsion:

$$\tau_T = 0.25 \text{ s} \tag{8.15}$$

$$T_{\max} = 70 \text{ N} \tag{8.16}$$

12 References

[1] M.V. Cook. *Flight Dynamics Principles*. Elsevier Butterworth-Heinemann, 1997.

[2] B. Etkin, L.D. Reid. *Dynamics of Flight, Stability and Control, 3rd Ed*. John Wiley & Sons, 1996.

[3] J.H. Blakelock. *Automatic Control of Aircraft and Missiles*, Second Edition. John Wiley and Sons, New York, 1991.

[4] R.S. Shevell. *Fundamentals of Flight*. Prentice-Hall, 1983.

[5] W.J. Hough. *Autonomous Aerobatic Flight of a Fixed Wing Unmanned Aerial Vehicle*. Masters thesis, Stellenbosch University, March 2007

[6] I.K. Peddle. *Autonomous Flight of a Model Aircraft*. Masters thesis, Stellenbosch University, April 2005.